UNIVERSITÀ DEGLI STUDI DI MESSINA

DIPARTIMENTO DI

SCIENZE CHIMICHE, BIOLOGICHE, FARMACEUTICHE ED AMBIENTALI

DOCTOR OF PHILOSOPHY IN CHEMICAL SCIENCES

Development of high-resolution chromatographic techniques based on mass spectrometry and infrared spectroscopy hyphenation

PhD thesis of:
Carmelo Coppolino

Supervisor:
Prof. Paola Agata Eustochia Donato

Coordinator:
Prof. Concetta De Stefano

CICLO XXXVI – A.A. 2022/2023 – SSD CHIM/01

Table of contents

Scope of the thesis

The present research thesis was focused on the development and application of liquid (LC) and gas-chromatographic (GC) techniques hyphenated to high-resolution tandem mass spectrometry (MS/MS) and solid-state infrared spectroscopy (*sd*-FTIR) for the characterization of complex matrices. Two fields of research have been followed in parallel, which implied the use of the two types of detectors.

The first part of the thesis describes the retrieval and characterization of biologically active peptides obtained from fish protein hydrolysates (FPHs), which exert well-known biological activities in the organism, by LC-MS/MS. Among the numerous biological activities of FPHs, short-length peptides have shown promising antimicrobial activities, high stability and low toxicity toward human cells. According to the principle of green and blue economy, a possible reuse of FPHs as source of active peptides would further benefit from easier manufacturing and cheaper production of short-length peptides, compared to the long-chain ones. Part of this research work has been carried out in the laboratory of Biochemistry, Technology and Innovation of Meat and Meat Products under the supervision of Professor Fidel Toldrá and Doctor Leticia Mora (Institute of Agrochemistry and Food technology of Valencia, Spain).

A second research topic has consisted in the development of prototype systems based on the hyphenation of LC and GC to a novel FTIR detector. The coupling of high-resolution, front-end separation to the unique identification capability of FTIR fingerprinting was aimed at achieving identification power for unknown components in complex mixtures, including regioisomers which often represent a challenging task in MS routine measurements.

The results achieved during the PhD course have been the subject of various research papers, as well as oral and poster communications listed at the end of this document.

Chapter 1

Chromatographic techniques

Chromatography is the most used separation technique in analytical chemistry. Indeed, when a complex matrix of unknown chemical compounds as the case of food sample needs to be qualitatively and quantitatively characterized, separation of its components considerably simplifies the analytical task.

According to the International Union of Pure and Applied Chemistry (IUPAC), chromatography is defined as "a physical method of separation in which the components to be separated are distributed between two phases, one of which is stationary (stationary phase) while the other (the mobile phase) moves in a definite direction" ("Chromatography," 2006). Depending on the nature of the mobile phase, three types of chromatography exist: liquid chromatography (LC), gas chromatography (GC) and supercritical fluid chromatography (SFC).

1.1 Chromatographic parameters

The chromatographic separation is based on the different interaction between each of the analytes with the two phases. As a consequence, the analytes are differently retained into the column and elute at different retention times (t_R). The result of a chromatographic run is the chromatogram, which is a plot of the intensity of the signal registered by the detector as a function of the time. Each of the analytes constituting the sample can be visualized as peaks with a gaussian shape. Each of them has a specific retention time (t_R) which correspond to the time when the maximum of the peak signal is registered.

Retention factor is the parameter which describes how much the analyte is retained by the column and can be calculated by rationing the time the analyte spends interacting with the stationary phase, also known as corrected retention time ($t'_R = t_R - t_0$) and the dead time (t_0), which is the time a completely not retained compound need to cross the column.

$$k' = \frac{t_R - t_0}{t_0} \quad (1.1)$$

The higher is the retention time and therefore the *k'*, the higher is its affinity for the stationary phase. The optimal k' is between 2 and 10.

Another important chromatographic parameter is selectivity (α) which represent the capacity of the stationary phase to separate two analytes and can be calculated as the ratio between the retention factors of the two analytes A and B:

$$\alpha = \frac{k'_B}{k'_A} \quad (1.2)$$

$\alpha > 1.2$ is desirable for a good separation.

Chromatographic separation is conceptually theorized in the same way as distillation. Indeed, the column is theoretically constituted of many "theoretical plates" in each of which the equilibrium of each analyte between the two phases is regulated by the distribution constant:

$$K_c = \frac{C_S}{C_M} \quad (1.3)$$

Where C_S and C_M are the concentrations of the analyte in the stationary and mobile phases respectively. Due to fact that during a chromatographic run the mobile phase flows continuously into the column, this equilibrium is never reached.

When the sample is injected into the chromatographic column, it constitutes a very sharp band which during its path along the column, it naturally broadens generating a gaussian shape. The extent of bandwidth broadening is defined by the efficiency and is measured in terms of theoretical plate number (N). Considering a gaussian shape peak N is calculated as follows:

$$N = \left(\frac{t_R}{\sigma}\right)^2 = \left(\frac{t_R}{w_b}\right)^2 = 5.54\left(\frac{t_R}{w_h}\right)^2 \quad (1.4)$$

Where t_R is the retention time of the peak, w_b is the base peak width and w_h the peak width at half height. Therefore, the higher is N, the narrower is the chromatographic peak, and consequently higher the efficiency.

Another parameter expressing column efficiency and related to N is the equivalent height of the theoretical plate (HETP o H), which can be calculated by rationing the column length (L) and N:

$$H = \frac{L}{N} \tag{1.5}$$

H was also studied by Van Deemter, who identified the parameters affecting the band broadening in chromatography (Van Deemter et al., 1956), which are included into the Van Demeter equation, which is specific for the packed columns:

$$H = A + \frac{B}{\bar{u}} + C\bar{u} \tag{1.6}$$

Where:

- **A** also known as Eddy diffusion is the dispersion of the analytes across the stationary phase, i.e. the little differences in the packing material bring to the formation of paths of different length, causing a band broadening. This parameter is proportional to the particle diameter (d_p) and λ which is a constant value depending on the packing:

$$A = 2\lambda d_p \tag{1.7}$$

- **B** is the longitudinal diffusion, which the solute is subjected to during its passage into the column, according to the concentration gradient. This term is dependent on the longitudinal diffusion coefficient D_m and the coefficient γ which is related to the stationary phase. B is inversely proportional to the column flow ($\bar{u}$). Indeed, using a lower flow rate the analytes have more time to diffuse. In liquid chromatography this term is negligible.

$$B = 2\gamma D_m \tag{1.8}$$

- **C** is the sum of resistance to the mass transfer in stationary (C_s) and in mobile phase (C_M), C = C_M + C_s, where

$$C_s = \frac{8kd_f^2}{\pi^2(1+k)^2 D_S} \tag{1.9}$$

C_s is a parameter proportional to the square of film thickness bonded to the packing particle (d_f^2) and reversely proportional to the diffusion coefficient of the solute in the

film (D_S). C_s also depends on the retention factor, in particular the expression $\frac{k}{(1+k)^2}$. High values of k mean that the analytes are highly soluble in the stationary phase and therefore this ratio decreases.

$$C_M = \frac{\omega d_p^2}{D_M} \tag{1.10}$$

C_M is proportional to the square of the particle diameter d_p^2 and reversely proportional to the diffusion coefficient of the solute in the mobile phase (D_M) and ω is a constant value.

The different contributions of the Van Deemter equations give rise to the Van Deemter curve which is reported in figure 1.1.

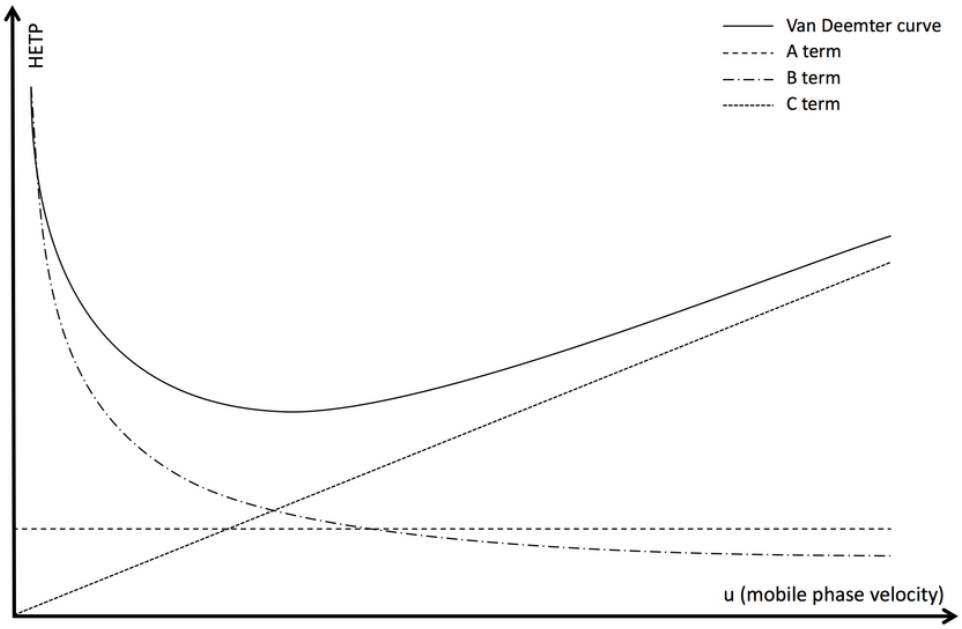

Figure 1.1 Plot of the van Deemter curve (Yu, 2016).

According to this equation and the relative plot in figure 1.1, there is an optimal mobile phase velocity which corresponds to the minimum value of H. The need for higher chromatographic efficiency has therefore led to the reduction of the packing particle diameter, reducing the A factor (equation 1.7) and consequently H. However, this results in an increase of the mobile phase resistance to cross the column when operating at regular flow rate. To this regard, all the instrumentation, including the

pumps, injection system, columns and connections were implemented in order to operate at higher pressures without any damages. Therefore, high-performance or high-pressure liquid chromatography (HPLC) and then ultra-high performance or ultra-high pressure liquid chromatography (UHPLC) have been developed. Columns normally used in analytical HPLC have a length comprised between 5 and 30 cm and an internal diameter of 2-2.1 or 4-4.6 mm.

The further introduction of capillary columns in gas chromatography by Golay led to the modification of the Van Deemter equation to the Golay equation:

$$H = \frac{B}{\bar{u}} + (C_S + C_M)\bar{u} \tag{1.11}$$

In this case, not being the column packed, the term A (eddy diffusion) was omitted, and an improvement of the efficiency was obtained.

The parameter B was dependent on the diffusion coefficient (D_G) of the analyte in the carrier gas, according to the following equation:

$$B = 2D_G \tag{1.12}$$

Also, in the case of capillary columns the term C (mass transfer) is the sum of mass transfer in the mobile phase (C_M) and in the stationary phase (C_S).

In particular C_S describes the velocity of the analyte diffusion between the stationary and the mobile phase. The faster is the transfer, the lower is this factor.

$$C_S = \frac{2kd_f^2}{3(1+k)^2 D_S} \tag{1.13}$$

Indeed, C_S depends on the stationary phase film thickness d_f, the diffusion coefficient of the analyte in the stationary phase D_S and the retention factor in particular the expression $\frac{k}{(1+k)^2}$. High values of k mean that the analytes are highly soluble in the stationary phase and therefore this ratio decreases. When k >20 a little decrease takes place. Moreover, since a large value of k results in a very long-time analysis, k value near to 20 is preferable.

The term C_M is described by the following equation:

$$C_M = \frac{(1+6k+11k^2)r_c^2}{24(1+k)^2 D_G} \quad (1.14)$$

Where r_c is the column radius.

The last chromatographic parameter is chromatographic resolution (R_S) which measures the degree of separation between two adjacent peaks, and it is calculated as follows:

$$R_S = \frac{t_{R_2} - t_{R_1}}{\frac{w_1 + w_2}{2}} \quad (1.15)$$

To obtain an appropriate separation of the two peaks, the resolution should be higher than 0.8. R_S is dependent on the already described parameters according to the following equation:

$$R_S = \frac{\sqrt{N}}{4}\left(\frac{\alpha-1}{\alpha}\right)\left(\frac{k_2}{1+k_2}\right) \quad (1.16)$$

R_S is proportional to the square root of N, so if the column length is doubled, R_S increases of 1.414. This explains how considerably R_S increases using very long columns. However, it results in a longer analysis time.

Column retentivity (k_2) also affect the resolution, but a substantial contribution is given only for analytes with low retention factors ($k_2 \leq 3$).

The greatest effect on resolution is given by the selectivity (α). That is the reason why the choice of the correct stationary phase based on the nature of the analytes is the most important factor for obtaining the best R_S.

1.2 Liquid chromatography

Liquid chromatography is the analytical technique of election for the separation of non-volatile or thermo-degradable compounds. In this case, the separation takes place inside a stainless-steel column packed with small size (µm) particles chemically functionalized. Separation of the analytes is based on the different affinity of each of the analytes between the stationary and the liquid mobile phase.

1.2.1 Types of liquid chromatographic separations

According to the goal of the separation HPLC systems can be classified into preparative and analytical chromatography. Preparative chromatography is generally used for the isolation and purification of a specific compound, for its identification or for the evaluation of its biological activity. On the other hand, analytical chromatography is used for the qualitative and quantitative characterization of a sample. Since the two types of chromatography requires different amount of sample, columns have different diameters. Whereas the preparative columns have a diameter comprised between 2.1 and 200 mm, the analytical ones between 2.1 and 4.6 mm.

As the table 1.1 shows, columns of reduced diameter have also been developed for the need of miniaturized analyses.

Table 1.1 Types of liquid chromatographic columns and the relative diameter.

Type	**Diameter**
Preparative	2.1 to >200 mm
Analytical	2.1–4.6 mm
Micro	1.0 mm
Capillary	300 μm–1 mm
Nano	25–300 μm

Many types of liquid chromatographic separations exist, and the choice depends on the nature of the sample. Normal phase (NP) HPLC uses a polar stationary phase and a non-polar mobile phase. On the other hand, in reversed phase (RP) HPLC the stationary phase is non-polar, and the mobile phase is polar. In particular, the stationary phase is made of a silica support functionalized with n-alkyl groups: octadecyl (C18) or octyl (C8). Typical mobile phase used for this type of separation is water with a more non-polar and water miscible solvent. Elution is generally performed by gradually increasing the percentage of the less polar mobile phase (gradient mode). In this way the analytes are eluted according to their different hydrophobicity from the

more to the less polar. This is the most used type, constituting the 80% of all of the HPLC applications (Wang, 2015).

Ion Exchange chromatography (IEC) is used for the separation of charged molecules. The stationary phase shows ionic functional groups which retain opposite charged analytes. Therefore, cationic ion exchange chromatography retains cations because the stationary phases possess a negatively charged group as phosphoric or sulfonic. On the other hand, anionic ion exchange chromatography retains anions being the stationary phase positively charged, because it possesses amino or quaternary ammonium group. As an example, in the peptide class, the acid peptides are better separated on anionic ion exchange columns (Pizzano et al., 1998), while acid peptides on cationic ion exchange columns (Sentandreu et al., 2003). In this type of separation, the elution is performed by increasing the ionic strength of the mobile phase. Better separation can be obtained by using non-volatile salts such as NaCl, but they are not compatible with mass spectrometry. To overcome this issue, after this separation an RP-HPLC or HILIC-HPLC need to be performed to eliminate these salts.

Another type of chromatographic separation is hydrophilic interaction liquid chromatography (HILIC). In this case, the stationary phase is polar, and consists of silica particles functionalized with polar groups, such as diol, amino, amide and cyano substituents similarly to NP-HPLC. However, in this case mobile phases are the same as the ones used in RP-HPLC but inverted, i.e. during the analysis the percentage of water increases (Buszewski & Noga, 2012). This type of separation offers many advantages over others. Indeed, it is the separation of choice for uncharged highly hydrophilic and amphiphilic compounds that are too polar to be well retained RP-HPLC, and at the same time do not have enough charge to interact with ion-exchange chromatography stationary phases (Buszewski & Noga, 2012). Moreover, having a water based mobile phase, it overcomes the drawback of NP-HPLC which using a non-polar mobile phase do not allow a proper solubilization of the polar analytes and can be efficiently coupled to Electro Spray ionization (ESI). Moreover, it allows separation of charged polar analytes, such as small peptides (Mora et al., 2007).

1.3 Gas chromatography

Gas chromatography is the separative technique used for the separation of volatile and thermostable compounds. In this case separation is based on the different affinity of the analytes with the stationary phase while the gas carrier (normally N_2, H_2 or He) flows into the chromatographic column.

The sample, generally liquid, is introduced into the chromatographic column by means of the injector which is set at a temperature higher than the most boiling point analyte. The chromatographic separation takes place into a capillary chromatographic column (0.25 µm of diameter) made of fused silica, which is open tubular (OT) and whose wall is coated with the stationary phase (wall coated open tubular WCOT). Being open tubular and being the mobile phase a gas, these columns generate a very low resistance to the flow, thus they can have a length up to 200 m.

The column can be of different nature according to the analyte to be separated. For samples with similar polarity compounds but quite different boiling points, it is not necessary for the stationary phase to be particularly selective, so a non-polar one is used. In this way, the compounds will elute in increasing order of boiling points. On the other hand, for samples with substances of different polarity but with fairly close boiling points, a polar stationary phase is preferable. In this case, separation depends more on the polarity of the analyte, meaning that the most polar will be more retained.

The chromatographic column is placed into an oven and separation can be performed keeping the temperature constant for the entire analysis (isothermal), or by gradually increasing the temperature (temperature-program).

Chapter 2

Mass spectrometry techniques

Mass spectrometry is a type of detector widely used in analytical chemistry either for its identification, or for its quantification capabilities because of the very low limit of detection it can reach. Moreover, thanks to the different types of interphases existing, it is widely used in combination with chromatographic techniques. Mass spectrometer is an analytical instrumentation capable of separating and consequently detecting the ions generated from the analytes present in the sample on the basis of their mass/charge (*m/z*) and is constituted of three main parts:

- **Ion source**, where the ions are generated from the analytes;
- **Mass analyser**, where the ions are separated according to their *m/z*;
- **Detector**, where the signal generated from the ions coming from the analyser is converted into an electric signal, which is further displayed as mass spectrum.

Mass analysers, detectors and some ion sources work in vacuum conditions, with the goal of not altering the trajectory of the ions and to avoid collisions with the neutral molecules.

2.1 Ion sources

To be analysed by mass spectrometry, it is necessary that the sample is in gaseous form and ionized. These are the tasks of the first part of a mass spectrometer: ion source. They are differently classified according to the nature of the introduced sample, for gas phase molecules such as the ones coming from a gas chromatograph the most used is electron ionization (EI). For liquid samples, for example the ones coming from liquid chromatography, electrospray ionization (ESI) and atmospheric pressure chemical ionization (APCI) are the typical ion sources. Finally in the case of solid samples Matrix-Assisted Laser Desorption Ionization (MALDI) is commonly used.

2.1.1 Ion sources for gaseous phase samples

Samples eluting from gas chromatography are already in the gaseous form, therefore in this case the ion source only needs to ionize the analytes. In this regard electron ionization is the most widely used source. In this technique, the ions coming from gas chromatography are subjected to a high energy electrical field (70 eV) in vacuum atmosphere to avoid collisions between the ions and other gas phase molecules. This high energy is far greater than the ionization energy of a molecule and provokes the loss of an electron bringing to the generation of the molecular ion as radical cation ($M^{+\bullet}$) as shown in the equation 2.1.

$$M + e^- \rightarrow M^{+\bullet} + 2e^- \quad (2.1)$$

Being $M^{+\bullet}$ instable, it fragments into more stable ions, giving rise to a fragmentation pattern which is highly reproducible at that energy. For this reason, this ionization technique allows the easy identification through comparison with mass spectral libraries. This advantage of EI has been also exploited for the coupling with liquid chromatography (nano-LC) with a big effort due to the necessity to remove the mobile phase, which is not compatible with the high vacuum of the mass spectrometer. (Famiglini et al., 2021).

Being the ionization energy so high it is defined hard ionization. However, such hard ionization leads to the reduced intensity, or the absence of the molecular ion (MI), making the molecular weight determination challenging. For this reason, the possibility to use milder ionization conditions has been exploited (Tranchida et al., 2019).

2.1.2 Ion sources for liquid phase samples

The hyphenation between liquid chromatography and mass spectrometry is much more complicated due to the presence of the mobile phase which is not compatible with the MS vacuum. For this reason, the LC-MS ion sources are able to eliminate the mobile phase, and this process takes place at atmospheric pressure, therefore they are classified as atmospheric pressure ionization (API) sources. Among these, electrospray ionization (ESI) is the most common and it is designed for the analysis of polar, thermally labile and also high molecular weight analytes such as proteins (Fenn, 2003;

Fenn et al., 1989, 1990). In this ionization technique, the solubilized sample or the eluent coming from the HPLC is vaporized by means of a nebulizing gas (N_2) to a fine aerosol by passing through a small steel capillary tube subjected to a high voltage (1-5kV). As a result, a cloud of electrically charged droplets is generated and passes through a flow of heated inert gas (desolvation gas, N_2) which eliminates the neutral molecules and evaporates the solvent from the droplets, causing to shrink in size. Thus, the charge density inside the droplets increases and consequently the repulsion forces between ions. When the electrostatic repulsion and the surface tension of the droplet become exactly equal, such a situation is known as the Rayleigh limit. When this limit is exceeded, the droplets explode (Coulomb explosion) releasing ions in gaseous form into the mass analyser. Being a soft ionization, it does not cause bond breakages, but only the protonation (positively charged ions) or deprotonation (negatively charged ions) of the analytes.

The advantage of ESI source is that it can generate ions of different charges $(M+nH)^{n+}$, which is particularly useful when it comes to high molecular weight molecules such as proteins, allowing the reduction of *m/z* up to 150kDa (Fenn et al., 1990). Isotopic pattern of the peak allows to understand the number of charges of the considered molecule and consequently the molecular weight. The miniaturization of this ionization technique (nano-ESI) leads to a huge improve of the sensitivity (Wood et al., 2003).

Atmospheric pressure chemical ionization (APCI) is another soft ionization technique similar to ESI, but it is specifically designed for the analysis of low and medium polarity molecules which ionizes with difficulty with ESI. The difference with APCI, is the presence in the ion source of a corona discharge needle whose discharge causes the ionization of the gas molecules (N_2), which ionize the solvent, and further the analytes.

The last atmospheric pressure ionization technique is Atmospheric Pressure Photo-Ionization (APPI), which is very similar to APCI, but in this case molecules are ionized by means of photoionization. It is used for the ionization of non-polar molecules.

2.1.3 Matrix assisted laser absorption (MALDI)

Matrix assisted laser absorption (MALDI) is another ionization source used for the ionization of solid sample such as a mixture of peptides. The sample is placed on a metal-plate solubilized in a solvent containing the matrix constituted of small organic molecules such as α-cyano-hydroxycinnamic acid or 2-5-dihydroxybenzoic acid, that have a strong absorption at the laser wavelength. As the solvent evaporates, crystals of the analyte-matrix mixture are formed. The plate is introduced into the source, which is in vacuum conditions and then is irradiated with a pulsed nitrogen laser. This causes the heating of the crystals by the accumulation of high amounts of energy through the excitation of the matrix molecules, which further transfer this energy to the analytes for their ionization. The ions generated by means of this technique are principally monocharged $(M+H)^+$.

2.2 Mass analysers

Mass analyser is the part of the mass spectrometer which separates the ions generated into the ion source and delivers them to the detector. There are many different types of mass analysers which are different in their functioning principle and in the mass resolution they can provide. They work in different modalities and can be classified in mass analysers which operate continuously (magnetic sector and quadrupole), in pulsed mode (time of flight), or through ion capture (ion trap, orbitrap and FTICR).

2.2.1 Quadrupole

The quadrupole analyser is one of the most used types of mass analyser because of its lower cost, compact design, durability and reliability. It can be considered as a mass filter since it allows a specific *m/z* to reach the detector depending on the electric field generated (Miller & Denton, 1986). It consists of four parallel cylindrical rods, where each opposing rod pair is connected together electrically, and between one pair of rods and the other, a radio frequency (RF) voltage with a DC offset voltage is applied. The combination of the RF and DC potentials induces the oscillation of the ions passing through the quadrupole in the z-direction following a spiral trajectory. Depending on the DC and the RF frequency, only ions of a specific *m/z* have a stable trajectory and thus can reach the detector. The others have an unstable trajectory and collide with the

rods. Therefore, the quadrupole operates as an ion filter. The variation of the two potentials let ions of different *m/z* to be filtered. Thus, the quadrupole can operate in two different modalities:

- Single ion monitoring (SIM), where only a specific *m/z* of the analyte of interest is monitored. This modality is highly selective because it allows the selection of just an analyte without the interference of others and is particularly useful for targeted analysis.
- Scan, where a range of *m/z* is monitored because of the variation of the DC and RF. In this case the sensitivity is reduced due to the higher duty cycle, but it can be used for untargeted analysis.

2.2.2 Time of Flight (ToF)

Time of flight (ToF) mass analyser is conceptually the easiest type of mass analyser. It basically separates the ions generated into the ion source on the basis of the time they spend to travel a specified distance consisting in the flight tube length. The ions coming from the source are previously accelerated into an acceleration grid by means of an electrical field applied (10^3-10^4 V) towards the detector. Therefore, an identical kinetic energy E_k is applied, which is calculated as follows:

$$E_k = \frac{1}{2}mv^2 \tag{2.2}$$

Where m is the mass of the ion, and v is its velocity. Due to the free field region, the ion speed is maintained constant along the tube:

$$v = \frac{d}{t} \tag{2.3}$$

Where d is the path the ions travel, and t the time they spend to reach the detector from the acceleration grid.

Replacing v, the kinetic energy equation become:

$$m = \frac{2E_k t^2}{d^2} \tag{2.4}$$

Since E_k and the flight tube length remain constant, mass is a function of the time the ions spend to travel along the flight tube. Depending on the ion mass and charge, they

move with different velocities into the tube, and specifically the lighter ions move with a higher velocity reaching first the detector. The latter registers the time ions spend to reach the detector (time of flight).

The more sophisticated ToF mass analysers employ reflectron and delayed estraction to obtain an improvement in mass resolution.

The reflectron reflects the ions accelerated back in the direction of the ion source before the detection (Cotter, 1999). This allows for corrections in small differences in the initial kinetic energy of the ions, which may occur during the acceleration, consequently improving mass resolution (Mamyrin et al., 1973).

Delayed extraction introduces a small delay (nanoseconds) in the electric pulse before acceleration of the ion coming from the ion source (Juhasz et al., 1997; Vestal et al., 1995). This small delay allows the ions formed to equilibrate in the acceleration grid and have a more uniform average momentum before acceleration.

This type of mass analyser is capable of achieving the widest mass range, allowing for the separation of ions with masses from few to over 100 kDa (Karas & Bahr, 1990). For this reason, they are the analysers of choice for the observation of singly charged high mass biomolecules such as proteins, and moreover they are the most used for performing peptide mass fingerprinting (Pappin, Hojrupt, & Bleasbyl, 1993; Thiede et al., 2005). Since ToF works in pulsed mode, it was initially coupled only with pulsed sources, such as MALDI, but then it was also interfaced with sources that provide a continuous flux of ions, such as ESI.

2.2.3 Orbitrap

Orbitrap is a mass analyser which makes use of a fourier transform to convert a signal produced by the oscillation of ions induced by an electric field in a trap into a mass value. This type of mass analyser is composed of three main parts: an inner spindle electrode covered by two hollow outer concave electrodes facing each other. The two outer electrodes are separated each other by a thin ring of dielectric material. A voltage potential is applied between the inner and the outer electrodes, creating a linear electric field between them. The ions are introduced tangentially into the orbitrap as a “packet” between the inner and outer electrodes through a hole present into one of the outer

electrodes. Due to the electric field between the inner and outer electrodes, the ion packet is bent towards the inner electrode while the tangential velocity of the ions creates an opposing centrifugal force. At a specific potential between the inner and outer electrodes, the ions remain in a spiral path around the inner electrode. However, due to the conical shape of the electrodes, a harmonic axial oscillation in the ions is induced. The outer electrodes also act as receiver plates that detect the back-and-forth axial harmonic motion of the ions. This signal image is digitized and transformed from the time domain to the frequency domain (Zubarev & Makarov, 2013). The axial harmonic frequencies are proportional to the *m/z* of the ions. One of the most important advantages of the orbitrap analysers is its high mass resolution, but it is not the same for all the *m/z*. Indeed, a decrease in resolution which is inversely proportional to the square-root of the measured *m/z*, having it a better resolving power at higher *m/z*. It gives the orbitrap the advantage in the analysis of high molecular weight molecules such as proteins (Haag, 2016).

2.2.4 Ion trap

Ion trap (IT) is a mass analyser that works similarly to the quadrupole. It consists of two hyperbolic ring electrodes which act in the same way of the metallic rods. They face each other and a hyperbolic ring electrode is placed in between them. The ions enter a small opening in the endcap of one of the electrodes. By means of an oscillating RF and a superimposed DC electric field, ions are trapped between the electrodes. In particular, the ions of an appropriate *m/z* value circulate in a stable orbit within the cavity surrounded by the ring.

Then, when the radiofrequency potential increases the orbits of the heavier ions becomes stable, while the ones of the lighter ions destabilize and are ejected by the trap (Dass, 2006; Haag, 2016). In this way ions are selectively released from the trap in increasing order of *m/z* by gradual changes in the RF potential and are further registered by the detector.

2.2.5 Tandem mass spectrometry

Mass spectrometers which employ two or more mass analysers are known as tandem mass spectrometers (MS/MS). They are particularly useful to obtain structural

information about the molecules because fragmentation takes place between the mass analysers.

Indeed, in tandem mass spectrometry, mass analysers are separated by a fragmentation or collisional chamber. When the ions are formed in the ion source, the first mass analyser separates the ions considering their *m/z*. Further, based on a specific selection criterion, a specific precursor ion is selected and subjected to fragmentation by means of collision-induced dissociation (CID) (Hayes R N & Gross M L, 1990).

This fragmentation occurs into a collision cell, where a chemically inert gas (argon or nitrogen) is introduced. Then, its collision with the ions causes their fragmentation at low pressure. During the collision, some of the kinetic energy of the gas molecules is transmitted and converted to the internal energy of the analyte ions, thus resulting in bond breakage of the analyte ion molecules (Cooks, 1995).

Finally, the precursor and its fragments are transmitted into the second mass analyser, which separates and sends them to the detector, which register the mass spectrum of both precursor and fragments. The spectrum thus obtained provides structural information of the analyte. There are many types of tandem mass spectrometry configurations: triple quadrupole (QqQ), Q-ToF, ToF-ToF, IT-TOF, Q-Orbitrap.

Triple quadrupole mass analyser is constituted of a collisional cell (Q_2) which is placed in the middle of the two quadrupoles (Q_1 and Q_3). Therefore, while Q_1 and Q_3 operate only as mass filters, Q_2 is a collisional cell. This configuration and the combination of the two modalities of work of quadrupole (Scan and SIM) allows different modalities of work.

- **Product Ion Scan:** a precursor ion is selected by Q_1 and delivered to the collisional cell, fragmented, and all the product ions are scanned into the Q_3, and further detected. Q_1 and Q_3 work in SIM and Scan modes respectively.

- **Precursor Ion Scan:** all the masses are scanned into the Q_1 and fragmented. Only a product is selected by the Q_3 and then detected. This modality is used when it is necessary to understand which are the precursors of a specific product ion. Q_1 and Q_3 works in Scan and SIM mode respectively.

- **Neutral Loss Scan:** all the masses are scanned in the Q_1 and then fragmented. Then the Q_3 scans all the product ions which have a set offset from the Q_1. This offset corresponds to a neutral loss that is commonly observed for the class of compounds. Therefore, all the precursors which undergo to the loss of a specific mass are detected. In this case both Q_1 and Q_3 work in scan mode.

- **Selected Reaction Monitoring:** a precursor is selected in the Q_1, fragmented and then a product is selected by Q_3 and further detected. Both Q_1 and Q_3 work in SIM. In **Multiple Reaction Monitoring (MRM)** more than a product ion can be selected from one or more precursor ions. This modality is extremely selective and sensitive and specifically used for targeted analysis.

Due to this high versatility and sensibility QqQ, is one of the most used tandem mass spectrometers.

An improvement of the triple quadrupole is the Q-ToF in which the second quadrupole is substituted with a time-of-flight mass analyser. In particular, the two analysers are orthogonally coupled so that the ions are accelerated in the perpendicular axis to the one of their initial directions of motion.

This configuration provides higher mass accuracy of precursors and products ions. This is of particular interest in the field of untargeted analyses, which are gaining considerable interest in the fields of proteomics and metabolomics. The aim of the untargeted analysis is to obtain a comprehensive evaluation of all the compounds present in a certain sample either if they are known or unknown. In this regard, liquid chromatography coupled to high resolution mass spectrometry (LC-HRMS) is currently the most prominent analytical platform, owing to its high mass resolution, mass accuracy, sensitivity, fast scan speed, and large dynamic range (Guo & Huan, 2020; Want, 2018).

Data-Dependent acquisition (DDA) and Data-Independent Acquisitions (DIA) are the most common strategies in untargeted analyses. In both techniques the MS performs an MS^1 full scan, followed by a different precursor selection for the MS/MS acquisition (MS^2). In DDA mode, the most intense precursors are selected from MS^1

and subjected to fragmentation, so that not all ions are fragmented. Therefore, a limitation of DDA is the detection and quantification of low abundance ions in MS^1, because they may not be selected for the fragmentation and consequently do not have MS^2 data associated with them. Moreover, this type of analysis is not reproducible because a relatively high variability of the selected analytes may be registered between replicate analyses of the same samples (Fernández-Costa et al., 2020).

On the other hand, in DIA all the precursors from MS^1 are subjected to the fragmentation and consequently generate MS^2 spectra of all the precursor ions. Therefore, a higher number of less abundant ions can be detected and quantified. However, the complexity of the resulting MS^2 is incredibly high because fragmentation of more than one precursor takes place, so it becomes difficult to link fragments with precursors. For this reason, DDA analyses is still more used than DIA.

Chapter 3

Infrared spectroscopy coupling to chromatographic techniques

Infrared spectroscopy (IR) is a powerful analytical technique used in chemistry, physics, and various scientific disciplines to study the interaction between matter and electromagnetic radiation in the infrared region of the electromagnetic spectrum. IR provides valuable information about the vibrational and rotational motions of molecules, making it a fundamental tool for identifying and characterizing organic and inorganic compounds. IR spectroscopy has applications in a wide range of fields, including chemistry, materials science, environmental science, pharmaceuticals, and forensic analysis. The principle behind infrared spectroscopy is based on the fact that molecules can absorb specific wavelengths of infrared light, which causes them to vibrate or rotate in characteristic ways. By measuring the energy of absorbed or transmitted infrared radiation, researchers can create detailed spectra that serve as unique molecular fingerprints for different substances. These spectra are typically represented as a graph of absorbance (or transmittance) versus wavelength or wavenumber.

Infrared spectroscopy is particularly valuable for elucidating the chemical structure of compounds, identifying functional groups, and determining the presence of specific bonds. It can be used for qualitative analysis, where it helps identify the chemical composition of unknown samples, and for quantitative analysis, where it quantifies the concentration of a particular component in a mixture.

There are two common types of infrared spectroscopy: dispersive infrared spectroscopy and Fourier-transform infrared spectroscopy (FTIR). FTIR is the most widely used method and is known for its high sensitivity and ability to provide rapid, comprehensive data. It has revolutionized the field of spectroscopy due to its speed and accuracy.

Infrared spectroscopy has found applications in various scientific, industrial, and research areas. It is used in environmental monitoring to detect pollutants, in the pharmaceutical industry to analyse drug compounds, and in forensic science for identifying trace evidence. Additionally, it plays a critical role in materials science for characterizing polymers, minerals, and surface coatings.

3.1 IR spectroscopy

The Infrared Spectroscopy is the region of the electromagnetic radiation comprised between 700 nm and 1 mm and is located between the visible light and the radio waves. It is a powerful tool for identifying organic and inorganic compounds because, apart from a few homonuclear molecules, such as O_2, N_2, and Cl_2, all organic and inorganic molecules absorb infrared radiation.

Furthermore, except for chiral compounds, each molecule has a unique infrared absorption spectrum (fingerprint). Thus, an exact overlap between the spectrum of a compound of a known structure and that of an analyte unambiguously identifies the analyte.

Infrared radiation has a particular energy able to generate the vibration of a molecule, more specifically a vibrational transition. Molecules are atoms linked by chemical bonds, which due to their elasticity, do not remain fixed, but they vibrate in the three-dimensional space relative to each other., giving rise to a continuous oscillatory motion. This motion, if accompanied by a variation in the moment of molecular electric dipole, can interact with the wave motion of an electromagnetic radiation, giving rise to absorption of the same. In this case, a spectrum called vibrational spectrum or even infrared spectrum (IR) will be observed, because it takes its name from the values of the frequencies of the absorbed radiation, which fall precisely in the spectral zone of the infrared.

Taking into consideration the easiest type of molecule, namely a diatomic molecule, it is constituted of two atoms which are held together at a certain distance from each other (distance of equilibrium r_e), by a series of attractive forces (between the electrons of one atom and the nuclei of the other) and repulsive forces (between the two positively charged nuclei and between the electrons of one atom and those of the

other). At the distance of equilibrium, all the forces are perfectly balanced. If the bond is compressed the repulsive forces would grow rapidly, increasing the potential energy of the molecule. Likewise, any attempt to drive away the two atoms would be counteracted by the attractive forces. In both cases the energy of the molecule would increase following the law described graphically in figure 3.1, which represents the potential energy of the molecule as a function of the internuclear distance.

As already said the minimum of the curve corresponds to the distance of equilibrium.

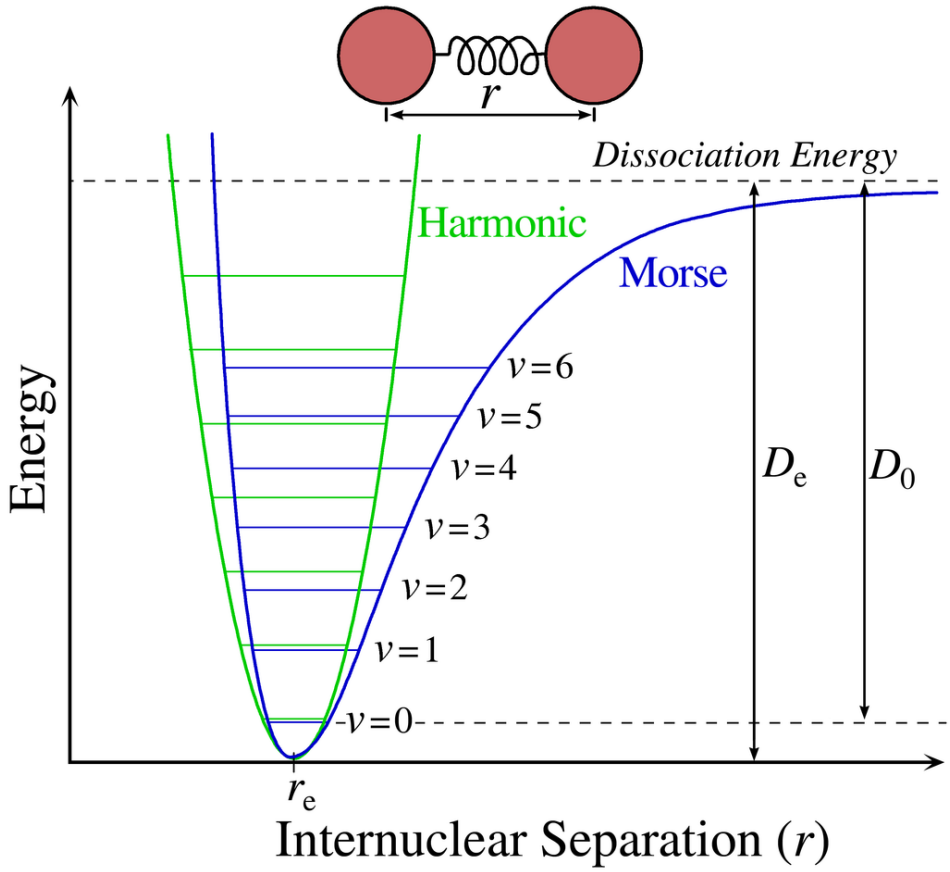

Figure 3.1 The Morse potential (in blue) and the harmonic oscillator potential (in green).

For little oscillations near r_e the energy follows a parabolic trend behaving as a harmonic oscillator, and consequently following the Hooke law. This establish that the elastic force is proportional to the elastic constant of the spring (k) and the amount of the shift from the r_e according to the following equation:

$$F = -k(r - r_e) \tag{3.1}$$

Therefore, the correspondent potential energy of the harmonic oscillator will be:

$$E = \frac{1}{2}k(r - r_e)^2 \tag{3.2}$$

Therefore, modifying the distance between the two masses the energy increase, but the frequency remains constant because it is not dependant on the distance.

$$\omega_{osc} = \frac{1}{2\pi c}\sqrt{\frac{k}{\mu}} \tag{3.3}$$

Where μ is the reduced mass:

$$\mu = \frac{m_1 m_2}{m_1 + m_2} \tag{3.4}$$

Where m_1 and m_2 are the two masses of spring.

K a constant which depends on the strength of spring and in the case of a molecule it depends on the bond order (single, double or triple bond). Therefore, according to the equation the vibrational frequency ω_{osc} increases with the increase of the bond order and the decrease of the masses of the atoms that constitute the molecule.

Since this is a microscopical system, molecular vibrational energy cannot vary continuously but for discrete amounts, therefore only well-defined amplitude vibrations are allowed. The allowed energy values can be obtained by solving the appropriate Schrödinger equation, which, for a simple harmonic oscillator whose potential energy is expressed by equation:

$$\varepsilon_\nu = \left(\nu + \frac{1}{2}\right)\omega_{osc} \tag{3.5}$$

Where ε_ν is the quantized energy, and ν is a whole number (1,2,3,4…) with the frequency expressed in cm^{-1}. Therefore, there is not a zero level of energy, but the lowest energy values allowed in diatomic molecule is $\frac{1}{2}\omega_{osc}$ and then , $\frac{3}{2}\omega_{osc}$, $\frac{5}{2}\omega_{osc}$ etc. It means that the vibrational energy cannot be zero, but the molecules always make small oscillations.

Moreover, the quantum levels are equally spaced by a quantity of ω_{osc}, as show the green curve of the Figure 3.1.

The interaction with an electromagnetic radiation, whose frequency correspond to the one related to the separation between the two levels according to the plank equation, can give place to an energy absorption with promotion of the molecule to the upper level, as long as the transition obeys the two selection rules that govern vibrational spectroscopy:

- The first is that vibrations are active spectroscopically only on condition that they give rise to a variation in the electric dipole moment of the molecule. Thus, homonuclear diatomic molecules, and therefore without dipole momentum such as H_2, N_2, O_2, Cl_2 ha, etc., do not any exhibit vibrational spectra.
- The second selection rule derives directly from the properties of vibrational wave functions obtained by reviewing the Schrödinger equation for the harmonic oscillator, which says that only vibrational transitions between two adjacent levels are allowed, for which it must be:

  $$\Delta\nu = \pm 1 \tag{3.6}$$

  By applying this rule, the energy variation that takes place during the variation corresponds to ω_{osc} obtained by subtracting $\varepsilon_{\nu+1} - \varepsilon_{\nu}$.

  Therefore, any transition between adjacent levels will give rise to a single spectral line, a frequency coinciding with the oscillation frequency of the molecule.

How are the molecules arranged on the various vibrational levels at ordinary temperatures? The answer to this question is formed by statistical thermodynamics and, in particular, by Boltzmann's law of distribution, which predicts that the ratio between the populations of two levels (non-degenerate) characterised by vibrational quantum numbers *i* and *j* and with energies respectively E_i, and E_j, is given by the formula.

$$\frac{N_i}{N_j} = e^{\frac{E_j - E_i}{kT}} \tag{3.7}$$

Where N_i and N_j are the two populations of the levels i and j. K is the Boltzmann constant and T the absolute temperature. By calculating this ratio, it is found from that only the lowest vibrational level $\nu = 0$ is populated and the prevalent transition is from $\nu = 0$ to $\nu = 1$.

As previously anticipated, the harmonic oscillator model is valid only for very small oscillations of the two atoms.

For greater amplitude vibrations, the potential energy curve deviates considerably from a parabola and therefore a much more complex function must be used. The function that well describes the behaviour of a diatomic molecule, is the so-called Morse function. In this model the levels of energy of the anharmonic oscillator are:

$$\varepsilon_\nu = \left(\nu + \frac{1}{2}\right)\omega_e - \left(\nu + \frac{1}{2}\right)^2 \omega_e \chi_e \tag{3.8}$$

Where χ_e is the anharmonicity constant.

In this case the energy levels are not equally spaced anymore, and the upper levels become closer and closer. Therefore, the frequency of the oscillation decreases with the increase of the amplitude of the oscillation.

Furthermore, another consequence of the anharmonicity is that the second selection rule is not valid anymore. Therefore, the transition between levels can be:

$$\boldsymbol{\Delta\nu} = \pm 1, \pm 2, \pm 3 \text{ etc.} \tag{3.9}$$

However, the probability that they happen decreases with the increase of the energetic jump.

The only visible transitions are the first two which are named first harmonic or fundamental and second harmonic which is not likely to happen. These bands are named overtone bands.

Other types of transitions that can be observed are the hot bands which correspond to the transition between the second and the following energy level. These are very weak band, which intensity increases with the increase of the temperature, due to the rise of population of the second vibrational level. Their frequency is $\omega_e = (1 - 4\,\chi_e)$.

In the case of a polyatomic molecule which is the normal case, due to the fact that they have different bonds, they can have multiple vibrations. The possible vibrations in a polyatomic molecule, consisting of n atoms, can be easily predicted as follows: being the molecule as a set of atoms not rigidly connected to each other, each of which can move along three perpendicular directions, it will possess in total 3n degrees of motional freedom, of which:

- 3 are the translational movements in the three-dimensional space.

- 3 are the rotational degree of freedom because they can rotate around three axes of inertia. 2 rotational degrees of freedom for the linear molecules because they cannot rotate around the binding axis.
- The remaining are vibrational degree of freedom: 3n-6, and 3n-5 for linear molecules.

Therefore, in theory the infrared spectrum of a molecule should show 3n-6 (3n-5 for linear molecules) absorption.

There are two types of vibrations for a polyatomic molecule:

- Stretching: variation of the bond length
- Bending: variation of the bond angle

In this regard, two types of vibrations can be distinguished in the IR spectrum:

Skeleton vibrations: they are observed in the fingerprint region 400-1500 cm^{-1} and is not easy to assign them the corresponding vibration because it is related to the entire molecule.

Group vibration: vibrations related to isolated and specific functional groups. The easiest to recognize are in the region between 4000-1500 cm^{-1}, therefore outside the fingerprint region.

3.2 Interferometer and interferogram

The most important part of the FTIR instrumentation is the interferometer, which is a device used to measure the interference pattern produced by the interaction of two electromagnetic waves. Many interferometers have been developed during the years, the Michelson interferometer, invented by Albert Abraham Michelson in the 1880s, is one of the oldest one and the probably the most diffused. Its functioning is represented in Figure .

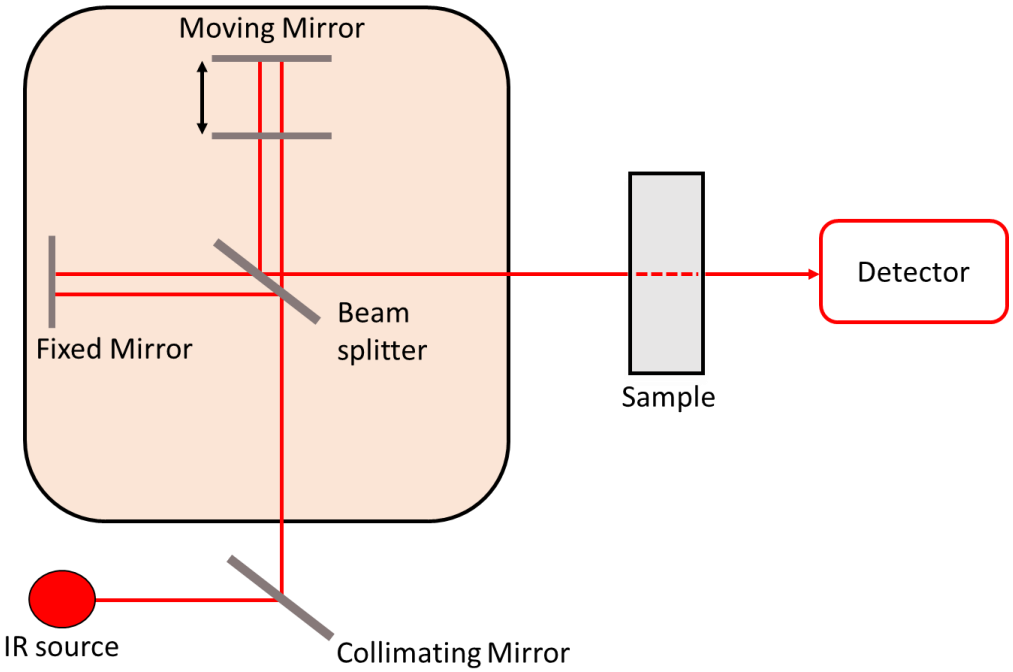

Figure 3.2 Scheme of a Michelson interferometer.

It consists of four arms: the bottom one contains the infrared source along with a collimating mirror, which reflects the incoming infrared rays making them parallel. The upper and left arm contains two mirrors: one which is in a fixed position, and the other vertically movable up and down. Finally, the last arm accommodates both the sample and then the detector. At the core of this interferometer, there lies an optical component called beam splitter.

The beamsplitter is specifically engineered to allow a portion of the incident light to pass through it while reflecting the rest of the light. In particular, the light that passes through the beamsplitter is directed towards the movable mirror, whereas the light that is reflected is directed towards the movable mirror (Figure 3.2).

After bouncing off these mirrors, the light beams return to the beamsplitter, merging back together to form a unified light beam which exits the interferometer, interacts with the sample, and ultimately reach the detector.

When superimposed, waves interact with each other, resulting in the addition of their amplitudes to form a single wave. In a Michelson interferometer, the light beams

reflected from the fixed and moving mirrors interfere according to the following relationship:

$$A_f = A_1 + A_2 \tag{3.10}$$

Where A_f is the final amplitude, A_1 and A_2 are the amplitudes of the fixed and the movable mirrors respectively. When A_f exceeds the amplitudes (A_1 and A_2), a constructive interference takes place. Conversely, if A_f is smaller, it leads to destructive interference.

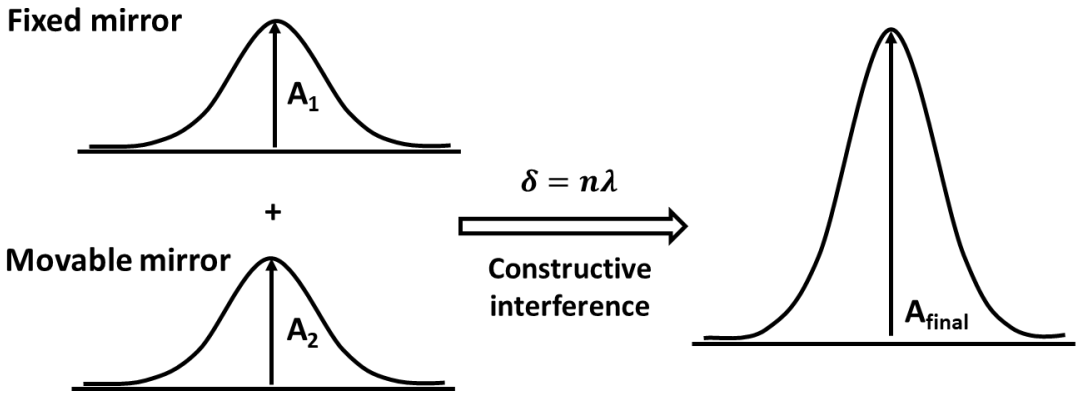

Figure 3.3 Two light beams which undergo to a constructive interference.

The principle of FTIR functioning, in particular how the infrared spectrum can be produced by the instrumentation can be explained by assuming that the light source is monochromatic and have a wavelength λ.

When the two mirrors are positioned at the same distance from the beam splitter, the light beams traverse identical distances. Therefore, when they recombine at the beam splitter, since their wave crests coincide, they interfere constructively, giving rise to a more intense beam compared to the individual ones. In this case the two beams are said to be in phase (figure 3.3).

In general, the two beams are in phase with each other when δ is multiple of their wavelength according to the following formula:

$$\delta = n\lambda \tag{3.11}$$

Where δ is the optical path difference, λ the wavelength and n any integer. The n=0 corresponds to the zero path difference (ZPD); The n = 1 value signifies that the light beams are precisely one wavelength out of phase, and the n=2 two wavelength out of phase, etc.

The mirror displacement is denoted as Δ. Therefore, at the ZPD Δ=0, but when it is not at this position, from a shift of Δ, results an optical path difference of 2Δ, because the light covers the displaced distance twice, traveling to and from the mobile mirror, according to the following equation:

$$\delta = 2\Delta \tag{3.12}$$

Moving the mobile mirror from or toward the beam splitter, the destructive interference increase and the resulting beam from the combination of the two reflected beams become weaker until at δ is equal to $\frac{1}{2}\lambda$. In this scenario, the light beam reflected off the moving mirror has travelled a distance equivalent to half a wavelength further, causing it to be 1/2 out of phase by of respect to the fixed mirror beam. This means that the peak of one beam now coincides with the trough of the other. In this case the two beams are completely out-of-phase and their amplitudes will cancel each other, giving rise to a destructive interference Figure 3. 3.4).

$$\delta = \left(n + \frac{1}{2}\right)\lambda \tag{3.13}$$

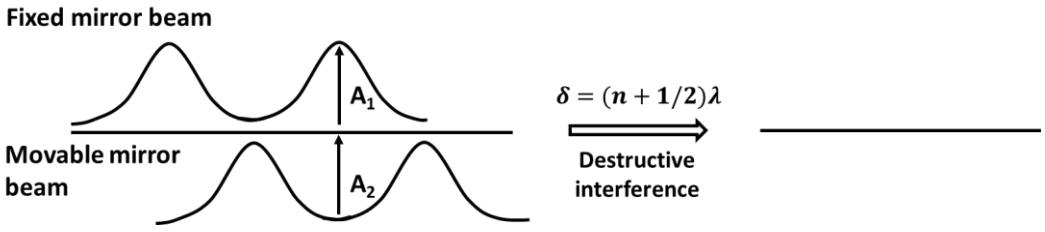

Figure 3.4 Two light beams which undergo a destructive interference.

Therefore, during the movement of the mirror, the intensity of the resulting beam which reach the detector changes. It means that at the ZPD ($\delta = 0$), being the two beams completely in phase the intensity of the beam is maximum but, moving the

movable mirror away or toward the beam splitter, the two beams start becoming out of phase until the minimum at $\delta = \frac{1}{2}\lambda$ (completely out of phase).

Keeping the mirror moving, the two beams become more in phase, and the resulting ray increases in intensity until it passes through a maximum at $\delta = \lambda$.

As the mirror continues to move, the intensity of the resulting ray becomes weaker again, passing through another minimum at $\delta = \frac{3}{2}\lambda$, and then becoming more intense again as it passes through another maximum at $\delta = 2\lambda$. The intensity of the resulting ray varies as it passes through maxima and minima, as determined by Equations 3.12 and 3.13 and shown in figure 3.5.

The measurement of the intensity transmitted by the interferometer as a function of the optical path difference between the two beams constitutes the so-called interferogram of the incident radiation. Therefore, the interferogram is the electrical signal that comes out of the detector, which must be converted into a spectrum to be read.

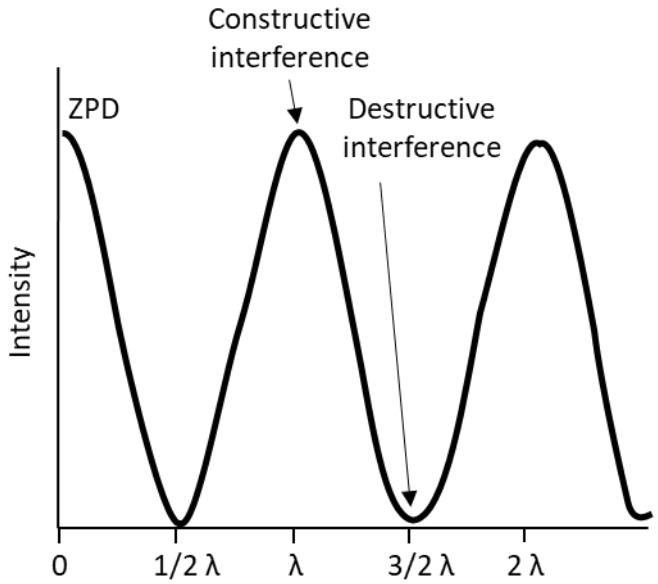

Figure 3.5 A plot of light intensity (or detector signal) versus optical path difference for a mirror moving away from the beamsplitter in a Michelson interferometer. Such a plot is called an interferogram. This is the interferogram for a single wavelength of light passing through the interferometer.

So far, the simplest case of monochromatic radiation has been described, and its graph is shown in figure 3.5. The graph is different when dealing with a polychromatic source, which is encountered in an FTIR spectrophotometer. Each individual wavelength of the incident IR radiation results in a characteristic interference profile as a function of the optical path difference (δ). The total interferogram measured by the detector is, therefore, the sum of all the interferograms produced by each individual wavelength.

To understand this, one can assume that wavelengths λ and 3λ pass through the interferometer together. Based on the previous equations, if we substitute 3λ with λ in these equations, we find that the maxima in the interferogram for 3λ occur at:

$$\delta = 3n\lambda \tag{3.14}$$

and that the minima in the interferogram for 3λ are given by:

$$\delta = 3\left(n + \frac{1}{2}\right)\lambda \tag{3.15}$$

The total interferogram is the sum of the individual interferograms generated by λ and 3λ (figure 3.6).

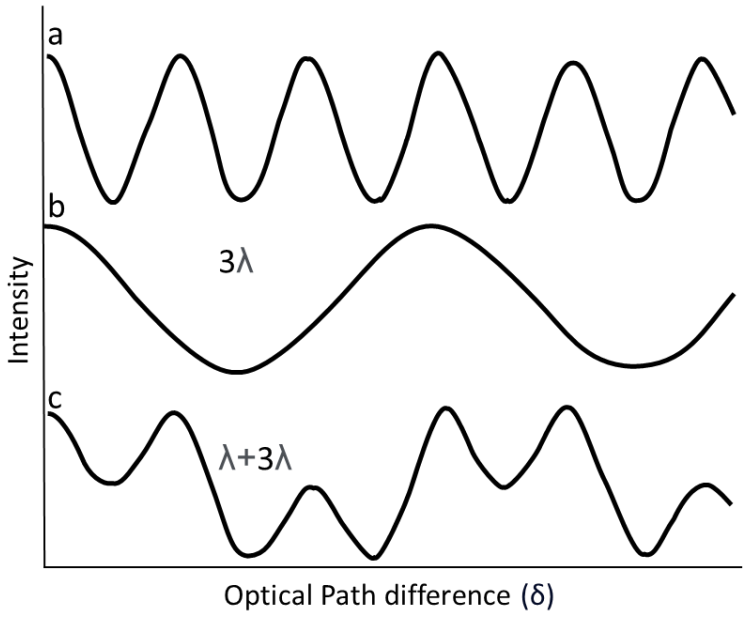

Figure 3.6 The interferograms of λ light (a), 3λ light (b), and their sum (c).

3.3 Interferogram

The interferogram is the signal measured by the detector, which exhibits a co-sinusoidal waveform, as show in figure 3.5, It exists a correlation between the frequency of a light wave and the frequency of the correspondent interferogram as follows:

$$F = \frac{(2\nu v)}{c} \tag{3.16}$$

Where F is the Fourier Frequency of the interferogram expressed in Hertz; ν is the frequency of the electromagnetic wave expressed in Hertz; v is the velocity of the moving mirror (assumed to be constant) in cm/s, and c is the speed of light expressed in cm/s.

Taking into consideration that the light speed (c) corresponds to the ratio between the frequency (ν) and the wavenumbers (W):

$$c = \frac{\nu}{W} \tag{3.17}$$

Using this equation, the previous equation (3.16) can be written as

$$F = 2\text{vW} \tag{3.18}$$

This equation states a direct relationship between the frequency of a light wave and the Fourier frequency (expressed in Hertz) of the corresponding interferogram.

Moreover, this equation demonstrates that there is a unique interferogram associated with each distinct wavenumber of light. As a result, it is not necessary to separate light with different wavenumbers in terms of time or space to distinguish them.

The infrared spectrum comprises two essential components: the intensity of light and the wavenumber. As the spectrum is derived from the interferogram, both intensity and wavenumber information are inherently embedded in the interferogram. The Fourier frequencies provide information about the wavenumbers of light contained in a given light source as described by the equation (3.18), while the intensity of a frequency is directly proportional to the amount of light detected at a specific wavenumber.

In the practical case of an interferometer, all the wavenumber emitted by the source pass through the interferometer simultaneously. Each of these wavenumbers corresponds to a unique interferogram with its own distinct Fourier frequency, and what the detector effectively records is the addition of these individual interferograms. In the case of a broad-spectrum infrared source emitting light at numerous wavenumbers, the resulting interferogram is illustrated in Figure 3.7.

There is a prominent rise in infrared intensity when the optical path difference is zero, commonly referred to as the "centerburst." This is because all wavelengths of light are in-phase and constructively interfere at this point.

The size of the centerburst corresponds to the total amount of infrared light reaching the detector.

While the optical path difference changes, the infrared intensity rapidly diminishes on both sides of the interferogram. These low-intensity regions on an interferogram are known as its "wings." The wings exhibit reduced intensity because, with the increasing optical path difference, the various Fourier frequencies progressively go out of phase with each other, leading to destructive interference.

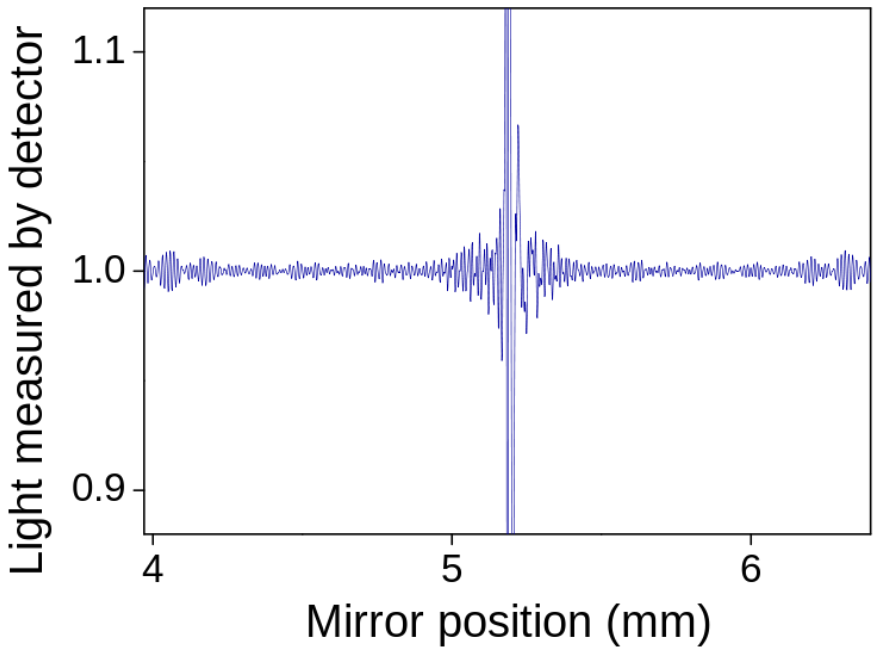

Figure 3.7 Interferogram.

3.4 IR spectrum

When the IR radiation emitted by the source passes through the interferometer, the spectrum of this radiation is optically transformed into an interferogram. The detector measures this interferogram and, through the fast Fourier transform (FFT), a mathematical operation performed by the computer, transforms it back into a spectrum. Thus, the fast Fourier transform (FFT) transforms the intensity of the incident IR radiation as a function of optical path difference (δ) into the intensity of the incident IR radiation as a function of wave number (cm^{-1}). Only in this way is the information obtained from a given sample readable.

If no sample is placed at the interferometer output, what is obtained is the background spectrum. The background spectrum includes spectral contributions from the external environment and the instrument itself. A large part of the environmental contribution is due to atmospheric gases, such as water vapour and carbon dioxide, which absorb in the IR, while the contribution of the instrument is due to the characteristics of all its elements (source, beam splitter, fixed and moving mirrors and detector) and particularly the temperature of the source. When the sample is placed at the interferometer output, the spectral contributions of the background spectrum are added to the latter. Since the objective is to obtain spectral information from the sample alone, the contributions from the external environment and the instrument must be subtracted. To do this, the instrument normalises the two spectra, the background, and the sample spectra, i.e. it relates them by subtracting the background from the sample. However, normalisation may not be sufficient for the subtraction of environmental contributions, so nitrogen is used. Nitrogen reduces water vapour and carbon dioxide concentrations. In addition, the reduction of humidity enables the preservation of moisture-sensitive optical parts of the instrument, such as the KBr windows used in beam splitters. Many currently manufactured instruments have interferometers sealed with a lid and a desiccant is placed underneath this lid to adsorb atmospheric gases.

Normally, the IR spectrum obtained from an FTIR spectrophotometer reports the sample absorptions in the mid-IR region, which ranges from 2.5 μm to 15 μm, or 4000 cm^{-1} to 666 cm^{-1}. In this region of the IR, the vibrations of the molecules' functional

groups are observed. The appearance of the bands appearing in this region can be analysed to see if there are specific functional groups within a molecule.

The IR spectrum obtained is conventionally divided into two zones: one ranging from 4000 cm^{-1} to 1500 cm^{-1} and another ranging from 1500 cm^{-1} to 666 cm^{-1}.

The former is the zone where all the stretches referring to the individual functional groups are recorded, while the second is a very complex zone because it is the zone in which, in addition to certain stretches, other complex vibrations referring to the molecule as a whole fall. This second zone is called the fingerprint. These complex vibrations cannot be defined because they are not related to individual functional groups but to the vibration of the molecule as a whole. As far as the first zone is concerned, from 4000 cm^{-1} to 2500 cm^{-1} the simple bond vibrations are observed, i.e. the vibrations of OH, NH and CH groups, so it is possible to determine the presence of amines, amides, phenols and alcohols; from 2500 cm^{-1} to 2000 cm^{-1} the vibrations of carbon-nitrogen and carbon-carbon triple bonds and allenes are observed; finally, from 2000 cm^{-1} to 1500 cm^{-1} the vibrations of the carbon-oxygen, carbon-nitrogen, carbon-carbon and nitrogen-oxygen double bonds are observed. The second zone of the mid-IR, although complex to analyse, can be exploited for identification because the absorptions in this zone are precisely characteristic of the molecules analysed (Mohamed et al., 2017).

The IR spectrum can be reported in absorbance using the following equation:

$$A = log \frac{P_0}{P} \tag{3.19}$$

Where 'A' is the absorbance, 'P_0' the intensity of the background spectrum and 'P' the intensity of the sample spectrum.

Absorbance (A) is also related to the concentration of molecules in a sample through Beer's law:

$$A = \varepsilon lc \tag{3.20}$$

Where 'ε' is the molar absorbance; 'l' the optical path length; 'c' the concentration.

The intensity of a peak in an IR spectrum calculated in absorbance is proportional to the concentration, which is why Beer's law can be used to determine the concentrations of molecules in a sample.

The IR spectrum can also be calculated in percent transmittance (%T), according to the following equation:

$$T\% = \frac{P}{P_0}\ 100 \tag{3.21}$$

Where '%T' is the percentage transmittance.

Absorbance (A) and percentage transmittance (%T) are mathematically correlated, and spectrum conversion can be easily performed using software. IR spectra are reported in absorbance or in percentage transmittance depending on the type of analysis to be performed after the spectrum is obtained. Since absorbance is directly proportional to concentration, IR spectra in absorbance are used to perform quantitative analysis; these spectra are also suitable for qualitative analysis and are used to perform library searches. However, as the peaks of the IR spectra recorded in percentage transmittance are not directly proportional to concentration, these cannot be used to perform quantitative analysis, but only for qualitative analysis.

3.5 GC-FTIR hyphenation

The high specificity of infrared spectroscopy led to the development of many different interfaces in order to achieve the hyphenation between gas chromatography and infrared spectroscopy detectors. As reported by different reviews (Ragunathan et al., 1999; Visser, 2002), infrared detection of analytes can be achieved in vapor or solid phase. Vapor phase is the easiest type because it simply consists in the passage of the eluting flow through a light pipe with IR transparent windows. However, it is characterized by a low sensitivity. On the other hand, solid phase configurations allow IR detection by means of the analyte entrapment on the surface of a rotating substrate at cryogenic temperatures. The rotation brings the analytes through the infrared beam allowing their real time detection. Two types of solid phase hyphenations were developed in which the analytes are immobilized in two different manners: Matrix isolation (MI) (Reedy et al., 1985) and solid deposition (*sd*) (Fuoco et al., 1986). While

the former consists in the entrapment of the analytes into a matrix cage of argon, in the latter the condensation on the surface takes place on an IR transparent moving window. Solid phase techniques allow the achievement of a lower detection limit compared to the one obtained by vapor phase because of its concentration on a solid spot. Moreover, the detection in the solid state allows an improved the spectral resolution up to 4 cm^{-1} (Salerno et al., 2020). Additionally, until the cryogenic temperature is maintained, the signal to noise ratio can be improved either by increasing the signal, concentrating the spot (by injecting more times the same sample) or by reducing the noise by averaging the analyte signal.

The information provided by infrared spectroscopy is mandatory for the univocal identification of a compound because it can provide fine structure details, which makes the spectrum unique and the library identification highly reliable.

3.6 HPLC-FTIR hyphenation

The issue of the coupling between HPLC and FTIR is the presence of the liquid mobile phase, whose absorption in the infrared interferes with the detection of the analytes. In fact, this has been the most important challenge in the development of such interfaces.

The simplest coupling with an FTIR detector in LC is to pass the effluent from the column through a flow cell with IR-transparent windows, so that the IR transmittance is continuously monitored. Despite its simplicity in maintenance and operation, the technique is limited by the poor sensitivity and spectral information that can be obtained, both of which are affected by the intense IR absorption of solvents, especially aqueous ones.

Since the major obstacle in using a flow cell is the presence of the solvent, couplings have been developed that can remove the solvent via an evaporative interface and then deposit the separated compounds on a moving substrate that is transparent to the IR. In this way, the IR spectra of the deposited compounds can be recorded independently of the LC conditions and the sensitivity of the FTIR detector can be fully utilised. With this interface, FTIR detection of the deposited trace can take place both in real time and 'off-line'; in fact, after LC separation is complete, the trace can be transferred to an FTIR detector that scans the deposit and the LC-FTIR chromatogram is

reconstructed by the software (Kok et al., 2003). In addition to the increase in sensitivity (below nanograms) and resolution (4 cm^{-1}), a further advantage of this technique based on trapping of analytes is the possibility, as already seen with GC-FTIR coupling, to scan the deposited analytes several times in order to obtain IR spectra with a better signal-to-noise ratio.

Several approaches based on various types of interfaces have been proposed over time to exploit the full potential of IR spectroscopy. Among these, nebulisation systems allow for greater flexibility, as they can tolerate a flow rate greater than 1 mL/min and therefore make it possible to use conventional diameter columns. These interfaces include thermospray, particle beam, electrospray, pneumatic nebuliser, and ultrasonic nebuliser (Somsen et al., 1998). Despite the ability to generate an aerosol from the flow of liquid exiting the column, none of these systems were capable of effectively separating the solvent vapour and non-condensable carrier gas from the particle stream.

Part I

Applications of high-resolution UHPLC-MS/MS

Chapter 4

Food bioactive peptides

Peptides represent an important class of biological molecules which are recognized for the wide variety of biological activities they play in the organism. Indeed, they are involved in a wide range of biological activities, such as neurotransmission, growth factors activity, hormonal functions, immunomodulation, and antimicrobial activity (Barman et al., 2023). Moreover, being a source of biologically active peptides, food proteins play a crucial role in diet, other than being one of the most important sources of essential amino acids (Toldrá et al., 2018).

Bioactive peptides are small molecules that are composed of 3-20 amino acids. According to their chain length, they can be classified in short and medium sized peptides. Whereas short sized peptides are made of up to five amino acid residues, medium sized are made of five to twenty amino acids (Lee et al., 2019). These peptides are naturally encrypted in an inactive form within a parent protein and are released through the enzymatic hydrolysis from the protein (Giromini et al., 2019), by proteolytic enzymes during gastrointestinal digestion (Escudero et al., 2012), during fermentation (Pihlanto-Leppälä, 2001) or during food processing (Arihara & Ohata, 2010).

Bioactive peptides can affect many different biological functions depending on their aminoacidic sequence and the location of the singles amino acids that form the peptide. These peptides affect many different biological functions, including antihypertensive, antioxidant, antimicrobial, opioid agonists or antagonists, immunomodulatory, antithrombotic, and anti-cancer activities (Mora et al., 2014; Toldrá et al., 2018). Many literature studies report the presence of biologically active peptides derived from food proteins. Milk-based product peptides were the first that have been studied for their health beneficial effects (Nongonierma & FitzGerald, 2016). Furthermore, meat proteins are reported to be a wealthy source of bioactive peptides (Escudero et al., 2010, Udenigwe and Howard, 2013), as well as fish proteins (Ferraro et al., 2013).

4.1 Generation of food bioactive peptides and bioavailability

As reported in figure 4.1 and anticipated in the previous paragraph, during fermentation and/or ripening food proteins are gradually hydrolysed to form small amino acid sequences. This proteolysis is operated by endogenous peptidases, and/or microbial peptidases in fermented food. Many studies indeed, report the formation of bioactive peptides consequently to food processing (Toldrá et al., 2018, 2020), for example in cured ham (Mora et al., 2015, 2016, 2020; Toldrá et al., 2020; Toldrá & Mora, 2021), dry-fermented sausages (Gallego, Mora, Escudero, et al., 2018) and cheese (Corrêa et al., 2014; Santiago-López et al., 2018).

However, the most important source of bioactive peptides is the industrial production by enzymatic hydrolysis by means of commercial peptidases or microorganisms in reactors and in controlled conditions (Toldrá et al., 2018). These methods are principally used for exploiting the food by-products for their valorization (Ryder et al., 2016).

Typical raw materials are indeed by-products from:

- Agricultural practices such as slaughterhouses, olivemill wastewater, cheese whey, winery sludge and citrus peel (Toldrá & Mora, 2021).
- Meat and fishery industry, which annually produces tons of by-products, such as trimmings, bones, skin and viscera (Ferraro et al., 2013; Lassoued et al., 2015; Mora et al., 2014; Rigano et al., 2021; Toldrá et al., 2016).

In this regard, industries are exerting substantial efforts to valorise by-products into useful sources and transform them into valuable resources and functional ingredients with a significant added-value and/or a strong economic potential. This, in order to obtain a reduction of both the disposal and raw materials supply, following the principle of circular economy.

To produce large amounts of bioactive peptides from these sources of proteins, hydrolysis is generally performed by means of commercial peptidases at industrial scale in controlled conditions (Dos Santos Aguilar & Sato, 2018). Controlled conditions mean controlled temperature, pH and quantity of enzyme added in order to

gain a fixed degree of hydrolysis (DH). The DH constitutes a good parameter for monitoring the extension of protein hydrolysis. Indeed, the functional properties of the protein hydrolysate depends on the DH and type of peptidase preparation used (Mune Mune, 2015). Although the DH is a very important control parameter, the final target is the number of bioactive peptides able to exert the desired activity.

Different types of enzymes can be employed for the hydrolysis, sortable according to their origin: microorganisms, animal, or plant sources. Typically, the former are the most used types because of the lower cost. This is the case of Alcalase from *Bacillus licheniformis*, Protamex from *Bacillus sp.*, Flavorzyme from *Aspergillus oryzae*, Neutrase from *Bacillus subtilis* or *Bacillus amyloliquefaciens*, Bioprase from *Bacillus sp.*, Thermolysin from *Bacillus stearothermophilus*, Prolidase from *L. casei*, and Corolase 7089 from *B. subtilis*.

The other enzymes, since they are obtained from animal or plant sources, they are more expensive. To this category belongs trypsin from bovine or pig pancreas and bromelain from pineapple stem (Toldrá et al., 2018). Regarding trypsin, it is an enzyme which operates a specific cleavage on the C-terminal side of lysine and arginine amino acid residues leading to the generation of medium-sized peptides (6-20 AAs) due to its specific cleavage mechanism (Capriotti, Cavaliere, et al., 2015). The choice of the enzyme is important in the biological activity of the produced peptides.

To carry out the biological activity, bioavailability of these bioactive peptide must be taken into consideration. Indeed, to exert their biologically activity and reach the target, the generated peptides must be ingested and must resist to the gastrointestinal digestion, where the action of salivary, stomachal, intestinal and pancreatic enzymes, which can lead to the partial or complete inactivation (Pepe et al., 2016). However, gastrointestinal digestion can also contribute to the generation of smaller bioactive peptides (Capriotti, Caruso, et al., 2015). Then they are absorbed intact through the intestinal barrier and reach the blood stream to exert their physiological action (Gallego et al., 2016). In this regard, the small sized peptides are more likely to be active because of their higher bioavailability related to the lower molecular weight that promotes the crossing of the biological barriers.

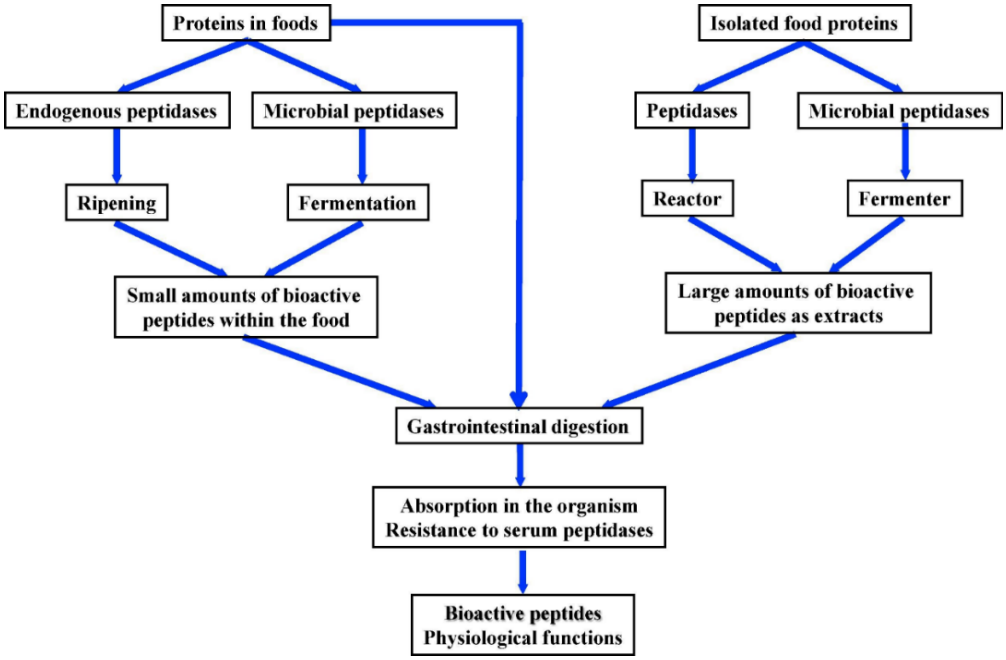

Figure 4.1 Scheme of the generation of bioactive peptides from food protein. Reproduced from Generation of bioactive peptides during food processing (Toldrá et al., 2018).

4.2 Analytical characterization of peptide

4.2.1 Peptide separation

Separation of peptides is mandatory for the improvement of peptide identification. In this regard, chromatographic techniques are the most used for this purpose. Reversed phase high performance liquid chromatography (RP-HPLC) is the most used for the analysis of this kind of molecules. In this regard, separation is based on the hydrophobicity of the peptides which is dependent on the peptide aminoacidic composition and peptide length. As mobile phase, the typical mobile phases are water as polar phase and acetonitrile as organic one, with the addition of the 0.1 % of formic or trifluoroacetic acid. Separation is normally performed in gradient mode, consisting in the gradual increase of the organic phase. In this way, peptides are separated according to their polarity, in order that the most polar elutes before and consequently the more apolar elutes later for their higher interaction with the stationary phase.

4.2.2 Peptide identification

Mass spectrometry is a necessary equipment for the identification of proteins and peptides. It is a widely used detector for a wide range of applications due to its capabilities to be coupled with chromatography techniques and for the very high sensitivity it can reach. In particular, the introduction of the soft ionization methods such as electrospray ionization (ESI) and Matrix-assisted Laser Desorption/Ionization (MALDI) has made possible their analysis.

Peptidomic approaches utilize several mass analysers: TOF, quadrupole, ion trap and, more recently due to its high resolving power, orbitrap or ion cyclotron resonance analysers (Hellinger et al., 2023).

Peptides identification is usually based on the bottom-up proteomics. It consists in an identification method based on the characterization of proteins by analysis of the peptides released from the proteolytic digestion. When it is performed on a mixture of proteins it is called shotgun proteomics (Zhang et al., 2013).

In this case, two identification strategies exist for the identification of proteins and peptides: Peptide mass fingerprinting (PMF), i.e., identification through mass spectrometry and identification by means of tandem mass spectrometry.

4.2.2.1 Peptide mass fingerprint

The peptide mass fingerprint of a protein is the sum of all the peptides generated by enzymatic digestion of a protein with a specific enzyme which have a specific cutting pattern. To this regard, trypsin has become the gold standard for protein digestion for shotgun proteomics. Trypsin is a serine protease which cleaves at the carboxyl side of arginine and lysine. This sequence-specific information has been used to filter identified peptides (Zhang et al., 2013). The identification is based on the comparison between the peptide experimental mass and the theoretical mass of the peptides contained into the protein present into the database. The absolute mass of a huge number of peptides should be equal to the theoretical mass of the peptides of the protein contained into the database. The identification is correct when the mass of a huge number of peptides is equal to the theoretical one and cover a large part of the protein sequence present in the database. (James et al., 1993; Pappin, Hojrupt, & Bleasby, 1993).

This technique is more useful when isolated proteins need to be analysed. However, when the complexity of the sample increases, the identification becomes more complex. Moreover, in the case of the peptides generated from proteolytic processes in which a mixture of enzymes is involved like in a cured or fermented food or enzymatic hydrolysis is performed by using a nonspecific enzyme, identification is challenging due to the non-specific cut of the proteolytic enzymes, and the consequent impossibility of comparison with the theoretical mass. In this case, the identification should be performed by analysis with tandem mass spectrometry (MS/MS).

4.2.2.2 Tandem mass spectrometry (MS/MS)

The types of fragment ions observed in an MS/MS spectrum depend on many factors including primary sequence, the amount of internal energy, charge state etc.

When it comes to proteomic field, in particular fragmentation of peptides obtained by protease digestion, collision induced dissociation (CID) is the most widely and traditionally used approach. In this case ions separated by the first mass analyser are subjected to the collision with an inert gas (nitrogen or argon) in a collision cell. By collision with the gas, kinetic energy is transferred to the molecule and some of it converted in internal energy. When the internal energy exceeds the energy of the weakest chemical bond, it is preferentially broken (Ma & Johnson, 2012).

In particular, fragmentation can occur in multiple sites (figure 4.2). For this reason, a specific nomenclature is used to indicate the type of fragment generated, which was proposed by (Roepstorff & Fohlman, 1984) and then modified by (Johnson et al., 1987).

Six types of fragments can be generated from a peptide skeleton (figure 4.3). Depending on which of the two extremity keeps its structure, they are classified as (a_n, b_n, c_n) for the ones which keep the N-terminal extremity, or (x_n, y_n, z_n) for the fragments which keep the C-terminal extremity. The subscript n indicates the number of aminoacidic residues that the fragment has.

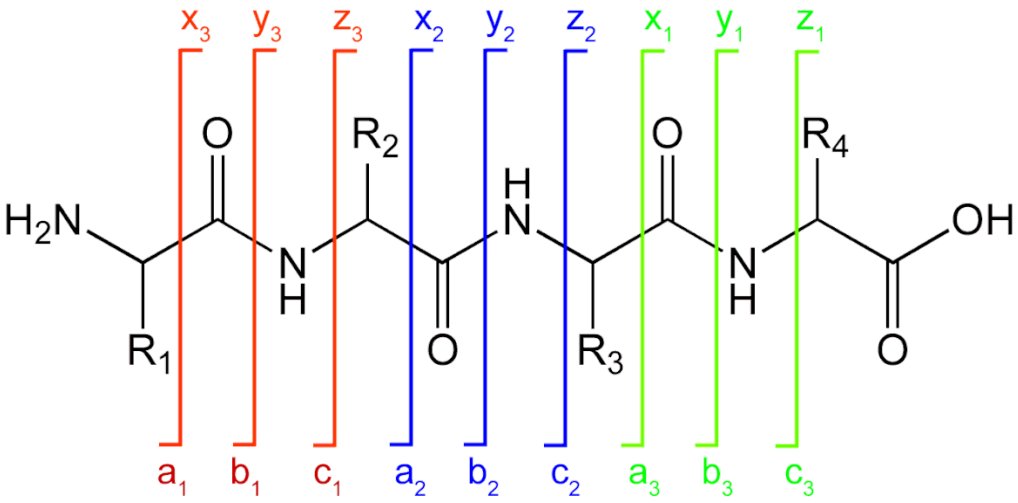

Figure 4.2 Fragmentation sites of a peptide.

However, since it is the weakest, cleavage typically occurs at the peptide amide bond, producing **b** ions, if the amino terminal fragment retains the charge, or **y** ions, if the carboxy-terminal fragment retains the charge. Moreover, cleavage doesn't occur equally along the peptide backbone, but it takes preferentially place near the glutamic acid, aspartic acid, and proline residues.

For the same reason of the preferential breakage of the weakest bond, CID may cause the fragmentation of post-translational modifications (PTMs) from aminoacidic side chains, precluding their study or by determining their loss from the amino acidic side chains (Sobott et al., 2009).

For this reason, electron-based dissociation techniques such as electron capture dissociation (ECD) and electron transfer dissociation (ETD), emerged as complementary for protein characterization. Indeed, these dissociation techniques provide alternative fragmentation patterns, with a predominant formation of c- and z-type ions (cleavage of the N-Cα bonds) with the preservation of the more labile PTMs (Zhang et al., 2013).

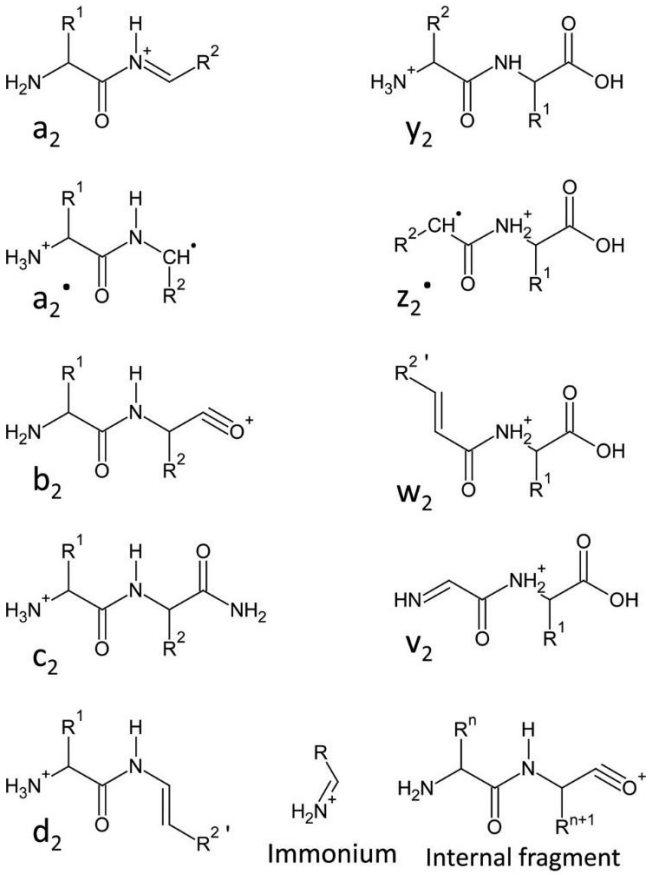

Figure 4.3 Types of ions that can be generated from the peptide fragmentation.

The MS/MS fragmentation spectra provide information about the mass difference between two consecutive ions of the same type allowing the determination of both identity and position of all amino acids and therefore to deduce the complete peptide sequence, if the fragmentation is successful. However, sometimes a double fragmentation takes place and not all fragments are generated at detectable level so that only a partial sequence can be deduced (Mann et al., 2001).

However, the information about the partial sequence and the peptide mass can be used for the database identification (Henzel et al., 1993; Mann et al., 1993).

4.2.3 Data analysis

Analysis of mass spectrometric data obtained is necessary because a huge number of mass spectra are obtained from a single analysis, and many ions are present in each of them. Therefore, information needs to be extracted for the peptide sequences

identification. Indeed, MS data are therefore elaborated to obtain a peak list, which contains data such as the *m/z* observed values of the precursor, the intensity, the number of charges for each of the detected and then fragmented ions, and their MS/MS fragmentation. As already mentioned, peptide identification of mass spectra without fragmentation is called PMF and refers to the identification of peptides generated through enzymes with cleavage specificity. However, when it comes to peptides generated by means of enzymes without cleavage specificity, peptide MS/MS fragmentation is necessary for the identification. In this regard, three strategies exist for the mass spectra interpretation.

4.2.3.1 De novo sequencing

This approach consists in the identification of the peptide sequences by manual interpretation of the MS/MS fragmentation spectra through the interpretation of the b and y masses. This identification approach is used for the identification of organism which are not sequenced and therefore are not included into protein databases. This approach is obviously the most time consuming because of the necessity of manually interpretation of all the MS/MS spectra generated from a single analysis.

4.2.3.2 Database search

In this approach, identification is performed by means of database search. In this case informatic tools are able to compare the experimental spectra with the fragmentation spectra experimentally obtained by the in-silico digestion of proteins contained into protein databases (Eng et al., 2011; James et al., 1993; Pappin, Hojrupt, & Bleasby, 1993; Yates et al., 1993).

The database search is performed after the by using specific parameters which corresponds to the experimentally used ones. For example, if the digestion is site-specific, this parameter should be selected for the database search.

As result, a list of peptides classified in function of the agreement between the experimental and the theorical spectra is provided. After the identification of the peptide sequence, each of them is assigned to an original protein, giving a score indicating the level of confidence of the assignment. Therefore, the greater the number of peptides identified for a given protein, the greater the confidence that they correspond to that protein (figure 4.4).

This is the most used identification approach, and it is performed on bioinformatic tools, such as MASCOT and SEQUEST, which are the most used commercial ones. Whereas other tools, such as MaxQuant (Cox & Mann, 2008) X!Tandem, OMSSA and ProbID are freely available. The software uses principally NCBInr and Uniprot as protein databases (Eng et al., 1994; Perkins et al., 1999). This is the most used technique for the identification of medium-sized peptides.

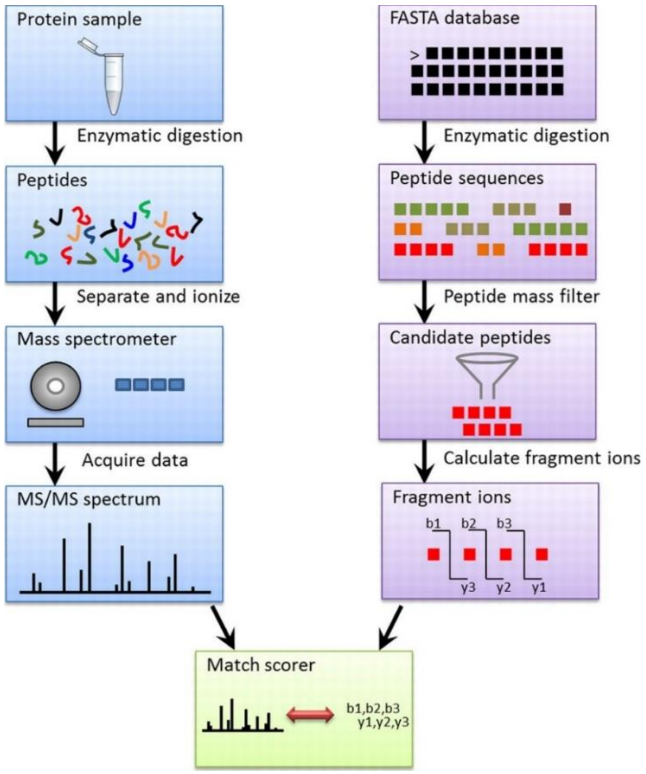

Figure 4.4 Protein identification mechanism by means of database search of MS/MS spectra. The MS/MS spectra are compared with the theoretical ones in-silico obtained by database protein fragmentation. (Eng et al., 2011).

Chapter 5

Circular economy in the food chain: retrieval and characterization of antimicrobial peptides from fish waste hydrolysates

5.1 Introduction

The increasing awareness of the negative effects of industrial growth on the environment is strongly pushing the transition from the conventional linear economy model to a more sustainable strategy, known as the circular economy (European Commission & Directorate-General for Environment, 2020). Within the food chain, the circular economy model places an emphasis on the valorisation of discards through their reuse, in order to minimize the waste disposal and the raw material consumption (Martínez-Vázquez et al., 2021; Morseletto, 2020). Indeed, the classic manufacturing-use-disposal approaches have proven to be ineffective and unsustainable over time, motivating the emergence of an alternative model (Di Vaio et al., 2023; Esposito et al., 2018). Fish and seafood take up a growing share of food consumption, due to awareness of their higher food conversion rates relative to other animal protein sources. In this concern, circular economy seeks new perspectives to redesign and innovate fish production and consumption, to enhance resource efficiency and contribute to inclusive and sustainable development (Fadeeva & Van Berkel, 2023). The blue economy model extends the circular economy principles of sustainability and reuse to activities impacting the world aquatic ecosystems. The purpose is to apply all necessary strategies for protecting the aquatic environment (including seas and coastline, oceans, rivers and lakes) (Vierros & De Fontaubert, 2017). It is reported from the last FAO state of world fisheries and aquaculture 2022 (FAO, 2022) that in the last 70 years, the total annual fisheries and aquaculture production (excluding

algae) has significantly expanded, going from 19 million (1950) to 178 million tonnes (2020). Consequently, an increase of the amount of waste production is reported. Tuna is one of the most popular and commercially valuable fish. Tuna cannery industry produces a number of discards as much as 70% of the original material, which are composed of dark muscle, gills, head, tail, skin, bone and viscera (Cutajar et al., 2022). From this material, only low economic value products are obtained, such as fishmeal, fertilizer, pet food and fish silage (Coppola et al., 2021). Yet this waste material contains high value generating molecules, such as polyunsaturated fatty acids (PUFAs), amino acids (AAs), enzymes, peptides, minerals and vitamins with many possible uses for production of value-added products (Donnarumma et al., 2021; Rigano et al., 2021). Specifically, fish-derived peptides are reported to have a wide variety of biological activities, including antimicrobial (Valero et al., 2020), antihypertensive (Yathisha et al., 2019), antidiabetic (Wan et al., 2023), anticancer (Yaghoubzadeh et al., 2020), immunomodulatory (Cai et al., 2022) and antioxidant properties (Capriotti, Cavaliere, et al., 2015). Among them, the antimicrobial activity is receiving specific attention, in the pursuit of new therapeutic agents against resistant microbes known as "superbugs" (Neubauer et al., 2017). To this regard, peptides represent possible alternative to conventional antimicrobial agents, because of the ability to inhibit resistant microorganisms. Different reports have evidenced that peptide activity is associated to a low risk of developing antimicrobial resistance (Mahlapuu et al., 2020; Thakur et al., 2022). Most studies have focused on bioactive peptides obtained from fish protein hydrolysates (FPH), which are the most studied type, and to a lesser extent to endogenous peptides (Cerrato, Aita, Cavaliere, et al., 2021). Antimicrobial peptides (AMPs) belong to the innate immunity of the host, and they represent the first line of defence against pathogens (Talapko et al., 2022). Endogenous peptides are naturally encrypted within inactive proteins and are released in their active form as a consequence of enzymatic hydrolysis (Giromini et al., 2019; Valero et al., 2020). Once activated, peptides elicit their effect by provoking cell membrane lysis, DNA and RNA synthesis inhibition or by interacting with key proteins or intracellular targets (Erdem Büyükkiraz & Kesmen, 2022). As a result, peptides are active against different types of microorganisms, including gram-positive and gram-negative bacteria, fungi and viruses (Bahar & Ren, 2013). Due to their wide

range of molecular targets, AMP physicochemical properties are highly variable. With particular regard to the interaction with membrane, positive charge and polarity are crucial physicochemical parameters (Pirtskhalava et al., 2021). The peculiar characteristics of AMPs make possible their application as pharmaceutical products, food additives in the food industry, feed additives for animal husbandry and aquaculture and in agriculture for plant protection (Erdem Büyükkiraz & Kesmen, 2022). Given the above, the aim of this work was the analytical characterization of the tuna waste protein hydrolysate in order to identify their peptides. Afterwards, to pave the way to the valorisation of these discards, peptide antimicrobial activity was predicted by using support vector-machine (SVM) learning prediction software. Peptide identification in protein hydrolysate is usually based on bottom-up proteomic procedure (Cerrato, Capriotti, et al., 2020), which is one of the most employed analytical strategies for protein identification when used with data-dependent acquisition (DDA) (Dupree et al., 2020). However, the high complexity of FPH generally poses a big challenge for peptide identification. The most employed analytical strategy is based on the use of ultra-high performance liquid chromatography coupled to high resolution tandem mass spectrometry (UHPLC-MS/MS). To this regard, separation by means of a single LC column is hardly ever enough for the large number of coelutions which may occur. Indeed, to enhance the separation power, the serial connection of three reversed phase (RP) HPLC columns resulted successful in increasing separation efficiency in terms of plate number, as well as peak capacity (Donato et al., 2009). Later on, four columns were connected in series and employed as the first dimension in RPLC × RPLC separation (Donato, Cacciola, Sommella, et al., 2011; Mondello et al., 2010). The different approaches exploited for comprehensive LC analysis of peptides and proteins have been reviewed, thoroughly (Donato, Cacciola, Mondello, et al., 2011). This research focused on the development of an efficient RP-UHPLC method for the separation and identification of FPH peptides, aiming to retrieving bioactive molecules from tuna fishery wastes. In silico evaluation of the identified AA sequences was afterwards performed to get useful information about the structure-related antimicrobial properties.

5.2 Materials and methods

5.2.1 Chemicals

All solvents, reagents and standard materials used in this research were purchased from Merck Life Science (Darmstadt, Germany). Water, acetonitrile (AcN) and formic acid (FA), all LC-MS grade, were used for UHPLC-MS/MS analyses of peptides. Distilled water, reagent-grade sodium hydroxide (NaOH), hydrochloric acid (HCl), ammonium formate (HCOONH4), trifluoroacetic acid (TFA) and trypsin from bovine pancreas (T4799) were used for protein extraction and digestion. A HPLC peptide standard mixture (Product No. H-2016) was used for UHPLCMS/ MS method optimization, consisting of GLY-TYR, VAL-TYR-VAL, methionine enkephalin acetate, leucine enkephalin, angiotensin II acetate.

5.2.2 Sample and sample preparation

Waste parts of yellowfin tuna (*Thunnus albacares*) were obtained from fresh samples purchased at a local fish market in Messina, Italy. For protein extraction, 20 g of tuna waste was homogenized in 9 volumes (180 mL) of ice-cold distilled water. The proteins in the suspension were solubilized under alkaline conditions, by adding 1 N NaOH to reach a pH value of 9.5. The suspension obtained was centrifuged for 25 min at 8000 g, and the supernatants were separated from the deposits. For enzymatic digestion, 100 mg of each protein fraction was pooled and dissolved in 10 mL of 0.01 M $HCOONH_4$ in water. Then, 1 N NaOH was added to reach a pH value of 8.0, and the solution was heated in a boiling water bath for 6 min. After cooling, trypsin was added to the solution in a substrate: enzyme ratio of 50:1, and the mixture was allowed to react at 37 °C for 4 h. The reaction was quenched by adding 0.1% TFA to a pH value of 2.0. The digest was filtered through a 0.45-μm nylon membrane (Whatman). Ten percent (*v/v*) of AcN containing 0.1% FA was added to each sample before injection for UHPLCMS/MS analysis.

5.2.3 Equipment and analytical conditions

Instrumentation for the UHPLC analyses consisted of Acquity Column Manager (CM), Acquity UPLC Class Binary Solvent Manager (BSM), Sample Manager (FTN);

the system was hyphenated to a Synapt G2-*Si* Q-ToF mass spectrometer via an ESI interface (Waters Corporation, Milford, MA, USA). Separations were performed on one or two (serially coupled) Ascentis Express Peptide ES-C18 columns, 150 × 2.1 mm, 2.7 μm d.p. (Merck Life Science, Darmstadt, Germany). A stainless-steel tube (5 cm L and 0.07 mm I.D.) was used as the column connector. The mobile phases were as follows: 0.1% FA in water (A) and 0.1% FA in AcN (B). The gradient was from 0 to 50% B in 15 min for the one-column set and 0 to 50% B in 30 min for the two-column set. The flow rate was 0.3 mL/min, the column oven was set at 35 °C, and the injection volumes were 2 μL and 4 μL for the one- and two-column configurations, respectively. The MS instrument was operated as follows: source polarity (ESI), positive; analyser mode, resolution; source temperature, 90 °C; desolvation temperature, 250 °C; desolvation gas (N2) flow, 650 L/h; nebulizer gas flow, 6.5 bar, sampling cone voltage, 40 V; capillary voltage, 2.5 kV. The MS method consisted of two concurrent cycle experiments: experiment 1 was a survey scan, followed by fast DDA scans (experiment 2). The survey scans were acquired at a resolution of 20 k in a scan range of 100–1800 Da, with a survey switching threshold of 10,000 at a scan time of 0.2 s (continuum data format). The DDA scans were acquired in the MS/MS range 50–1800 Da, with a scan time of 0.2 s, under the following conditions: maximum number of ions selected for MS/MS from a single MS Survey scan, 5; stop MS/MS criteria: accumulated TIC threshold 10e5; dynamic peak exclusion: 30 s; collision energy (Trap CE): *m/z* dependent ramp applied for low (100 *m/z*, 15–25 V) and high mass (1800 *m/z*, 55–65 V). No criteria other than intensity were applied for peak selection. The Q-ToF spectrometer was calibrated daily by infusing a sodium formate 2-propanol/water solution. A Leucine enkephalin solution (*m/z* 556.2771, positive ionization mode) was used as LockSpray reference compound, for internal lock-mass correction. MassLynx ver. 4.1 software (Waters Corporation, Milford, USA) was employed for data acquisition and processing.

5.2.4 Identification of FPH peptides

ProteinLynx Global SERVER (PLGS) ver. 3.0.3 software (Waters Corporation, Milford, USA) was used to create MS/MS datasets containing information on precursor ions, derived fragments, charge status and intensity. The MS/MS datasets as

.pkl files were subjected to MASCOT MS/MS ion search (ver. 2.3.02), selecting the SwissProt database and restricting the search to the *Thunnini* taxonomy. Parameters for the database search were as follows: enzyme, trypsin; maximum missed cleavages, 2; variable modifications, oxidation (M) and deamidation (N, Q). A precursor mass tolerance of 20 ppm and a fragment mass tolerance of 0.6 Da were selected. Significance threshold was set at 0.05, and ion score cut-off was 25. Results were validated trough MS/MS spectra manual checking, with particular reference to "*b*" and "*y*" (N-terminal and C-terminal, respectively) fragment ions, commonly obtained by the CID technique.

5.2.5 Evaluation of the physicochemical properties and antimicrobial activity

Among the physicochemical properties, hydrophobicity and isoelectric point were calculated. The former was computed as grand average of hydropathicity (GRAVY) which calculates the sum of the hydropathy values of all the AAs divided by the sequence length (Kyte & Doolittle, 1982). Peptide sequences were investigated by iAMPpred (Meher et al., 2017) for antimicrobial activity prediction.

5.3 Results and discussion

Fish protein hydrolysate (FPH) is reported to have different properties, which make it applicable in many fields (Halim et al., 2016). In this study, a tryptic digest of tuna waste was characterized by bottom-up UHPLC-MS/MS approach, followed by bio-informatic tools able to predict the antimicrobial activity.

5.3.1 Chromatographic separation and peptide identification

Separation of tuna waste protein hydrolysate was obtained by RP-UHPLC. As expected, the use of one column for peptide separation resulted in a huge number of coelutions. Being the theoretical plate number proportional to the column length, the separation efficiency was roughly doubled by serially connecting two identical columns. The gradient was proportionally expanded to keep the same retention factors, and the injection volume was doubled. Plate number (N) and peak capacity (n_c) values (table 5.1) were determined on the single and double-column setup, by analysis of a peptide standard mixture consisting of compounds of increasing hydrophobicity. As

expected, *N* was roughly almost doubled in the two columns set and was measured taking angiotensin II acetate as reference peptide. The peak capacity (*nc*) increased from 168 to 232 and was calculated from the average peak widths of the five standard peptides spanning the whole elution gradient (GLY-TYR, VAL-TYR-VAL, methionine enkephalin acetate, leucine enkephalin, angiotensin II acetate). Figure 5.1 shows the comparison between the chromatographic profiles obtained by the two analytical setups, from which is evident that a large number of coelutions were resolved by doubling the stationary phase length.

Table 5.1 Chromatographic and performance parameters obtained on the one- and two-column setups (Ascentis Express Peptide ES-C18, 150 × 4.6 mm L × I.D., 2.7 µm d.p.).

	Column	
	1 × 15 cm	**2 × 15 cm**
ΔP (bar)	243	478
Run Time (min)	15	30
N	≈ 26475	≈ 52640
$w_{average}$ (min)	0.18	0.13
***n_c**	168	232
Identified AA sequences	73	194

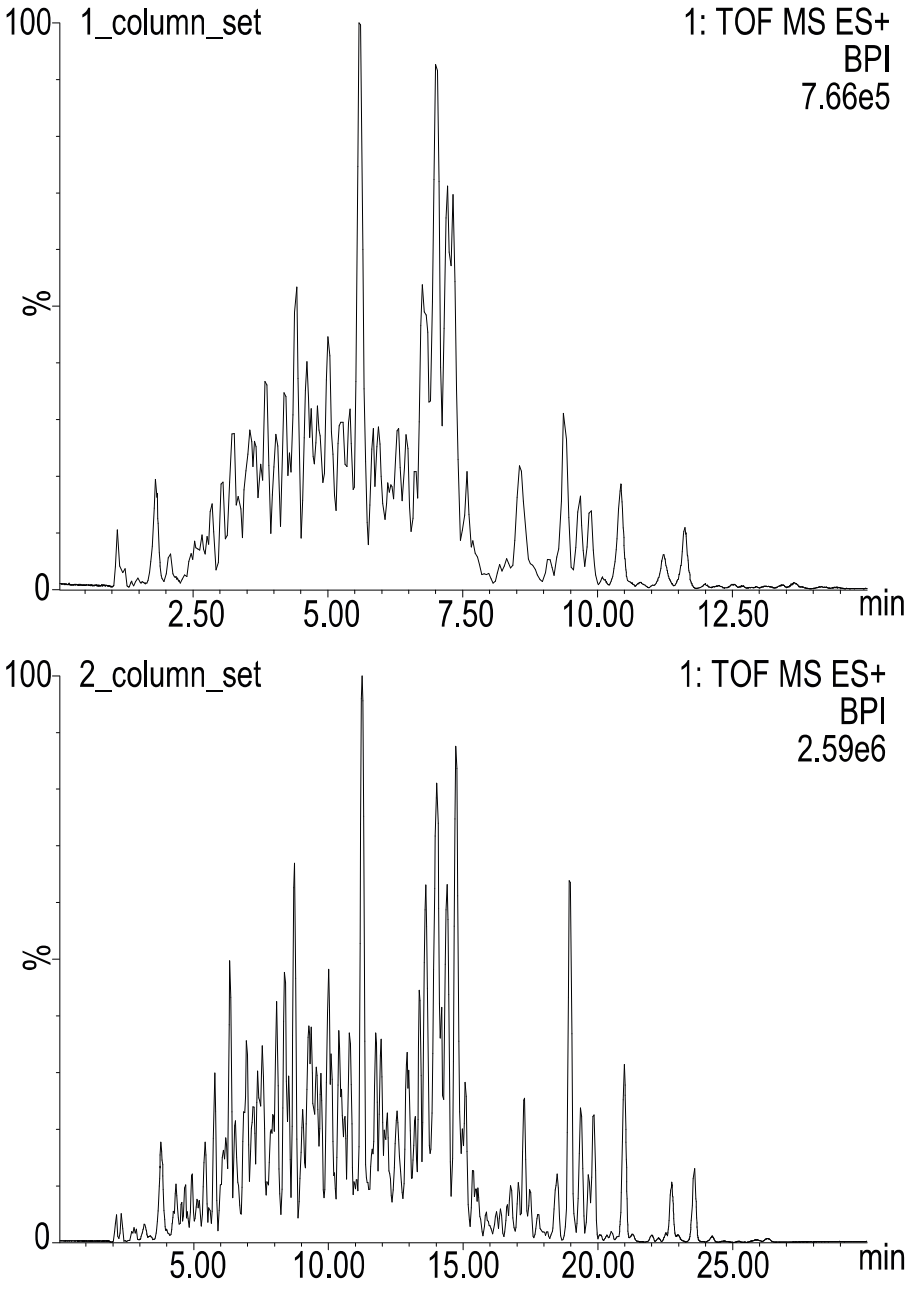

Figure 5.1 RP-UHPLC-ESI QToF MS fingerprint of the tryptic tuna waste hydrolysate (base peak intensities). Separation on one or two Ascentis Express Peptide ES-C18 column at 35 °C, 150 mm L × 2.1 mm I.D., 2.7 μm d.p.. Mobile phases: 0.1% FA in water (A) and 0.1% FA in AcN (B), 0 to 50% B in 15 min or 30 min, at 0.3 mL/min. Injection volume: 2 μL or 4 μL.

Identification of the protein hydrolysate was performed by using an established peptidomic approach, based on bottom-up proteomics. The issue of this approach is the lack of genomic information for non-model organisms as *Thunnus albacares*. Therefore, identification was based on the similarity to proteins reported for close organisms (Cerrato, Capriotti, et al., 2020; Piovesana et al., 2016). In this study, database search was performed restricting the search to the taxonomy of *thunnini*, allowing the identification of peptides belonging to 21 different proteins. The use of a double-column setup allowed the identification of more than twofold the number of peptides, in detail 194 AA sequences against 73 identified on a single column (table 5.1). The higher peak capacity allowed to obtain cleaner mass spectra, free from contaminations from less abundant ions; this is shown in figure 5.2, for the triple-charged peptide eluted at 9.37 and 18.94 min on the one-column and two-column set, respectively. Accordingly, a higher number of precursor ions were selected and subjected to fragmentation, in the DDA approach. As a result, a higher number of MS/MS spectra could be obtained, leading to a higher number of identified AA sequences.

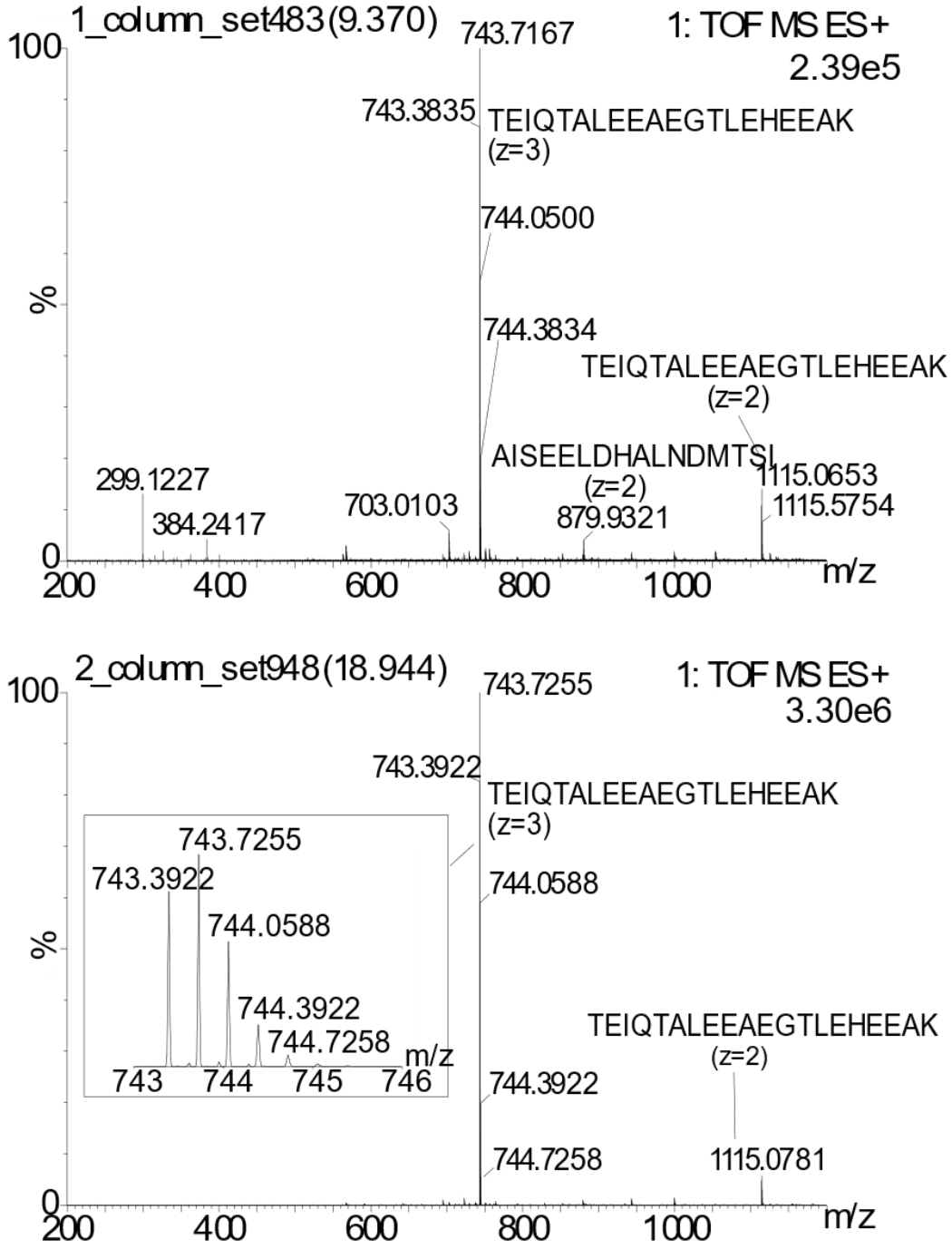

Figure 5.2 QToF MS (ESI+) spectrum at r_T 9.37 min (one-column set) and at r_T 18.94 min (two-column set) of the tuna FPH chromatographic separation in figure 5.1.

5.3.2 Evaluation of the antimicrobial activity

The exaggerated use of antibiotics is leading to the increase of resistance mechanisms to the common drugs, so that future infections might no longer be treated with common antibiotics (Xie et al., 2017). For this reason, novel antimicrobial agents need to be discovered, and peptides represent a valid alternative to the common ones. Antimicrobial peptides can be classified according to the target microorganisms (Talapko et al., 2022), and computational approaches were recently developed for antimicrobial activity screening of peptides. Indeed, this strategy is more advantageous compared to biochemical assays, because it is less time and cost expensive, whenever the number of compounds to be tested is high (Bose et al., 2022). In this study, the antibacterial, antifungal and antiviral activities of the identified AA sequences were evaluated using an in-silico approach to predict antimicrobial activity based on a SVM learning model (Meher et al., 2017). Three different features were taken into consideration: peptide composition (AA sequences), peptide structure (α-helix, β-sheet and turn structure propensity) and peptide physicochemical properties (isoelectric point, hydrophobicity, and net-charge). Regarding the physicochemical features, hydrophobicity, which is relevant for the interaction and disruption of bacteria cellular wall (Erdem Büyükkiraz & Kesmen, 2022), was evaluated as grand average of hydropathy (GRAVY). GRAVY is the sum of the hydrophobicity values of the AA constituents, assigned in the Kyte and Doolittle's hydropathy scale, divided for the number of AAs (Kyte & Doolittle, 1982). According to this scale, all AAs possess hydrophobicity values comprised between − 4.5 (arginine, the most hydrophilic AA) and + 4.5 (isoleucine, the most hydrophobic AA). As a result, 83% of these peptides had a negative GRAVY value, being predominantly hydrophilic. However, 49% of the peptides had a GRAVY value comprised between − 1 and 0, thus intermediate polarity. Polarity is one of the most important features involved in the interaction with the bacterial wall, allowing to approach lipid and phospholipid components (Erdem Büyükkiraz & Kesmen, 2022). GRAVY distribution of the identified AA sequences is displayed in Figure 5.3. These results were in accordance with the ones reported in literature found from the medium-sized peptides obtained by simulated gastrointestinal digestion of tuna muscle (Cerrato, Capriotti, et al., 2020). The majority (62%) of peptides identified in this work consisted of a number of AAs comprised between 6

and 13. Isoelectric point of the identified sequences was also calculated, and the results are shown in figure 5.4. It was found that 89% of the sequences have an isoelectric point lower than 7, meaning that they are negatively charged at physiological pH. Although AMPs are known to be preferentially positively charged, which is necessary for the interaction with negatively charged bacteria wall (Talapko et al., 2022), there are literature studies (Huan et al., 2020) reporting that also negatively charged AMPs are antimicrobial. On the basis of these physicochemical characteristics, a prediction of the potential antimicrobial activity was also carried out with specific online available bioinformatic tools, i.e. iAMPpred. From this evaluation, 44 out of 194 sequences (23%) scored above 0.5 and were potentially antimicrobial. Among them, 24 sequences were predicted to have antibacterial properties, 27 antiviral and 9 antifungal properties. Moreover, for some peptides multiple activities were predicted: seven sequences had both antibacterial and antifungal potential activity, five sequences had antiviral and antifungal activity, seven sequences had antibacterial and antiviral activity, and three sequences were predicted scored positively for a combination of antibacterial, antiviral and antifungal properties. The results of antimicrobial prediction for the tuna peptides are reported in table 5.2.

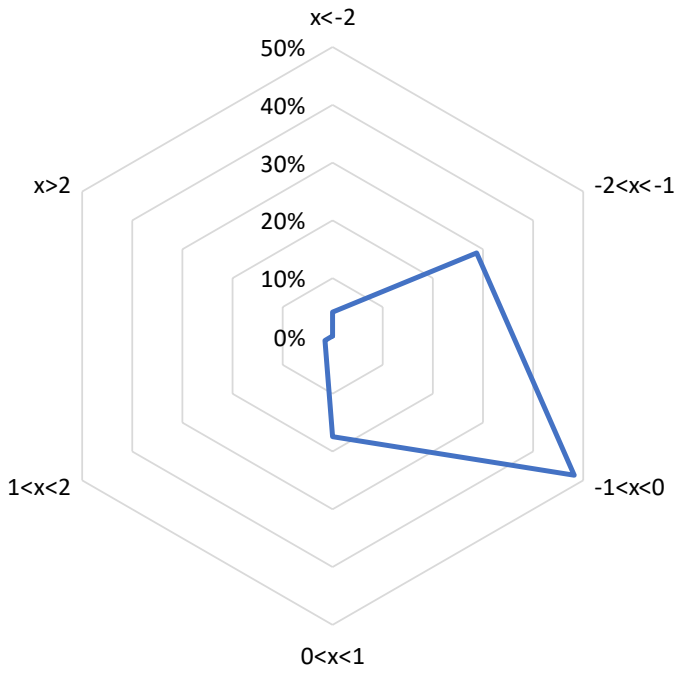

Figure 5.3 Distribution of the grand average of hydropathy (GRAVY) values for the identified peptides.

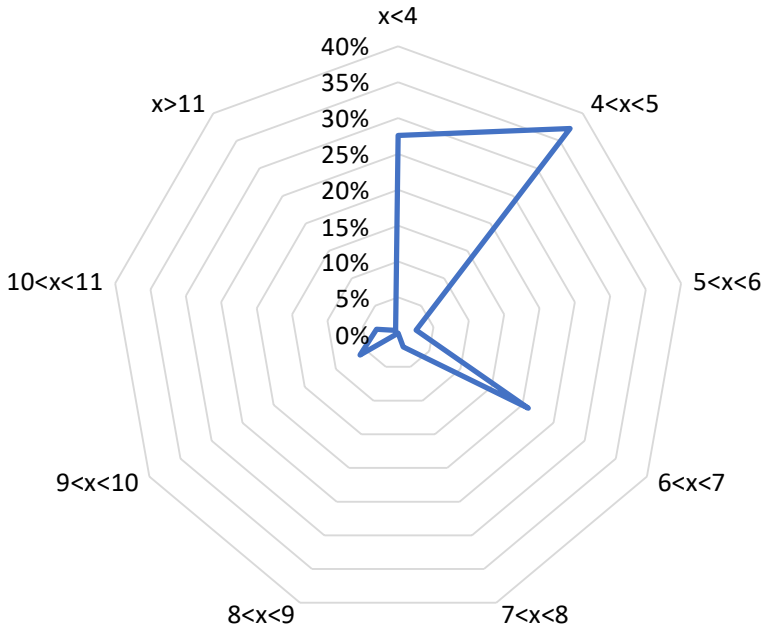

Figure 5.4 Distribution of the isoelectric point calculated for the identified peptides.

5.4 Conclusions

In this work, a UHPLC-MS/MS method was developed for the characterization of protein hydrolysates derived from industrial yellowfin tuna (*Thunnus albacares*) wastes. A total of 194 unique AA sequences were obtained in a protein sequence database search, by carrying out peptide identification by homology in the *Thunnini* taxonomy, as it is the most convenient and less time-consuming approach. Among the numerous biological activities of FPH, short length AMPs have been shown to have enhanced antimicrobial activities, higher stability and lower toxicity for human cells. Hereby, in silico predicting models allowed to make a quick screening of the identified sequences, reducing the amount of the more expensive and time-consuming biological assays. As a result, 44 AA sequences were predicted as antimicrobial, with potential antiviral, antifungal or antibacterial activity, or a combination of more than one. More studies should be carried out to confirm the potentiality of these short AA sequences as possible therapeutics, as alternative to common antimicrobial medicines to which infectious agents are developing resistance. Furthermore, antimicrobial properties of the retrieved peptides could be exploited in the formulation of nutraceuticals and, more

generally, in the industry food for product preservation. To this concern, a possible reuse of FPH as source of AMPs within the blue economy model would further benefit from easier manufacturing and cheaper production of short length peptides, compared to the long-chain ones.

Table 5.2 The AA sequences identified with MASCOT MS/MS ion search. For each sequence identified, the correlated protein description is reported, together with the protein score, protein mass, and number of peptide sequences found to belong to the same protein (protein match). Peptide information: experimental *m/z*, calculated *m/z*, experimental *z*, mass error in ppm (average error: 1.93 ppm), calculated relative mass, number of missed cleavages (miss. cleav.), aminoacid residues before and after the sequence.

Protein description	**Prot. score**	**Prot. mass**	**Prot. match.**	**Pep. exp. *m/z***	**Pep. calc. *m/z***	**Pep. exp. *z***	**Pep. delta (ppm)**	**Pep calc. mr**	**Miss. Cleav.**	**AA res. before**	**AA sequence**	**AA res. after**	**AMP results**		
													Antibacterial	**Antiviral**	**Antifungal**
Myosin heavy chain-1 OS=Thunnus orientalis OX=8238 GN=myh-1 PE=2 SV=1	24556	222036	182	560.3040	560.3039	1	0.18	559.2966	0	K	GNLEK	M	0.158	0.091	0.129
Myosin heavy chain-1 OS=Thunnus orientalis OX=8238 GN=myh-1 PE=2 SV=1	24556	222036	182	561.2991	561.2991	1	0.00	560.2918	0	R	ADLSR	E	0.038	0.118	0.103
Myosin heavy chain-1 OS=Thunnus orientalis OX=8238 GN=myh-1 PE=2 SV=1	24556	222036	182	588.3102	588.3100	1	0.34	587.3027	0	R	NDALR	I	0.147	0.211	0.324
Myosin heavy chain-1 OS=Thunnus orientalis	24556	222036	182	646.3400	646.3406	1	-0.93	645.3333	0	R	QIEEK	D	0.474	0.668	0.375

OX=8238 GN=myh-1 PE=2 SV=1															
Myosin heavy chain-1 OS=Thunnus orientalis OX=8238 GN=myh-1 PE=2 SV=1	24556	222036	182	332.1595	332.1602	2	-1.96	662.3057	0	R	MDLER	A	0.598	0.401	0.364
Myosin heavy chain-1 OS=Thunnus orientalis OX=8238 GN=myh-1 PE=2 SV=1	24556	222036	182	716.3018	716.3032	1	-1.95	715.2959	0	R	GHEDMK	E	0.685	0.449	0.381
Myosin heavy chain-1 OS=Thunnus orientalis OX=8238 GN=myh-1 PE=2 SV=1	24556	222036	182	365.7142	365.7140	2	0.68	729.4133	1	R	RGADAIK	G	0.721	0.151	0.393
Myosin heavy chain-1 OS=Thunnus orientalis OX=8238 GN=myh-1 PE=2 SV=1	24556	222036	182	366.2075	366.2080	2	-1.37	730.4014	0	K	VLADWK	Q	0.620	0.849	0.214
Myosin heavy chain-1 OS=Thunnus orientalis OX=8238 GN=myh-1 PE=2 SV=1	24556	222036	182	742.3706	742.3730	1	-3.23	741.3657	0	K	HVETEK	T	0.414	0.209	0.158

Myosin heavy chain-1 OS=Thunnus orientalis OX=8238 GN=myh-1 PE=2 SV=1	24556	222036	182	786.4458	786.4468	1	-1.27	785.4395	0	R	NVQGQLK	D	0.482	0.260	0.203
Myosin heavy chain-1 OS=Thunnus orientalis OX=8238 GN=myh-1 PE=2 SV=1	24556	222036	182	788.4504	788.4513	1	-1.14	787.4440	0	K	NLEVSVK	D	0.237	0.599	0.072
Myosin heavy chain-1 OS=Thunnus orientalis OX=8238 GN=myh-1 PE=2 SV=1	24556	222036	182	802.4556	802.4669	1	-14.08	801.4596	1	R	KLEGDLK	L	0.583	0.163	0.192
Myosin heavy chain-1 OS=Thunnus orientalis OX=8238 GN=myh-1 PE=2 SV=1	24556	222036	182	830.4601	830.4618	1	-2.05	829.4545	0	R	LQDLVDK	L	0.631	0.389	0.305
Myosin heavy chain-1 OS=Thunnus orientalis OX=8238 GN=myh-1 PE=2 SV=1	24556	222036	182	855.4566	855.4571	1	-0.58	854.4498	0	K	SIHELEK	A	0.295	0.113	0.195
Myosin heavy chain-1 OS=Thunnus orientalis OX=8238	24556	222036	182	897.4681	897.4676	1	0.56	896.4603	0	R	HIEEEIK	A	0.537	0.280	0.355

GN=myh-1 PE=2 SV=1															
Myosin heavy chain-1 OS=Thunnus orientalis OX=8238 GN=myh-1 PE=2 SV=1	24556	222036	182	459.2374	459.2380	2	-1.31	916.4614	0	R	AALEQTER	G	0.076	0.306	0.062
Myosin heavy chain-1 OS=Thunnus orientalis OX=8238 GN=myh-1 PE=2 SV=1	24556	222036	182	462.7556	462.7555	2	0.22	923.4964	0	R	SLSTELFK	M	0.250	0.100	0.167
Myosin heavy chain-1 OS=Thunnus orientalis OX=8238 GN=myh-1 PE=2 SV=1	24556	222036	182	961.4772	961.4771	1	0.10	960.4698	0	K	EQVAMVER	R	0.364	0.129	0.221
Myosin heavy chain-1 OS=Thunnus orientalis OX=8238 GN=myh-1 PE=2 SV=1	24556	222036	182	498.2433	498.2433	2	0.00	994.4720	0	K	YETDAIQR	T	0.047	0.245	0.149
Myosin heavy chain-1 OS=Thunnus orientalis OX=8238 GN=myh-1 PE=2 SV=1	24556	222036	182	501.7811	501.7826	2	-2.99	1001.5506	0	K	DALVSQLTR	G	0.005	0.035	0.015

Myosin heavy chain-1 OS=Thunnus orientalis OX=8238 GN=myh-1 PE=2 SV=1	24556	222036	182	502.7492	502.7484	2	1.59	1003.4822	0	R	ELEEISER	L	0.368	0.300	0.310
Myosin heavy chain-1 OS=Thunnus orientalis OX=8238 GN=myh-1 PE=2 SV=1	24556	222036	182	508.7719	508.7722	2	-0.59	1015.5298	0	R	ANSLAANLDK	K	0.463	0.578	0.791
Myosin heavy chain-1 OS=Thunnus orientalis OX=8238 GN=myh-1 PE=2 SV=1	24556	222036	182	529.7658	529.7649	2	1.70	1057.5152	0	R	QLNDLNGQR (NQ)	A	0.322	0.285	0.304
Myosin heavy chain-1 OS=Thunnus orientalis OX=8238 GN=myh-1 PE=2 SV=1	24556	222036	182	531.2544	531.2542	2	0.47	1060.4937	0	K	ANSEVAQWR (NQ)	T	0.204	0.183	0.047
Myosin heavy chain-1 OS=Thunnus orientalis OX=8238 GN=myh-1 PE=2 SV=1	24556	222036	182	1074.5435	1074.5426	1	0.84	1073.5353	0	R	ADIAESQVNK	L	0.057	0.876	0.054
Myosin heavy chain-1 OS=Thunnus orientalis OX=8238	24556	222036	182	1084.6372	1084.6361	1	1.01	1083.6288	0	R	VQLELNQIK	S	0.120	0.576	0.082

GN=myh-1 PE=2 SV=1															
Myosin heavy chain-1 OS=Thunnus orientalis OX=8238 GN=myh-1 PE=2 SV=1	24556	222036	182	553.7736	553.7736	2	0.09	1105.5325	0	R	LDEAEALAMK (M)	G	0.245	0.444	0.135
Myosin heavy chain-1 OS=Thunnus orientalis OX=8238 GN=myh-1 PE=2 SV=1	24556	222036	182	379.8752	379.8756	3	-1.14	1136.6050	0	K	NALAHAVQSAR	H	0.283	0.307	0.125
Myosin heavy chain-1 OS=Thunnus orientalis OX=8238 GN=myh-1 PE=2 SV=1	24556	222036	182	572.8190	572.8197	2	-1.13	1143.6247	1	R	ANSLAANLDKK	Q	0.656	0.540	0.850
Myosin heavy chain-1 OS=Thunnus orientalis OX=8238 GN=myh-1 PE=2 SV=1	24556	222036	182	1175.6149	1175.6154	1	-0.43	1174.6081	0	R	TIEDQLSELK	A	0.026	0.738	0.062
Myosin heavy chain-1 OS=Thunnus orientalis OX=8238 GN=myh-1 PE=2 SV=1	24556	222036	182	590.7826	590.7833	2	-1.18	1179.5520	0	R	LQTENGEFSR	Q	0.033	0.142	0.044

Myosin heavy chain-1 OS=Thunnus orientalis OX=8238 GN=myh-1 PE=2 SV=1	24556	222036	182	1181.6046	1181.6048	1	-0.17	1180.5975	0	K	EFETSQLLSK	I	0.070	0.185	0.058
Myosin heavy chain-1 OS=Thunnus orientalis OX=8238 GN=myh-1 PE=2 SV=1	24556	222036	182	593.2779	593.2784	2	-0.84	1184.5422	0	K	EQDTSAHLER	M	0.019	0.038	0.037
Myosin heavy chain-1 OS=Thunnus orientalis OX=8238 GN=myh-1 PE=2 SV=1	24556	222036	182	612.8141	612.8146	2	-0.82	1223.6146	1	R	TKYETDAIQR	T	0.040	0.236	0.122
Myosin heavy chain-1 OS=Thunnus orientalis OX=8238 GN=myh-1 PE=2 SV=1	24556	222036	182	1245.6552	1245.6573	1	-1.69	1244.6500	0	K	DIDDLELTLAK	V	0.372	0.481	0.288
Myosin heavy chain-1 OS=Thunnus orientalis OX=8238 GN=myh-1 PE=2 SV=1	24556	222036	182	626.8177	626.8177	2	0.00	1251.6208	0	K	DAQLHLDDAVR	G	0.211	0.156	0.100
Myosin heavy chain-1 OS=Thunnus orientalis OX=8238	24556	222036	182	632.2895	632.2886	2	1.42	1262.5626	0	R	ELESEVDAESR	R	0.067	0.063	0.101

GN=myh-1 PE=2 SV=1															
Myosin heavy chain-1 OS=Thunnus orientalis OX=8238 GN=myh-1 PE=2 SV=1	24556	222036	182	641.7754	641.7753	2	0.16	1281.5360	0	R	EQYEEEQEAK	G	0.531	0.625	0.430
Myosin heavy chain-1 OS=Thunnus orientalis OX=8238 GN=myh-1 PE=2 SV=1	24556	222036	182	656.8936	656.8954	2	-2.74	1311.7762	1	R	LQDLVDKLQLK	V	0.666	0.260	0.256
Myosin heavy chain-1 OS=Thunnus orientalis OX=8238 GN=myh-1 PE=2 SV=1	24556	222036	182	438.5523	438.5530	3	-1.60	1312.6371	1	K	KEQDTSAHLER	M	0.013	0.029	0.029
Myosin heavy chain-1 OS=Thunnus orientalis OX=8238 GN=myh-1 PE=2 SV=1	24556	222036	182	673.3342	673.3334	2	1.26	1344.6521	0	K	VAEQELVDASER	V	0.038	0.058	0.031
Myosin heavy chain-1 OS=Thunnus orientalis OX=8238 GN=myh-1 PE=2 SV=1	24556	222036	182	675.8476	675.8487	2	-1.55	1349.6827	0	K	QAYTQQIEELK	R	0.294	0.665	0.345

Myosin heavy chain-1 OS=Thunnus orientalis OX=8238 GN=myh-1 PE=2 SV=1	24556	222036	182	692.3337	692.3356	2	-2.67	1382.6565	1	K	ELTYQTEEDKK	N	0.213	0.351	0.308
Myosin heavy chain-1 OS=Thunnus orientalis OX=8238 GN=myh-1 PE=2 SV=1	24556	222036	182	693.3090	693.3094	2	-0.50	1384.6041	0	K	VQHEMEEAQER	A	0.466	0.284	0.337
Myosin heavy chain-1 OS=Thunnus orientalis OX=8238 GN=myh-1 PE=2 SV=1	24556	222036	182	694.8591	694.8582	2	1.37	1387.7017	0	R	NGLMLAEIEELR (NQ)	A	0.114	0.539	0.046
Myosin heavy chain-1 OS=Thunnus orientalis OX=8238 GN=myh-1 PE=2 SV=1	24556	222036	182	705.3362	705.3362	2	0.00	1408.6578	0	K	AITDAAMMAEELK (M)	K	0.337	0.587	0.301
Myosin heavy chain-1 OS=Thunnus orientalis OX=8238 GN=myh-1 PE=2 SV=1	24556	222036	182	729.8738	729.8754	2	-2.19	1457.7362	0	K	IEDEQSLGAQLQK	K	0.124	0.711	0.225
Myosin heavy chain-1 OS=Thunnus orientalis OX=8238	24556	222036	182	488.2409	488.2413	3	-0.89	1461.7021	1	K	LAEKDEEMEQIK	R	0.253	0.415	0.137

GN=myh-1 PE=2 SV=1															
Myosin heavy chain-1 OS=Thunnus orientalis OX=8238 GN=myh-1 PE=2 SV=1	24556	222036	182	744.8576	744.8569	2	1.01	1487.6991	0	R	IEELEEEIE AER	A	0.477	0.424	0.346
Myosin heavy chain-1 OS=Thunnus orientalis OX=8238 GN=myh-1 PE=2 SV=1	24556	222036	182	502.9349	502.9352	3	-0.66	1505.7838	1	K	QAYTQQIE ELKR	H	0.320	0.618	0.342
Myosin heavy chain-1 OS=Thunnus orientalis OX=8238 GN=myh-1 PE=2 SV=1	24556	222036	182	505.2403	505.2403	3	-0.07	1512.6991	1	R	KVQHEMEE AQER	A	0.364	0.204	0.261
Myosin heavy chain-1 OS=Thunnus orientalis OX=8238 GN=myh-1 PE=2 SV=1	24556	222036	182	507.9263	507.9266	3	-0.53	1520.7578	1	K	AITDAAMM AEELKK	E	0.358	0.605	0.374
Myosin heavy chain-1 OS=Thunnus orientalis OX=8238 GN=myh-1 PE=2 SV=1	24556	222036	182	767.3671	767.3676	2	-0.65	1532.7206	0	R	LQDAEESIE AVNSK (NQ)	C	0.013	0.868	0.023

Myosin heavy chain-1 OS=Thunnus orientalis OX=8238 GN=myh-1 PE=2 SV=1	24556	222036	182	520.9392	520.9399	3	-1.28	1559.7977	1	R	RNGLMLAEIEELR (NQ); (M)	A	0.082	0.464	0.045
Myosin heavy chain-1 OS=Thunnus orientalis OX=8238 GN=myh-1 PE=2 SV=1	24556	222036	182	405.4575	405.4581	4	-1.48	1617.8032	2	K	LAEKDEEMEQIKR	N	0.193	0.360	0.154
Myosin heavy chain-1 OS=Thunnus orientalis OX=8238 GN=myh-1 PE=2 SV=1	24556	222036	182	812.9534	812.9545	2	-1.35	1623.8944	0	R	VGLLHSQNTSLINTK	K	0.075	0.115	0.106
Myosin heavy chain-1 OS=Thunnus orientalis OX=8238 GN=myh-1 PE=2 SV=1	24556	222036	182	815.4386	815.4440	2	-6.56	1628.8733	1	R	QIEEKDALVSQLTR	G	0.006	0.470	0.015
Myosin heavy chain-1 OS=Thunnus orientalis OX=8238 GN=myh-1 PE=2 SV=1	24556	222036	182	1645.8096	1645.8102	1	-0.36	1644.8029	0	R	LQGEVEDLMIDVER	A	0.143	0.130	0.056
Myosin heavy chain-1 OS=Thunnus orientalis OX=8238	24556	222036	182	824.8953	824.8960	2	-0.85	1647.7774	0	R	LEEAGGATAAQIEMNK (M)	K	0.218	0.688	0.149

GN=myh-1 PE=2 SV=1															
Myosin heavy chain-1 OS=Thunnus orientalis OX=8238 GN=myh-1 PE=2 SV=1	24556	222036	182	550.6257	550.6249	3	1.45	1648.8528	2	K	KAITDAAMMAEELKK	E	0.444	0.607	0.516
Myosin heavy chain-1 OS=Thunnus orientalis OX=8238 GN=myh-1 PE=2 SV=1	24556	222036	182	827.3713	827.3710	2	0.42	1652.7273	0	K	MEIDDLSSNMEAVAK (NQ)	S	0.117	0.213	0.085
Myosin heavy chain-1 OS=Thunnus orientalis OX=8238 GN=myh-1 PE=2 SV=1	24556	222036	182	856.8949	856.8954	2	-0.53	1711.7761	0	R	QAEEAEEQANTHLSR	Y	0.085	0.216	0.074
Myosin heavy chain-1 OS=Thunnus orientalis OX=8238 GN=myh-1 PE=2 SV=1	24556	222036	182	862.4111	862.4103	2	0.93	1722.8060	1	K	QKYEEGQSELEGAQK	E	0.257	0.351	0.311
Myosin heavy chain-1 OS=Thunnus orientalis OX=8238 GN=myh-1 PE=2 SV=1	24556	222036	182	930.4427	930.4471	2	-4.73	1858.8796	0	K	LEQQVDDLEGSLEQEK	K	0.170	0.430	0.177

Myosin heavy chain-1 OS=Thunnus orientalis OX=8238 GN=myh-1 PE=2 SV=1	24556	222036	182	943.4645	943.4662	2	-1.75	1884.9177	0	K	QADSVAELGEQIDNLQR	V	0.022	0.637	0.047
Myosin heavy chain-1 OS=Thunnus orientalis OX=8238 GN=myh-1 PE=2 SV=1	24556	222036	182	663.3306	663.3321	3	-2.31	1986.9745	1	K	LEQQVDDLEGSLEQEKK	L	0.173	0.372	0.137
Myosin heavy chain-1 OS=Thunnus orientalis OX=8238 GN=myh-1 PE=2 SV=1	24556	222036	182	668.3041	668.3034	3	1.00	2001.8884	0	K	MEGDLNEMEIQLSHANR (M)	Q	0.055	0.221	0.040
Myosin heavy chain-1 OS=Thunnus orientalis OX=8238 GN=myh-1 PE=2 SV=1	24556	222036	182	668.3350	668.3358	3	-1.20	2001.9855	0	K	NLQQEISDLTEQIGETGK	S	0.022	0.774	0.058
Myosin heavy chain-1 OS=Thunnus orientalis OX=8238 GN=myh-1 PE=2 SV=1	24556	222036	182	505.7676	505.7697	4	-4.20	2019.0497	1	R	NVQGQLKDAQLHLDDAVR	G	0.139	0.181	0.067
Myosin heavy chain-1 OS=Thunnus orientalis OX=8238	24556	222036	182	1045.0176	1045.0184	2	-0.77	2088.0222	1	K	TKLEQQVDDLEGSLEQEK	K	0.081	0.275	0.074

GN=myh-1 PE=2 SV=1															
Myosin heavy chain-1 OS=Thunnus orientalis OX=8238 GN=myh-1 PE=2 SV=1	24556	222036	182	529.5028	529.5044	4	-3.02	2113.9884	1	K	KMEGDLNEMEIQLSHANR	Q	0.042	0.216	0.037
Myosin heavy chain-1 OS=Thunnus orientalis OX=8238 GN=myh-1 PE=2 SV=1	24556	222036	182	555.0364	555.0366	4	-0.36	2216.1172	2	K	TKLEQQVDDLEGSLEQEKK	L	0.100	0.222	0.068
Myosin heavy chain-1 OS=Thunnus orientalis OX=8238 GN=myh-1 PE=2 SV=1	24556	222036	182	743.3563	743.3570	3	-0.94	2227.0491	0	K	TEIQTALEEAEGTLEHEEAK	I	0.080	0.209	0.044
Myosin heavy chain-1 OS=Thunnus orientalis OX=8238 GN=myh-1 PE=2 SV=1	24556	222036	182	1119.0555	1119.0559	2	-0.31	2236.0971	0	K	LEADLVHIQGEVDDSIQEAR	N	0.033	0.223	0.015
Myosin heavy chain-1 OS=Thunnus orientalis OX=8238 GN=myh-1 PE=2 SV=1	24556	222036	182	1183.1010	1183.1034	2	-1.99	2364.1921	1	K	KLEADLVHIQGEVDDSIQEAR	N	0.039	0.248	0.014

Myosin heavy chain-1 OS=Thunnus orientalis OX=8238 GN=myh-1 PE=2 SV=1	24556	222036	182	624.0783	624.0791	4	-1.20	2492.2870	2	K	KKLEADLVHIQGEVDDSIQEAR	N	0.056	0.264	0.017
Myosin heavy chain-1 OS=Thunnus orientalis OX=8238 GN=myh-1 PE=2 SV=1	24556	222036	182	946.8082	946.8087	3	-0.56	2837.4043	1	K	ALQEAHQQTLDDLQAEEDKVNTLTK	A	0.024	0.182	0.045
Myosin heavy chain-1 OS=Thunnus orientalis OX=8238 GN=myh-1 PE=2 SV=1	24556	222036	182	984.4715	984.4754	3	-3.96	2950.4043	1	K	HVETEKTEIQTALEEAEGTLEHEEAK	I	0.094	0.106	0.039
Myosin heavy chain-1 OS=Thunnus orientalis OX=8238 GN=myh-1 PE=2 SV=1	24556	222036	182	1027.1724	1027.1737	3	-1.30	3078.4993	2	K	KHVETEKTEIQTALEEAEGTLEHEEAK	I	0.079	0.087	0.033
Tropomyosin OS=Thunnus thynnus OX=8237 PE=2 SV=1	5988	32694	47	575.3400	575.3399	1	0.17	574.3326	0	K	VLTDK	L	0.584	0.308	0.612
Tropomyosin OS=Thunnus thynnus OX=8237 PE=2 SV=1	5988	32694	47	717.3520	717.3526	1	-0.84	716.3453	0	K	ENALDR	A	0.053	0.184	0.234

Tropomyosin OS=Thunnus thynnus OX=8237 PE=2 SV=1	5988	32694	47	717.4501	717.4505	1	-0.56	716.4432	0	R	LATALTK	L	0.707	0.325	0.334
Tropomyosin OS=Thunnus thynnus OX=8237 PE=2 SV=1	5988	32694	47	718.3630	718.3617	1	1.81	717.3544	0	K	LEEAEK	A	0.341	0.228	0.247
Tropomyosin OS=Thunnus thynnus OX=8237 PE=2 SV=1	5988	32694	47	361.6767	361.6771	2	-0.97	721.3395	0	R	AEFAER	S	0.301	0.224	0.184
Tropomyosin OS=Thunnus thynnus OX=8237 PE=2 SV=1	5988	32694	47	733.3726	733.3727	1	-0.14	732.3654	0	R	AELSEGK	C	0.038	0.087	0.048
Tropomyosin OS=Thunnus thynnus OX=8237 PE=2 SV=1	5988	32694	47	766.3724	766.3730	1	-0.78	765.3657	0	K	YEEVAR	K	0.414	0.217	0.344
Tropomyosin OS=Thunnus thynnus OX=8237 PE=2 SV=1	5988	32694	47	777.3400	777.3373	1	3.47	776.3300	0	K	AADESER	G	0.107	0.109	0.172
Tropomyosin OS=Thunnus thynnus OX=8237 PE=2 SV=1	5988	32694	47	789.4420	789.4465	1	-5.70	788.4392	0	K	TVTNNLK	S	0.441	0.178	0.222
Tropomyosin OS=Thunnus thynnus OX=8237 PE=2 SV=1	5988	32694	47	425.7021	425.7024	2	-0.70	849.3902	1	R	AMKDEEK	M	0.500	0.325	0.300
Tropomyosin OS=Thunnus thynnus OX=8237 PE=2 SV=1	5988	32694	47	438.2266	438.2271	2	-1.14	874.4396	0	K	SLEAQAEK	Y	0.128	0.459	0.175

Tropomyosin OS=Thunnus thynnus OX=8237 PE=2 SV=1	5988	32694	47	894.4662	894.4679	1	-1.90	893.4606	1	R	KYEEVAR	K	0.247	0.126	0.204
Tropomyosin OS=Thunnus thynnus OX=8237 PE=2 SV=1	5988	32694	47	940.4475	940.4483	1	-0.85	939.4410	0	K	HIAEEADR	K	0.242	0.077	0.096
Tropomyosin OS=Thunnus thynnus OX=8237 PE=2 SV=1	5988	32694	47	503.2456	503.2460	2	-0.79	1004.4774	1	R	AEQAESDKK	A	0.179	0.322	0.222
Tropomyosin OS=Thunnus thynnus OX=8237 PE=2 SV=1	5988	32694	47	358.5241	358.5244	3	-0.84	1072.5513	1	K	LDKENALDR	A	0.103	0.306	0.219
Tropomyosin OS=Thunnus thynnus OX=8237 PE=2 SV=1	5988	32694	47	1131.6089	1131.6078	1	0.97	1130.6005	0	K	MELQEIQLK	E	0.274	0.665	0.237
Tropomyosin OS=Thunnus thynnus OX=8237 PE=2 SV=1	5988	32694	47	578.8326	578.8323	2	0.60	1155.6499	0	K	LVIIEGDLER	T	0.248	0.672	0.126
Tropomyosin OS=Thunnus thynnus OX=8237 PE=2 SV=1	5988	32694	47	591.7799	591.7799	2	0.00	1181.5452	1	K	EDKYEEEIK	V	0.401	0.430	0.332
Tropomyosin OS=Thunnus thynnus OX=8237 PE=2 SV=1	5988	32694	47	1243.6519	1243.6529	1	-0.80	1242.6456	0	R	IQLVEEELDR	A	0.140	0.404	0.173
Tropomyosin OS=Thunnus thynnus OX=8237 PE=2 SV=1	5988	32694	47	629.3377	629.3379	2	-0.32	1256.6612	0	K	QLEDDLVGLQK	K	0.363	0.232	0.099

Tropomyosin OS=Thunnus thynnus OX=8237 PE=2 SV=1	5988	32694	47	666.8217	666.8232	2	-2.17	1331.6317	0	K	ATDAEGEVASLNR	R	0.004	0.071	0.016
Tropomyosin OS=Thunnus thynnus OX=8237 PE=2 SV=1	5988	32694	47	467.2556	467.2562	3	-1.28	1398.7467	1	R	RIQLVEEELDR	A	0.133	0.345	0.276
Tropomyosin OS=Thunnus thynnus OX=8237 PE=2 SV=1	5988	32694	47	1552.7370	1552.7377	1	-0.45	1551.7304	0	K	TIDDLEDELYAQK	L	0.085	0.315	0.185
Tropomyosin OS=Thunnus thynnus OX=8237 PE=2 SV=1	5988	32694	47	799.3832	799.3833	2	-0.06	1596.7519	1	K	GTEDELDKYSEALK	D	0.025	0.099	0.124
Tropomyosin OS=Thunnus thynnus OX=8237 PE=2 SV=1	5988	32694	47	880.4056	880.4064	2	-0.91	1758.7982	0	K	AISEELDHALNDMTSI(NQ)	-	0.015	0.245	0.025
Tropomyosin OS=Thunnus thynnus OX=8237 PE=2 SV=1	5988	32694	47	723.6781	723.6780	3	0.18	2168.0120	2	K	GTEDELDKYSEALKDAQEK	L	0.043	0.109	0.124
Tropomyosin OS=Thunnus thynnus OX=8237 GN=TM PE=2 SV=1	5557	32742	42	688.3881	688.3876	1	0.73	687.3803	0	K	LEVAEK	S	0.116	0.051	0.049
Tropomyosin OS=Thunnus thynnus OX=8237 GN=TM PE=2 SV=1	5557	32742	42	382.1953	382.1953	2	0.13	762.3759	0	R	AELSESK	C	0.079	0.201	0.098

Tropomyosin OS=Thunnus thynnus OX=8237 GN=TM PE=2 SV=1	5557	32742	42	917.4327	917.4323	1	0.44	916.4250	0	K	NIAEEADR	K	0.105	0.259	0.152
Tropomyosin OS=Thunnus thynnus OX=8237 GN=TM PE=2 SV=1	5557	32742	42	460.7137	460.7140	2	-0.65	919.4134	0	K	GTEDELEK	Y	0.136	0.127	0.134
Tropomyosin OS=Thunnus thynnus OX=8237 GN=TM PE=2 SV=1	5557	32742	42	511.2430	511.2435	2	-0.88	1020.4723	1	R	AEQSESDKK	A	0.113	0.476	0.171
Tropomyosin OS=Thunnus thynnus OX=8237 GN=TM PE=2 SV=1	5557	32742	42	561.2691	561.2702	2	-1.87	1120.5257	0	K	MEMQDVQLK	E	0.475	0.397	0.319
Tropomyosin OS=Thunnus thynnus OX=8237 GN=TM PE=2 SV=1	5557	32742	42	581.3032	581.3036	2	-0.60	1160.5925	1	R	LKGTEDELEK	Y	0.094	0.091	0.088
Tropomyosin OS=Thunnus thynnus OX=8237 GN=TM PE=2 SV=1	5557	32742	42	586.8298	586.8297	2	0.17	1171.6448	0	K	LVVIESDLER	T	0.049	0.271	0.033
Tropomyosin OS=Thunnus thynnus OX=8237 GN=TM PE=2 SV=1	5557	32742	42	645.3211	645.3240	2	-4.42	1288.6333	0	K	QLEDDLVAMQK	R	0.252	0.219	0.176

Tropomyosin OS=Thunnus thynnus OX=8237 GN=TM PE=2 SV=1	5557	32742	42	703.3338	703.3314	2	3.48	1404.6481	0	K	SATDAEGDVASLNR	R	0.007	0.105	0.051
Tropomyosin OS=Thunnus thynnus OX=8237 GN=TM PE=2 SV=1	5557	32742	42	887.9104	887.9119	2	-1.63	1773.8091	0	K	SISEELDHALNDMTSI	-	0.016	0.240	0.032
Myosin light chain 3 OS=Thunnus thynnus OX=8237 GN=mlc3 PE=2 SV=1	4838	18544	35	586.3030	586.3018	1	2.05	585.2945	0	K	HIMSV	-	0.596	0.500	0.401
Myosin light chain 3 OS=Thunnus thynnus OX=8237 GN=mlc3 PE=2 SV=1	4838	18544	35	865.4419	865.4414	1	0.58	864.4341	0	K	QVDTFQK	G	0.423	0.331	0.159
Myosin light chain 3 OS=Thunnus thynnus OX=8237 GN=mlc3 PE=2 SV=1	4838	18544	35	471.7535	471.7538	2	-0.64	941.4930	0	R	ALGQNPTNK	D	0.134	0.035	0.084
Myosin light chain 3 OS=Thunnus thynnus OX=8237 GN=mlc3 PE=2 SV=1	4838	18544	35	477.7377	477.7377	2	0.10	953.4607	0	K	EAFGLFDR	V	0.071	0.169	0.058
Myosin light chain 3 OS=Thunnus thynnus OX=8237 GN=mlc3 PE=2 SV=1	4838	18544	35	480.2914	480.2923	2	-1.77	958.5699	0	R	IVLSTLGEK	M	0.061	0.328	0.148

Myosin light chain 3 OS=Thunnus thynnus OX=8237 GN=mlc3 PE=2 SV=1	4838	18544	35	617.7902	617.7903	2	-0.08	1233.5659	0	K	EGNGTVMGAELR (NQ)	I	0.039	0.127	0.018
Myosin light chain 3 OS=Thunnus thynnus OX=8237 GN=mlc3 PE=2 SV=1	4838	18544	35	1287.5852	1287.5852	1	0.00	1286.5779	0	K	GTYDDYVEGLR	V	0.059	0.196	0.219
Myosin light chain 3 OS=Thunnus thynnus OX=8237 GN=mlc3 PE=2 SV=1	4838	18544	35	1338.7122	1338.7126	1	-0.30	1337.7053	0	R	LNFDTFLPMLK	Q	0.318	0.274	0.407
Myosin light chain 3 OS=Thunnus thynnus OX=8237 GN=mlc3 PE=2 SV=1	4838	18544	35	680.3315	680.3323	2	-1.18	1358.6500	0	K	ILGNPTADDMANK	R	0.114	0.169	0.182
Myosin light chain 3 OS=Thunnus thynnus OX=8237 GN=mlc3 PE=2 SV=1	4838	18544	35	511.2564	511.2560	3	0.85	1530.7460	1	K	ILGNPTADDMANKR (M)	L	0.064	0.095	0.138
Myosin light chain 3 OS=Thunnus thynnus OX=8237 GN=mlc3 PE=2 SV=1	4838	18544	35	580.6128	580.6138	3	-1.78	1738.8196	1	R	VFDKEGNGTVMGAELR (NQ); (M)	I	0.019	0.054	0.017
Myosin light chain 3 OS=Thunnus thynnus OX=8237 GN=mlc3 PE=2 SV=1	4838	18544	35	592.9604	592.9615	3	-1.80	1775.8625	0	R	VGDNQVAFNQVADIMR	A	0.167	0.133	0.087

Myosin light chain 3 OS=Thunnus thynnus OX=8237 GN=mlc3 PE=2 SV=1	4838	18544	35	1015.1112	1015.1110	3	0.23	3042.3110	0	K	MSEPEIDALMTGQEDENGSVHYEAFVK (NQ); (M)	H	0.063	0.038	0.026
Procollagen alpha 1 type I (Fragment) OS=Thunnus orientalis OX=8238 PE=2 SV=1	4787	137640	37	558.2889	558.2882	1	1.25	557.2809	0	R	GEPGAK	G	0.083	0.144	0.061
Procollagen alpha 1 type I (Fragment) OS=Thunnus orientalis OX=8238 PE=2 SV=1	4787	137640	37	351.6816	351.6822	2	-1.56	701.3497	0	K	APDPFR	G	0.281	0.262	0.261
Procollagen alpha 1 type I (Fragment) OS=Thunnus orientalis OX=8238 PE=2 SV=1	4787	137640	37	392.7060	392.7067	2	-1.66	783.3987	0	R	GAAGPQGAR	G	0.128	0.071	0.077
Procollagen alpha 1 type I (Fragment) OS=Thunnus orientalis OX=8238 PE=2 SV=1	4787	137640	37	847.3787	847.3792	1	-0.59	846.3719	0	K	GESGDTGPK	G	0.048	0.092	0.064
Procollagen alpha 1 type I (Fragment) OS=Thunnus	4787	137640	37	426.2164	426.2166	2	-0.35	850.4185	0	R	GFSGLDGAK	G	0.790	0.236	0.521

orientalis OX=8238 PE=2 SV=1															
Procollagen alpha 1 type I (Fragment) OS=Thunnus orientalis OX=8238 PE=2 SV=1	4787	137640	37	858.4064	858.4065	1	-0.12	857.3992	0	K	GETGPQGGR	G	0.112	0.165	0.119
Procollagen alpha 1 type I (Fragment) OS=Thunnus orientalis OX=8238 PE=2 SV=1	4787	137640	37	438.1964	438.1964	2	0.11	874.3781	0	R	GEAGEAGER	G	0.134	0.158	0.171
Procollagen alpha 1 type I (Fragment) OS=Thunnus orientalis OX=8238 PE=2 SV=1	4787	137640	37	451.2222	451.2224	2	-0.33	900.4301	0	R	GPAGSSGSPGK	D	0.296	0.167	0.163
Procollagen alpha 1 type I (Fragment) OS=Thunnus orientalis OX=8238 PE=2 SV=1	4787	137640	37	983.5267	983.5269	1	-0.20	982.5196	0	K	QGPAGLVGER	G	0.012	0.018	0.013
Procollagen alpha 1 type I (Fragment) OS=Thunnus orientalis OX=8238 PE=2 SV=1	4787	137640	37	994.5069	994.5065	1	0.40	993.4992	0	R	GPAGASGPAGPR	G	0.045	0.043	0.052

Procollagen alpha 1 type I (Fragment) OS=Thunnus orientalis OX=8238 PE=2 SV=1	4787	137640	37	550.2784	550.2782	2	0.36	1098.5418	1	K	GADGAPGKNGVR (NQ)	G	0.509	0.145	0.352
Procollagen alpha 1 type I (Fragment) OS=Thunnus orientalis OX=8238 PE=2 SV=1	4787	137640	37	602.2700	602.2711	2	-1.83	1202.5276	1	K	GDRGEAGEAGER	G	0.044	0.100	0.131
Procollagen alpha 1 type I (Fragment) OS=Thunnus orientalis OX=8238 PE=2 SV=1	4787	137640	37	664.3345	664.3357	2	-1.81	1326.6568	0	R	GFPGLPGQSGEPGK	Q	0.141	0.077	0.109
Procollagen alpha 1 type I (Fragment) OS=Thunnus orientalis OX=8238 PE=2 SV=1	4787	137640	37	1480.7495	1480.7503	1	-0.54	1479.7430	0	R	GESGPAGVAGPAGAAGVR	G	0.029	0.029	0.017
Procollagen alpha 1 type I (Fragment) OS=Thunnus orientalis OX=8238 PE=2 SV=1	4787	137640	37	760.8693	760.8711	2	-2.37	1519.7276	0	K	SSGPPVPGPMGPMGPR	G	0.404	0.207	0.302
Procollagen alpha 1 type I (Fragment) OS=Thunnus	4787	137640	37	890.4092	890.4113	2	-2.36	1778.8080	0	R	GFTGMQGLPGTPGSMGER	G	0.333	0.215	0.242

orientalis OX=8238 PE=2 SV=1															
Procollagen alpha 1 type I (Fragment) OS=Thunnus orientalis OX=8238 PE=2 SV=1	4787	137640	37	611.9821	611.9829	3	-1.31	1832.9268	0	K	GEPGPAGLQGLIGPAGEEGK	R	0.048	0.181	0.046
Procollagen alpha 1 type I (Fragment) OS=Thunnus orientalis OX=8238 PE=2 SV=1	4787	137640	37	637.3206	637.3207	3	-0.16	1908.9402	1	K	TGDRGESGPAGVAGPAGAAGVR	G	0.009	0.018	0.009
Procollagen alpha 1 type I (Fragment) OS=Thunnus orientalis OX=8238 PE=2 SV=1	4787	137640	37	659.0073	659.0084	3	-1.62	1974.0032	0	K	VGPAGISGQDGRPGPAGPTGAR	G	0.021	0.018	0.026
Procollagen alpha 1 type I (Fragment) OS=Thunnus orientalis OX=8238 PE=2 SV=1	4787	137640	37	995.5078	995.5213	2	-13.51	1989.0279	1	K	GEPGPAGLQGLIGPAGEEGKR	G	0.029	0.142	0.039
Procollagen alpha 1 type I (Fragment) OS=Thunnus orientalis OX=8238 PE=2 SV=1	4787	137640	37	1040.4900	1040.4902	2	-0.19	2078.9658	0	R	GETGPSGPAGFAGPPGADGQPGAK	G	0.037	0.064	0.049

Procollagen alpha 1 type I (Fragment) OS=Thunnus orientalis OX=8238 PE=2 SV=1	4787	137640	37	1099.0680	1099.0628	2	4.73	2196.1110	1	R	VGPPGPAGASGPPGPLGPMGKDGAR	G	0.088	0.057	0.101
Procollagen alpha 1 type I (Fragment) OS=Thunnus orientalis OX=8238 PE=2 SV=1	4787	137640	37	811.0589	811.0606	3	-2.05	2430.1598	1	R	GPAGSSGSPGKDGMNGLPGPIGPPGPR (NQ); (M)	G	0.270	0.094	0.157
Myosin light chain 1 OS=Thunnus thynnus OX=8237 GN=mlc1 PE=2 SV=1	3573	21272	26	636.3091	636.2988	2	16.19	1270.5830	0	K	AGYEDYVEGLR	V	0.073	0.114	0.201
Myosin light chain 1 OS=Thunnus thynnus OX=8237 GN=mlc1 PE=2 SV=1	3573	21272	26	655.3299	655.3321	2	-3.36	1308.6496	0	K	VAYNQIADIMR (M)	A	0.177	0.218	0.093
Myosin light chain 1 OS=Thunnus thynnus OX=8237 GN=mlc1 PE=2 SV=1	3573	21272	26	711.8337	711.8338	2	-0.14	1421.6530	0	K	LLGMPSAEDMTNK (M)	R	0.197	0.294	0.178
Myosin light chain 1 OS=Thunnus thynnus OX=8237 GN=mlc1 PE=2 SV=1	3573	21272	26	722.3358	722.3356	2	0.35	1442.6565	0	K	VEFSADQIEDYK	E	0.041	0.302	0.032

Myosin light chain 1 OS=Thunnus thynnus OX=8237 GN=mlc1 PE=2 SV=1	3573	21272	26	726.3785	726.3819	3	-4.68	2176.1238	0	R	VEFEGFLP MLQTIINSP NK	A	0.028	0.297	0.019
Myosin light chain 1 OS=Thunnus thynnus OX=8237 GN=mlc1 PE=2 SV=1	3573	21272	26	778.7420	778.7436	3	-2.05	2333.2089	1	K	RVEFEGFLP MLQTIINSP NK (NQ)	A	0.018	0.266	0.020
Myosin light chain 1 OS=Thunnus thynnus OX=8237 GN=mlc1 PE=2 SV=1	3573	21272	26	793.7079	793.7095	3	-2.02	2378.1066	1	K	VEFSADQIE DYKEAFGL FDR	V	0.025	0.116	0.017
Myosin light chain 2 OS=Thunnus thynnus OX=8237 GN=mlc2 PE=2 SV=1	3483	18978	25	632.3611	632.3614	1	-0.47	631.3541	0	R	DGIISK	D	0.880	0.574	0.565
Myosin light chain 2 OS=Thunnus thynnus OX=8237 GN=mlc2 PE=2 SV=1	3483	18978	25	432.2291	432.2291	2	0.00	862.4436	0	R	FTPEEIK	N	0.164	0.407	0.125
Myosin light chain 2 OS=Thunnus thynnus OX=8237 GN=mlc2 PE=2 SV=1	3483	18978	25	538.7683	538.7683	2	0.09	1075.5219	0	K	NEELEAMI K	E	0.312	0.476	0.087
Myosin light chain 2 OS=Thunnus thynnus OX=8237 GN=mlc2 PE=2 SV=1	3483	18978	25	603.8051	603.8093	2	-6.96	1205.6040	0	K	EAFTIIDQN R	D	0.068	0.342	0.113

Myosin light chain 2 OS=Thunnus thynnus OX=8237 GN=mlc2 PE=2 SV=1	3483	18978	25	629.3550	629.3561	2	-1.75	1256.6976	1	K	VLDPDATGTIKK	E	0.365	0.141	0.293
Myosin light chain 2 OS=Thunnus thynnus OX=8237 GN=mlc2 PE=2 SV=1	3483	18978	25	1274.6757	1274.6773	1	-1.26	1273.6700	0	R	DVLASMGQLNVK	N	0.271	0.211	0.130
Myosin light chain 2 OS=Thunnus thynnus OX=8237 GN=mlc2 PE=2 SV=1	3483	18978	25	1361.6958	1361.6947	1	0.81	1360.6874	0	K	GADPEDVILSAFK	V	0.064	0.182	0.019
Myosin light chain 2 OS=Thunnus thynnus OX=8237 GN=mlc2 PE=2 SV=1	3483	18978	25	534.9618	534.9628	3	-1.87	1601.8665	1	K	LKGADPEDVILSAFK	V	0.310	0.412	0.083
Myosin light chain 2 OS=Thunnus thynnus OX=8237 GN=mlc2 PE=2 SV=1	3483	18978	25	910.4789	910.4811	2	-2.42	1818.9476	1	K	EAFTIIDQNRDGIISK	D	0.286	0.415	0.163
Myosin light chain 2 OS=Thunnus thynnus OX=8237 GN=mlc2 PE=2 SV=1	3483	18978	25	955.9407	955.9408	2	-0.05	1909.8669	0	K	NMWAAFPPDVAGNVDYK (M)	N	0.300	0.132	0.143
Myosin light chain 2 OS=Thunnus thynnus	3483	18978	25	994.4941	994.4954	2	-1.26	1986.9761	0	K	EASGPINFTVFLTMFGEK	L	0.034	0.235	0.026

OX=8237 GN=mlc2 PE=2 SV=1															
Myosin light chain 2 OS=Thunnus thynnus OX=8237 GN=mlc2 PE=2 SV=1	3483	18978	25	778.3958	778.3958	3	0.04	2332.1654	1	R	DVLASMGQLNVKNEELEAMIK (NQ)	E	0.054	0.315	0.028
Myosin light chain 1 OS=Katsuwonus pelamis OX=8226 GN=mlc1 PE=2 SV=1	2986	21336	24	680.3315	680.3323	2	-1.18	1358.6500	0	K	ILGNPSAEDMANK	R	0.061	0.275	0.079
Myosin light chain 1 OS=Katsuwonus pelamis OX=8226 GN=mlc1 PE=2 SV=1	2986	21336	24	511.2564	511.2560	3	0.85	1530.7460	1	K	ILGNPSAEDMANKR (M)	V	0.027	0.172	0.057
Myoglobin OS=Thunnus albacares OX=8236 GN=mb PE=1 SV=2	1252	15650	9	832.4391	832.4399	2	-0.90	1662.8651	0	R	NVMGIIIADLEANYK	E	0.429	0.327	0.076
Myoglobin OS=Thunnus albacares OX=8236 GN=mb PE=1 SV=2	1252	15650	9	1127.5725	1127.5749	2	-2.08	2253.1351	1	R	NVMGIIIADLEANYKELGFSG	-	0.322	0.644	0.129
Myoglobin OS=Thunnus albacares	1252	15650	9	756.4087	756.4096	3	-1.23	2266.2070	0	K	FAGIAQADIAGNAAISAHGATVLK	K	0.975	0.394	0.785

OX=8236 GN=mb PE=1 SV=2															
Myoglobin OS=Thunnus alalunga OX=8235 GN=mb PE=2 SV=3	1112	15657	8	756.4087	756.4096	3	-1.23	2266.2070	0	K	FAGIAQAD LAGNAAIS AHGATVLK	K	0.956	0.468	0.742
Beta-actin (Fragment) OS=Thunnus maccoyii OX=8240 PE=2 SV=1	856	36916	6	581.3105	581.3129	2	-4.04	1160.6111	0	K	EITALAPST MK	I	0.113	0.219	0.147
Beta-actin (Fragment) OS=Thunnus maccoyii OX=8240 PE=2 SV=1	856	36916	6	586.2894	586.2892	2	0.34	1170.5638	0	R	HQGVMVG MGQK	D	0.575	0.527	0.508
Beta-actin (Fragment) OS=Thunnus maccoyii OX=8240 PE=2 SV=1	856	36916	6	599.8552	599.8564	2	-2.00	1197.6982	0	-	AVFPSIVGR PR	H	0.157	0.060	0.355
Beta-actin (Fragment) OS=Thunnus maccoyii OX=8240 PE=2 SV=1	856	36916	6	895.9468	895.9496	2	-3.13	1789.8846	0	K	SYELPDGQ VITIGNER	F	0.004	0.176	0.012
Myosin light chain 2 OS=Katsuwonus pelamis OX=8226 GN=mlc2 PE=2 SV=1	830	19038	6	674.3398	674.3432	2	-5.04	1346.6718	0	K	GADPEDVI VSAFK	V	0.062	0.073	0.015
Hemoglobin beta chain OS=Thunnus thynnus OX=8237 PE=1 SV=1	435	16302	3	809.3894	809.3934	2	-4.94	1616.7722	0	R	YFGAYGDL STPDAIK	G	0.024	0.061	0.071

Hemoglobin beta chain OS=Thunnus thynnus OX=8237 PE=1 SV=1	435	16302	3	968.5045	968.5068	2	-2.32	1934.9989	0	R	SIIAGIFANLNYEDIGPK (NQ)	A	0.715	0.540	0.387
Parvalbumin OS=Katsuwonus pelamis OX=8226 GN=Kat p 1 PE=2 SV=1	365	11435	3	510.7703	510.7717	2	-2.64	1019.5287	0	K	AFAIIDQDK	S	0.567	0.236	0.188
Parvalbumin OS=Katsuwonus pelamis OX=8226 GN=Kat p 1 PE=2 SV=1	365	11435	3	581.3284	581.3294	2	-1.63	1160.6441	0	K	IGVDEFAALVK	H	0.515	0.278	0.134
Parvalbumin OS=Katsuwonus pelamis OX=8226 GN=Kat p 1 PE=2 SV=1	365	11435	3	590.7887	590.7903	2	-2.62	1179.5659	0	K	SGFIEEEELK	L	0.172	0.197	0.160
Hemoglobin subunit beta OS=Thunnus thynnus OX=8237 GN=hbb PE=1 SV=1	355	16171	3	968.5045	968.5068	2	-2.32	1934.9989	0	R	SIIAGFIANLNYEDIGPK (NQ)	A	0.713	0.538	0.388
Hemoglobin subunit alpha OS=Thunnus thynnus OX=8237 GN=hba PE=1 SV=1	294	15436	2	558.7852	558.7859	2	-1.16	1115.5571	0	K	SADAIGADALGR	M	0.210	0.120	0.102
Hemoglobin subunit alpha OS=Thunnus	294	15436	2	630.8695	630.8692	2	0.55	1259.7237	0	K	FLASVALALAER	Y	0.042	0.248	0.021

thynnus OX=8237 GN=hba PE=1 SV=1															
Calmodulin A OS=Thunnus orientalis OX=8238 GN=CaM-A PE=3 SV=1	154	16827	1	1245.5414	1245.5436	2	-1.77	2489.0726	0	R	EADIDGDGQVNYEEFVQMMTAK	-	0.070	0.128	0.049
Fructose-bisphosphate aldolase A (Fragment) OS=Thunnus albacares OX=8236 GN=ALDOA PE=1 SV=1	154	3912	1	706.3638	706.3721	2	-11.75	1410.7296	0	-	PHAFPFLTPEQK	K	0.289	0.348	0.137
Heat shock protein beta-1 OS=Thunnus orientalis OX=8238 GN=hspb1 PE=2 SV=1	154	23038	1	991.5599	991.5621	2	-2.17	1981.1095	0	K	VTSSLSPEGLLTVEAPLIR	Q	0	0.025	0.005
Alpha-amylase OS=Thunnus orientalis OX=8238 PE=2 SV=1	52	57530	1	612.7910	612.7985	4	-12.20	2447.1647	2	K	VADYMNKLIDMGVAGFRVDACK 2 (M)	H	0.560	0.251	0.313

Chapter 6

Characterization of antioxidant peptides fish protein hydrolysate and evaluation of gastrointestinal effect

6.1 Introduction

The wide range of molecules that can be generated from the combination of different amino acids can also lead to antioxidant molecules, which can have many different applications. Antioxidant compounds are essentials in preventing lipid oxidation of food and of biological membranes which naturally occurs in presence of oxygen. Antioxidant molecules and thus peptides thanks to this radical scavenging activity prevent this oxidation. Indeed, besides their potential as therapeutic agents they can also be employed as food additives, and anti-aging and photoprotective components in cosmetics (Zhu et al., 2022). Moreover, there are literature studies that have demonstrated that the antioxidant peptides can inhibit lipid peroxidation during food storage and transport, maintaining their value and prolonging the expire date (Samaei et al., 2020). There are many peptides which have been discovered to be antioxidant, the BIOPEP database as an example reports a number of 840 peptides (Minkiewicz et al., 2019).

The aim of this work was to evaluate the antioxidant activity of fish protein hydrolysate obtained by means of alcalase hydrolysis. Moreover, antioxidant activity of the in vitro gastrointestinal digestion was evaluated, to assess the stability of the hydrolysate to the digestion. Furthermore, peptides sequences were identified by means of HPLC-MS/MS in order to discover the presence of bioactive sequences.

6.2 Materials and methods

6.2.1 Chemicals and materials

All chemicals, reagents, and organic solvents of the highest grade available were purchased from Sigma-Aldrich (St. Louis, MO, USA) unless otherwise stated. Trifluoroacetic acid (TFA) was supplied by Romil Ltd (Cambridge). Mass-grade solvents used for medium-sized peptides were purchased from VWR International (Milan, Italy). Optima® LC-MS grade water and acetonitrile (ACN), used for short peptide analysis, were purchased from Thermo Fisher Scientific (Waltham, Massachusetts, USA). Bond elut C18 EWP cartridges (50 mg) were purchased from Agilent (Santa Clara, USA).

6.2.2 Fish samples and treatment

Fishes (*Micromesistius poutassou*) were purchased in a fish market in Valencia, Spain. Fillet and by-products (head, tail, and bones) were separated and differently treated. They were both triturated, by using a blender for the fillet and a hammer for the by-products. Then the samples were stored at −80 °C and freeze-dried on a scanvac coolsafe freeze-dryer (LaboGene, Denmark). Lyophilized by-product samples were grinded with pestle, then blended, and finally reduced to a fine powder in a mixer mill MM 400 (Retsch) for 90 sec at the frequency of 25 Hz. On the other hand, lyophilized muscle samples were grinded with pestle, and further reduced to a fine powder into a mixer mill MM 400 (Retsch) for 45 sec at the frequency of 25 Hz. Finally, muscle and by-products were labelled as M and BP respectively and stored at -20 °C for further use.

6.2.3 Moisture and protein content evaluation

Moisture of the two triturated samples was determined by drying 3 g of each sample on a laboratory thermobalance (HB43 Halogen, Metter Toledo, USA) until the weight was stable. Protein content was measured by Dumas combustion based on AOAC method 992.15-1992 (Association of Official Agricultural Chemists (AOAC), 1996).

6.2.4 Alcalase hydrolysis of by-products

Byproduct powder sample was reconstituted with the original quantity of water (77.95 %). Then 8 g were dissolved in 4 mL of bidistilled water and pH was increased to 8 with NaOH 10 M. Enzymatic hydrolysis of the sample was performed in duplicate with Alcalase 2.4 L 2% in reaction flasks placed on a Carousel 6 Plus Reaction Station™ (radleys, UK) at 65 °C with the gentle agitation generated by stir bars. After two hours the enzymatic activity was inhibited by a heat shock at 95 °C for 10 min. Sample was then freeze-dried and labelled as BPH-ALC and stored at -20°C for further use.

6.2.5 Ultrasound assisted alcalase hydrolysis of by-products

16 g of reconstituted sample were solubilized in 8 mL of bidistilled water, and pH was adjusted to 8 with NaOH 10 M. Alcalase 2.4 L 2% was added and the sample was subjected to ultrasounds by means of a probe-type 19 mm ultrasonic horn (SONICS Vibra-cell, VCX750, USA) pulse on for 2'', and off for 4'', using a frequency of 20 kHz and a power of 750 W, for two hours at 65 °C. Then, enzymatic activity was inhibited by a heat shock at 95 °C for 10 min. Sample was then freeze-dried and labelled as BPH-US+ALC stored at -20°C for further use.

6.2.6 Evaluation of degree of hydrolysis (DH)

Degree of hydrolysis (DH) of the two hydrolysates was determined according to the protocol (Nielsen et al., 2001). 36 µL of sample or blank or serine standard (0.9516 meqv/L in bidistilled water) were added to each microwell in triplicate, together with 270 µL of OPA reagent prepared according to the protocol reported in literature (Nielsen et al., 2001). Then they were mixed for 5s. OPA reacted with α-amino groups of peptides forming an adduct whose absorbance at 340 nm was measured on a Fluorescence multi-mode microplate reader CLARIOstar® Plus after two minutes. OD is the optical density. Measurements were performed in triplicate. Then DH was calculated according to (Nielsen et al., 2001).

6.2.7 Simulated gastrointestinal digestion

The in vitro gastrointestinal digestion (GID) of the three samples (M, BPH-ALC and BPH-US+ALC) was performed following the INFOGEST procedure reported by (Brodkorb et al., 2019; Minekus et al., 2014). Enzymatic activities, together with the preparation of digestive fluids (simulated salivary fluid (SSF), simulated gastric fluid (SGF) and simulated intestinal fluid (SIF)) were determined according to the protocol reported in the same references (Brodkorb et al., 2019; Minekus et al., 2014). Briefly, the oral phase was reproduced by diluting 1 g of reconstituted sample or control (1 mg of water) with 1 mL of simulated salivary fluid (1:1, w:v) without the addition of amylase. Then the oral bolus was acidified with HCl 2 M until pH 3 was reached and diluted (1:1 v/v) with SGF, then pepsin (2000 U/mL) was added to simulate the gastric phase and incubated for 2 hours. The reaction was then stopped by increasing the pH to 7 with NaOH 2 M. The last step of digestion, intestinal phase was simulated by diluting (1:1 v/v) the gastric chyme with the SIF containing pancreatin (based on trypsin activity to achieve 100 U/mL) and bile extract (10 mM) and incubated for 2 hours. Digestion was then stopped by heating at 100 °C for 5 minutes and then the samples were cooled in an ice bath. Samples were at this point centrifuged at 8000 rcf for 10 min at the temperature of 4 °C in an Avanti J-26S-XP centrifuge (Beckman Coulter). The supernatant was then stored at -20 °C until analyses.

The entire digestion was carried out inside reaction flasks placed into a Carousel 6 Plus Reaction Station™ (radleys, UK) kept at the temperature of 37 °C with the constant agitation generated by magnetic stir bars. Samples subjected to digestion were hydrated with the original amount of water calculated with the humidity, and the blank samples consisted in 1 mL water. Samples were labelled as (M-DGI, BPH-ALC-DGI, BPH-US+ALC-DGI).

6.2.8 Antioxidant assays

6.2.8.1 DPPH free radical-scavenging assay

DPPH radical scavenging activity of all samples was measured according to the protocol reported by (Bersuder et al., 1998). 100 µL of sample (M and BP at 10 mg/mL, BPH-ALC and BPH-US+ALC at 10 mg/mL, M-DGI at 5.5 mg/mL, BPH-ALC-DGI and BPH-US+ALC-DGI at 6.3 mg/mL) or blank or positive control were

mixed with 500 µL of ethanol and 125 µL of DPPH solution (0.02% in ethanol). Water was used as blank, while BHT (20 mg/mL) was used as positive control. The mixtures were incubated for 60 min in the dark at room temperature and then the reduction of DPPH radicals was measured at 517 nm by using an UV-Vis spectrophotometer (Cary 60 UV–visible spectrophotometer, Agilent Technologies, CA, USA). Lower absorbance values indicated higher free radical scavenging activity.

The radical scavenging activity was calculated as follows:

$$\text{DPPH activity } (\%) = \frac{(\text{Absorbance negative control} - \text{Absorbance sample})}{\text{Absorbance negative control}} \times 100 \quad (6.1)$$

Trolox at different concentration levels (0.02 to 0.3 mM) was measured to obtain a calibration curve. Results were expressed as nmol of trolox equivalent antioxidant capacity (TEAC) per mg of sample. Measurements were performed in triplicate.

6.2.8.2 ABTS radical-scavenging capacity

The ABTS assay was determined according to the (Re et al., 1999) method and modified by (Gallego et al., 2020; Gallego, Mora, & Toldrá, 2018). Briefly, 11.4 mg of ABTS were solubilized in 3 mL of potassium persulfate (2.45 mM) mixed and stored at room temperature overnight to produce the radical cation $ABTS^{\cdot+}$ (ABTS stock solution). Before the analysis, ABTS working solution was prepared by diluting ABTS stock solution with Phosphate buffer saline (PBS, 50 mM, pH 7.4) until the absorbance of 0.70 ± 0.02 at 734 nm was reached. A total of 10 µL of sample (M and BP at 10 mg/mL, BPH-ALC and BPH-US+ALC at 5 mg/mL, M-DGI at 0.6 mg/mL, BPH-ALC-DGI and BPH-US+ALC-DGI at 0.6 mg/mL) or blank or positive control was mixed with 990 µL of ABTS working solution and incubated for 6 min in the dark. Then absorbance at 734 nm was measured on a UV-Vis spectrophotometer (Cary 60 UV–visible spectrophotometer, Agilent Technologies, CA, USA). Trolox at different concentration levels (0.05 to 2 mM) was used to obtain a standard curve. Results were expressed as nmol of trolox equivalent antioxidant capacity (TEAC) per mg of sample. Ascorbic acid (4mM in PBS) was used as positive control. Measurements were performed in triplicate.

6.2.8.3 Ferric-reducing antioxidant power (FRAP) assay

The ferric-reducing power activity was evaluated following the procedure reported by (Huang et al., 2006). In brief, 70 µL of each sample (M and BP at 10 mg/mL, BPH-ALC and BPH-US+ALC at 5 mg/mL, M-DGI at 5.5 mg/mL, BPH-ALC-DGI and BPH-US+ALC-DGI at 6.3 mg/mL) were mixed with 70 µL of sodium phosphate buffer (200 mM, pH 6.6) and 70 µL of potassium ferricyanide (10 mg/mL) and incubated for 20 min at 50 °C. Then, 70 µL of TCA (100 mg/mL) were added and then the mixture was centrifuged with a MPW-150R centrifuge (2000 rpm for 10 min). Then 250 µL of the supernatant were mixed with 250 µL of bidistilled water and 50 µL of ferric chloride, measuring the absorbance at 700 nm. Higher absorbance values indicate higher ferric-reducing antioxidant power. BHT (20 mg/mL) was used as positive control. Measurements were performed in triplicate.

6.2.8.4 Oxygen radical absorbance capacity (ORAC)

ORAC antioxidant test was performed following the procedure described by (Dávalos et al., 2004) with the modification of (Gallego, Mora, & Toldrá, 2018). Briefly, 140 µL of sample (M and BP at 0.05 mg/mL, BPH-ALC and BPH-US+ALC at 0.0025 mg/mL, M-DGI at 0.009 mg/mL, BPH-ALC-DGI and BPH-US+ALC-DGI at 0.0105 mg/mL) in sodium phosphate buffer (75 mM, pH 7.4) were mixed with 70 µL of fluorescein (200 nM) and incubated for 15 min at the temperature of 37 °C in the dark. Then 70 µL of AAPH were added (80 mM), and the fluorescence was measured every minute for 100 min using excitation and emission wavelength of 485 and 538, respectively using a Fluorescence multi-mode microplate reader CLARIOstar® Plus. Different concentration level of Trolox (from 1.5 to 16 µM) were used to build a calibration curve, and tryptophan (1.5 µM) was used as positive control. The area under curve (AUC) was calculated for each sample by integrating the relative fluorescence curve, and the values were plotted against the concentration of Trolox. Results were expressed as nmol of TE (Trolox equivalents) per mg of sample. Measurements were performed in triplicate.

6.2.9 Statistical analysis

To evaluate significant differences of antioxidant activity among mean values of the different samples, Analysis of variance (ANOVA) followed by Tukey's Honest

Significant Difference (HSD) test was performed, with a significance level of $p < 0.05$. These statistical analyses were carried out using XLSTAT trial version.

6.2.10 HPLC-MS/MS characterization

6.2.10.1 Purification of fish extracts and hydrolysates

All freeze-dried samples were dissolved in H_2O 0.1% (*v/v*) trifluoroacetic acid (TFA) at a concentration of 4 mg mL^{-1}, sonicated for 30 min, and centrifuged at 8100 x *g* at 4 °C for 15 min to remove debris. Later, two 500 µL aliquots of each sample (corresponding to around 2 mg) were purified to obtain medium- and short-sized peptide extracts.

6.2.10.2 Purification of medium-sized peptides

Medium-chain peptides were enriched by SPE on Bond elut C18 EWP cartridges (50 mg) as previously described (Cerrato, Aita, Cavaliere, et al., 2021), with minor modifications. Before sample loading, the adsorbent was washed with 3 mL of ACN and 3 mL of H_2O 0.1% (*v/v*) TFA. Each sample (500 µL) was diluted to 3 mL with H_2O 0.1% TFA and loaded. After loading, the cartridge was washed with 3 mL of H_2O 0.1% TFA, and peptides were eluted with 500 µL of ACN/0.1% TFA 50:50 (*v/v*). The eluate was evaporated at 45°C in the Speed-Vac SC250 Express (Thermo Savant, Holbrook, NY, USA). The residue was reconstituted in 100 µL of H_2O 0.1% FA.

6.2.10.3 Purification of di- and tripeptides

Short peptides were purified using Ultrafiltration (UFM) Discs, 1 kDa NMW (Ultracel®) regenerated cellulose, 44.5 mm in diameter as described (Cerrato et al., 2023). Firstly, membranes were pre-treated and rehydrated in H_2O for 1 h to remove impurities from the manufacturing process or additives used for stabilization. After that, the membranes were washed three times with pure water and stored before use. Then, the filter was rinsed three times with 3 mL of MeOH, once with 1 mL of deionized H_2O 0.1% (*v/v*) TFA and stored before use. Each sample (500 µL) was diluted to 3 mL with pure H_2O, loaded onto the membrane, and filtered by a Millipore classic glass filter holder. The filtrate, containing short-chain peptides, was recovered and dried. The residue was reconstituted in 200 µL of pure H_2O.

6.2.10.4 Analysis of medium-chain peptide mixture by nano-HPLC-MS/MS

Medium-chain peptide mixtures were analyzed by nanoHPLC-MS/MS on an Ultimate 3000 (Thermo Fisher Scientific, Bremen, Germany) coupled to an Orbitrap Elite mass spectrometer (Thermo Fisher Scientific). The medium-chain peptide mixture was analyzed as previously described (Cerrato, Capriotti, et al., 2020), with some modifications. Twenty µL of sample was online preconcentrated on a µ-precolumn (Thermo Fisher Scientific, 300 µm i.d. × 5 mm Acclaim PepMap 100 C18, 5 µm particle size, 100 Å pore size) at 10 µL/min flow rate of a premixed mobile phase containing H_2O 0.1 % (*v/v*) TFA. Separation was conducted on an EASY-Spray column (Thermo Fisher Scientific, 15 cm × 75 µm i.d. PepMap C18, 3 µm particles, 100 Å pore size) operated at 300 nL/min and 35 °C. A 90 min-long gradient was employed using H_2O and ACN as mobile phases A and B, respectively, both with 0.1 % formic acid. The following linear gradient was used: 1 % B for 5 min; 1–5 % B in 2 min; 5–35 % B in 90 min; 35–90 % B in 3 min. Finally, the column was washed at 90 % B for 10 min and then equilibrated at 1 % B for 30 min. Peptide spectra were acquired in the 300–2000 *m*/*z* range at 30,000 resolution (full width at half maximum, FWHM, at *m*/*z* 400) for the full scan. MS/MS spectra were acquired at 15,000 resolution (FWHM, at *m*/*z* 400) in top 10 data-dependent acquisition (DDA) mode on monoisotopic precursors and with the rejection of singly charged ions and unassigned charge states. Precursors were fragmented by higher-energy collisional dissociation (HCD) with 35 % normalized collision energy and 2 *m*/*z* isolation window and 30 ms activation time. Dynamic exclusion was enabled with a repeat count of 1 and a repeat duration of 30 s with an exclusion duration of 20 s. For each sample, three technical replicates were performed. Raw data files were acquired by Xcalibur software (version 2.2, Thermo Fisher Scientific). Peptide spectra matching was achieved using MaxQuant (http://maxquant.org/, version 1.6.3.4) (Cox & Mann, 2008) with the Andromeda search engine (Cox et al., 2011). The database used for spectra matching was UniProtKB for *Gadidae* family (https://www.uniprot.org/taxonomy/8045, taxon ID 8045, downloaded from UniProt website on 04/12/2023, 64881 entries). Reverse database search was enabled, and a database of common contaminants was used to remove false positive identifications. Oxidation on methionine and acetyl on protein N-term were set as a variable modification. Maximum 2 modifications were

considered for each peptide. Digestion was unspecific and minimum peptide length was set to 5. Spectra were matched considering HCD fragmentation with a 20 ppm error on product ions and a 10 ppm error on precursor ions.

6.2.10.5 Analysis of short-chain peptide mixture by UHPLC-MS/MS

Short-chain peptide mixtures were analyzed by LC-HRMS in a suspect screening fashion as previously described (Cerrato, Aita, et al., 2020) using a Vanquish binary pump coupled to a hybrid quadrupole-Orbitrap Q Exactive mass spectrometer (Thermo Fisher Scientific) through a heated electrospray source (HESI). Samples were separated by a Kinetex XB-C18 (100 × 2.1 mm, particle size 2.6 μm, Phenomenex, Torrance, CA, USA) operated at 40 °C. A 35 min-long gradient was employed using H_2O and ACN as mobile phases A and B, respectively, both with 0.1 % TFA. Spectra were acquired in the positive ion mode range *m/z* 150–750 with a resolution (full width at half maximum, FWHM, *m/z* 200) of 70,000. For each sample, three individual runs were acquired using a dedicated inclusion list containing the exact *m/z* of the protonated ions of all unique di- and tripeptide masses. The inclusion list was prepared using MatLab R2018, as previously described (Cerrato, Aita, et al., 2020). The acquisition of the higher collisional dissociation (HCD) MS/MS spectra was performed using the top 5 data-dependent acquisition (DDA) mode at 35 % normalized collision energy and 35,000 (FWHM, *m/z* 200) resolution. All samples were run in triplicate. The identification of the short endogenous peptidome was achieved by processing RAW data files and blank samples using a dedicated data processing workflow implemented on Compound Discoverer 3.1 (Thermo Fisher Scientific) by our research group (Cerrato, Aita, et al., 2020). Data pre-processing tool includes the extraction of the masses from RAW data files, their alignment, removal of black signals, features that were not associated with at least one MS/MS spectrum, as well as features whose masses were not present in the mass list. Control DGI was used as a process blank to simultaneously remove contaminants and peptides deriving from the hydrolytic enzymes. After data-preprocessing, the identification of the short sequences was carried out by manual interpretation of the MS/MS spectra aided either by using the compound class scoring tool, which allowed to automatically match the experimental MS/MS spectra to the typical product ions deriving from amino acids at N-terminus, C-terminus, and in the middle of the sequence, or by comparison with in-

silico spectra generated by mMass (Strohalm et al., 2010). Leucine (Leu) and isoleucine (Ile) in a sequence were distinguished by comparing the RT and abundance of diagnostic ion at *m/z* 69.0698 of the two peptide isomers when both were annotated (Xiao et al., 2016). The sec-butyl group of Ile is more polar (lower RT) and more stable as a carbocation (higher abundance of *m/z* 69.0698) than the isobutyl group of Leu. Otherwise, Leu/Ile were annotated as Xle (J), which implies either of the two amino acids.

6.3 Results and discussion

6.3.1 Antioxidant activity assays

The antioxidant activity of the samples was evaluated by DPPH free radical scavenging assay, ABTS radical scavenging assay, Oxygen Radical Absorbance Capacity (ORAC) and Ferric-reducing antioxidant power (FRAP) assay.

Different tests were performed as they are based on different properties and there is not a standardized assay for the antioxidant activity evaluation. ABTS, DPPH and FRAP are generally classified as electron transfer (ET) based methods, even if DPPH and ABTS can also act as hydrogen transfer methods (HAT) as well as ORAC (Prior et al., 2005).

Antioxidant activity of the fish muscle sample was evaluated before and after gastrointestinal digestion. Whereas DPPH and FRAP antioxidant tests showed a decrease of the antioxidant activity after the simulated gastrointestinal digestion, ABTS radical-scavenging assay and ORAC showed a higher antioxidant activity (figure 6.1). This can be related to the fact that these differences in antioxidant activity can be related to the different selectivity of the test. Since peptides are constituted of amino acids of different nature, they have different physicochemical properties. In this regard, DPPH and FRAP correlate well with the peptide hydrophobicity, whereas no correlation exists with hydrophobicity and ABTS and ORAC tests. A similar trend resulted from the simulated gastrointestinal digestion of dry-cured ham (Gallego et al., 2020).

Regarding the by-product samples (figure 6.2), alcalase hydrolysis and ultrasound assisted hydrolysis were evaluated as possible sources of antioxidant peptides. In three of the four tests (DPPH, ABTS and ORAC), the increase of the antioxidant activity

from the control (BP) to the hydrolysed samples (BPH US+ALC and BPH ALC) was statistically significative ($P > 0.05$). Moreover, ultrasound assisted reaction has led to a higher antioxidant activity which is statistically significant in DPPH and ABTS assays.

Furthermore, the effect of simulated gastrointestinal digestion was evaluated on the antioxidant properties of these hydrolysates, to understand the effective bioavailability once they are subjected to the digestion. A statistically significant increase of the antioxidant activity was registered in ABTS (for both BPH US+ALC and BPH ALC), and in DPPH (only for BPH ALC) assays. Only in FRAP assay (BPH US+ALC) a statistically significant decrease of the antioxidant activity was registered.

The action of alcalase, and further GI enzymes leads to the breakdown of peptides, release of amino acids and/or exposition of internal groups, affecting the size, amount and physico-chemical characteristics, thus affecting their antioxidant capacity. In fact, the amino acid composition and structure of peptides as well as their solubility in the reaction media have the greatest influence on the antioxidant activity (Samaranayaka & Li-Chan, 2011; Sarmadi & Ismail, 2010).

Sometimes peptides showing in vitro bioactivity are inactive in the human body after ingestion mainly due to the action of salivary, gastric and intestinal enzymes, that hydrolyse them into smaller size peptides that lose their bioactivity. What is more, small bioactive peptides can be hydrolysed in the intestine by peptidases of the microbial flora, by brush border peptidases in the epithelium of the intestinal membrane, or even by peptidases in the blood stream. Thus, in vivo assays are always necessary in order to confirm the physiological effects of bioactive peptides in the organism.

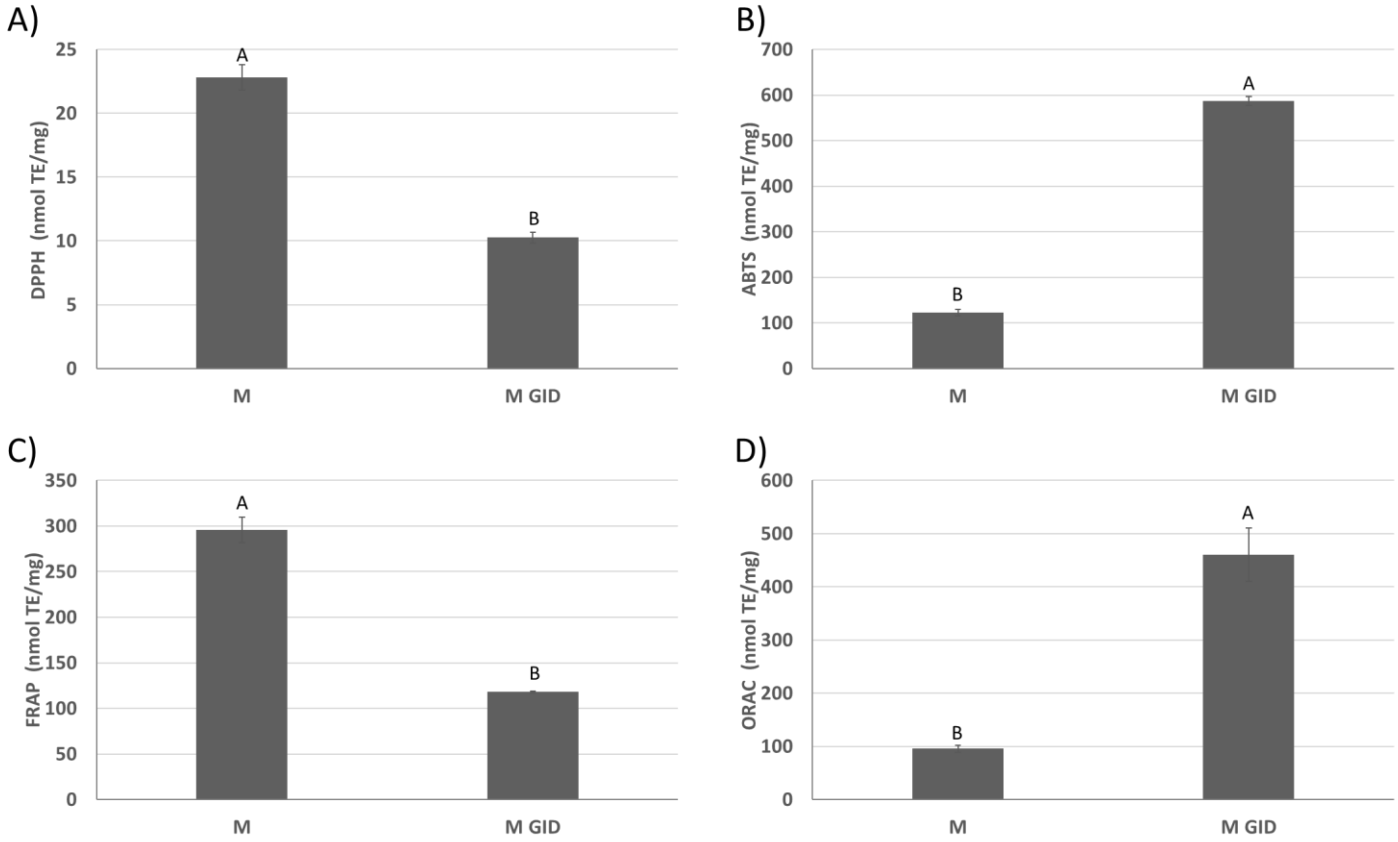

Figure 6.1 Antioxidant activity of the undigested and digested fish muscle samples expressed as Trolox Equivalent (nmol TE/mg of sample) and determined by (A) DPPH free radical scavenging assay, (B) ABTS radical scavenging assay, (C) Oxygen Radical Absorbance Capacity ORAC, (D) Ferric-reducing antioxidant power (FRAP) assay. Results are expressed as means ± standard deviation. Capital letter indicates significant differences between digestion steps: before (M) and after digestion (M GID) within the same sample ($P < 0.05$).

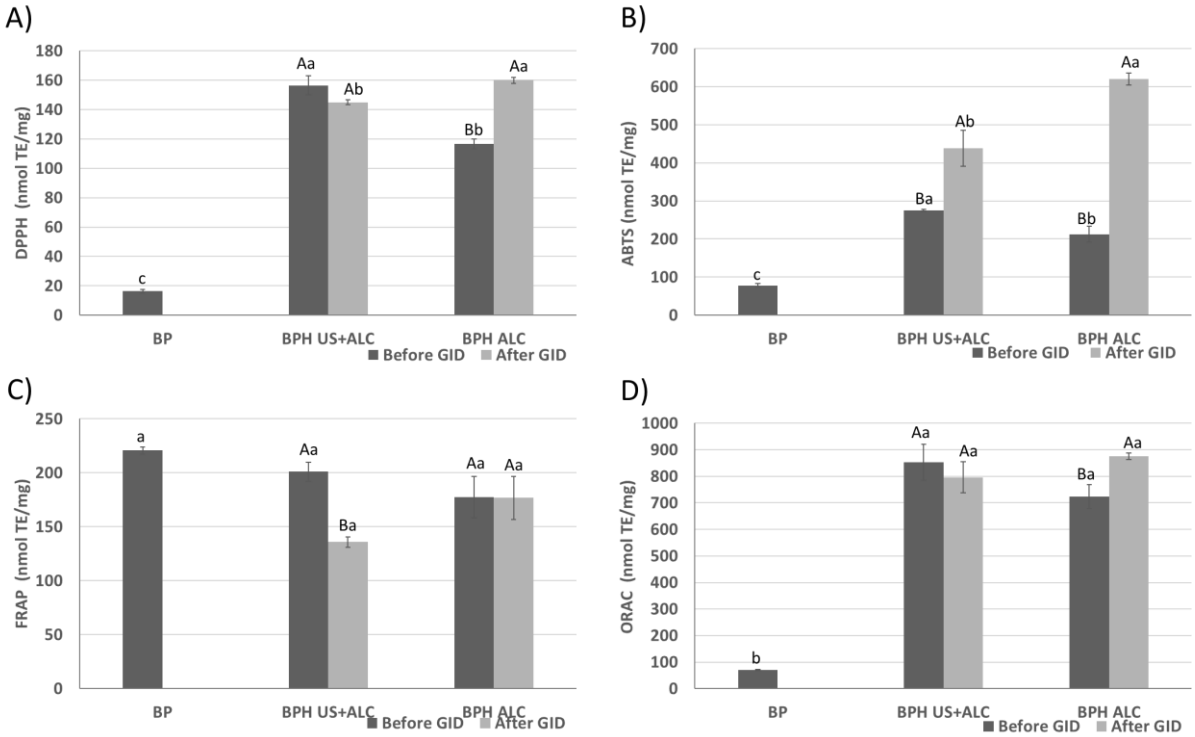

Figure 6.2 Antioxidant activity of the fish by-product samples: not hydrolysed (BP), hydrolysed with ultrasound assisted alcalase hydrolysis (BPH US+ALC) before and after gastrointestinal digestion (before GID and after GID) and with alcalase hydrolysis (BPH ALC) before and after digestion. The antioxidant activity was determined by (A) DPPH free radical scavenging assay, (B) ABTS radical scavenging assay, (C) Ferric-reducing antioxidant power (FRAP), (D) Oxygen Radical Absorbance Capacity ORAC assay. Results are expressed as means of Trolox Equivalent (nmol TE/mg of sample) ± standard deviation. Lowercase letter indicates significant differences between samples within the same digestion step, i.e. before GID, between BP, BPH US+ALC, BPH ALC and after GID between BPH US+ALC, BPH ALC ($P < 0.05$). Capital letter indicates significant differences between digestion steps, before and after digestion within the same sample i.e. BPH US+ALC (before and after digestion) BPH ALC (before and after digestion) ($P < 0.05$).

6.3.2 Nano-HPLC medium sized peptide characterization

The number of medium sized peptide sequences identified are reported in table 6.1. Regarding the by-product sample, the hydrolysis and the further gastrointestinal digestion step have led to the breakdown of the proteins and peptide sequences, leading to the reduction of their chain-length. The number of proteins and peptides identified in each of the samples of by-products and muscle is reported in table 6.1.

Since the peptides under the length of five aminoacids cannot be identified by means of this methodology, a reduction of the identified sequences was found from the initial sample to the hydrolyzed and further digested one. This explains the higher antioxidant activity of the samples which have been subjected to the proteolysis. Moreover, the higher quantity of medium-sized peptides of BPH US ALC compared to BPH ALC means that the ultrasound assisted resulted less effective in the peptide bond breakage, even if the degree of hydrolysis resulted not so different, indeed it was 11.53% ± 1.02 and 12.03% ± 0.94 for the BPH ALC and BPH US ALC respectively. The same trend was found from the undigested and digested muscle sample, even if a higher percentage of proteins and peptides was found compared to byproduct. This can be related to the fact that fish muscle contains more proteins than by-products. Protein percentage were indeed 95.98% ± 0.65 and 68.59 ± 1.80 for muscle and by-products respectively.

Table 6.1 Number of protein and peptide sequences identified in each of the samples of by-products and muscle.

	Peptide sequences	**Protein sequences**
BP	218	44
BPH ALC	147	58
BPH ALC DGI	7	6
BPH US ALC	394	67
BPH US ALC DGI	2	11
M	744	67
M DGI	45	23

6.3.3 Short sized peptide characterization

The peptide size is one of the most important characteristics for their biological activity. Therefore they can easily be absorbed, resisting to hydrolysis by

gastrointestinal proteases and serum peptidases, and can be transported in their biological target (Wang et al., 2019).

Regarding the antioxidant activity, although there is not a strict relationship between the antioxidant activity and the molecular weight of the peptides, most of the reported antioxidant peptides from food proteins are usually between 3 and 6 amino acids showing MWs lower than 1000 Da (Zou et al., 2016). However, due to different reasons they are more difficult to identify and therefore a different method for the identification is needed. This can be attributed to three different issues:

1. These classes of peptides have a wide range of physicochemical properties, principally polarity, are molecular weight, polarity and acid-base properties, which makes not perfectly suitable the typical C18 reverse phase (RP) separation, standardly employed in proteomics and medium-sized peptidomics (Cerrato, Aita, Montone, et al., 2021).
2. Short-chain peptides have a poor ionization efficiency when the common electrospray ionization is used. In fact, short-chain peptides generate low-abundance and singly charged precursor ions, hindering the use of common nano-HPLC-MS approaches which are mainly based to multi-charged ions.
3. Peptide sequences cannot be confidently identified by common proteomics software. Such short-chain sequences, in fact, cannot be uniquely attributed to proteins present in the databases because they are shared between more proteins (Cerrato, Aita, et al., 2020).

To overcome these issues di- and tripeptides were analysed separately. Indeed, they have been isolated by means of Ultrafiltration (UFM) and then the suspect screening approach developed by (Cerrato, Aita, et al., 2020) was used for the precursor selection. In this case, the selection is based on an inclusion list containing the exact *m/z* of the protonated ions of all unique di- and tripeptide masses, gaining a lower sensitivity, and therefore the identification of a higher number of sequences. This method allowed to overcome the issues of both DDA and DIA. A total of 415 di and tripeptides have been identified in all the samples, of which 36 were generated by autolysis of the DGI enzymes and therefore discarded. 55 of them had areas smaller than the background noise threshold (10^6) in the DGI-treated samples meaning that they were not resistant to the gastrointestinal digestion.

The remaining 324 peptides which is the majority demonstrated to be resistant to the gastrointestinal digestion and potentially, being also small sized, they can potentially cross the intestinal barrier and reach the blood stream to exert their biological activity. This explains the maintenance of the in vitro antioxidant activity after the gastrointestinal digestion.

6.4 Conclusions

The enzymatic hydrolysis performed by means of alcalase has led to an increase in the antioxidant activity of the byproduct sample, demonstrating the possibility of valorisation of this byproduct into a source of antioxidants. Moreover, the activity demonstrated to not decrease after the gastrointestinal digestion, meaning that these peptides are resistant to the digestion, or in any case new antioxidant peptides are formed. Of course, many other factors influence the bioavailability, therefore in vivo studies are necessary to confirm the activity. Further studies need to be performed for assessing the most active peptides by in silico antioxidant activity evaluation.

Part II

Development of High-resolution LC-FTIR prototype

Chapter 7

The online coupling of liquid chromatography to fourier transform infrared spectroscopy using a solute-deposition interface: a proof of concept

7.1 Introduction

The effectiveness of liquid chromatography (LC) hyphenated to spectroscopic detection in providing structural information about non-volatile and polar constituents of complex samples is undisputed. However, accurate identification of isomeric compounds remains a challenge for most analytical methods, and additional information may be required, for example, for confident discrimination of conformational isomers. Basically, three distinct techniques may serve this purpose: mass spectrometry (MS), nuclear magnetic resonance (NMR), and Fourier transform infrared spectroscopy (FTIR). The advantages of MS include the capacity for extremely low detection limits and the availability of high-performance LCMS interfaces; at the same time, differentiation of compound isomers requires dedicated experiments based upon specific consecutive fragmentation processes, usually performed by electrospray multistage MS or high-resolution MS ($ESIHRMS^n$) (Bianco et al., 2020; Schwarzenberg et al., 2014). In spite of the experimental complexity, the physical connection of LC and NMR has been pursued using different strategies, including on-flow, stopped-flow, and loop-storage operation, to achieve unequivocal structural information for the individually isolated compounds (Gathungu et al., 2020). However, the rather poor sensitivity of NMR remains a limiting factor, and additional techniques such as the use of multiple trapping, solid-phase cartridges, or cryogenic probes were deemed necessary when dealing with limited sample amounts (Exarchou et al., 2003). Vibrational spectroscopy, including FTIR and Raman techniques, has

long been valued for its ability to uniquely identify a wide range of samples in a rapid and non-destructive manner by providing a distinctive fingerprint of the molecules. Specifically, absorption of the IR beam in the mid-IR spectrum (4000–400 cm^{-1}) by the functional groups in a molecule result in stretching, bending, deformation, or a combination of these vibrations, which provide a unique spectral fingerprint of each chemical or biochemical compound (Balan et al., 2019). Thus, the information obtained by mid-IR spectroscopy is more useful at the analytical level than the overtone and harmonic vibrations that are provided by the near-IR region (12,500–4000 cm^{-1}) (Hashimoto & Badarla, 2019). Modern FTIR instrumentation would, in principle, allow for spectra to be recorded from nanograms or even picograms of pure substances, and would thus meet the requirements for the detection of analytes at the levels usually achieved in LC (Andersen et al., 2016; Kebukawa et al., 2019). Unfortunately, absorption from the mobile phase can obscure detection of the LC-eluted analyte bands, and this has posed a great challenge for the coupling of LC and FTIR. Moreover, the interference from water in the mid-IR region is a major hurdle, since it can hinder light penetration into the sample and furthermask some key information useful for molecular recognition (Hackshaw et al., 2020; Pachetti et al., 2020). As a consequence, progress in LC-FTIR hyphenation has been a slower and more difficult route relative to its gas chromatography counterpart (GC-FTIR).

Early online LC-FTIR techniques based on the flowcell approach achieved very limited success, as authoritatively reviewed by (Somsen et al., 1999; Somsen & Visser, 2000) and references therein). In this configuration, the effluent from an LC column is passed through an IR-transparent cell, and the IR spectra of the separated compounds are acquired continuously, in a similar fashion as in online LC with UV-Vis spectroscopy. In spite of the ease of operation and maintenance, this technique is severely limited by the low sensitivity (requiring 1000–10,000 ppm injections of the analytes) and the scarce spectral information obtained, both of which are affected by the IR absorption of the solvents, and especially when aqueous LC eluents are used. A second approach, relying on LC solvent elimination prior to IR detection, provides a number of advantages: (i) removing or minimizing the solvent and air interference, (ii) maximizing the optical absorptivity, and (iii) preserving the chromatographic resolution (Kuehl & Griffiths, 1979). Solvent-elimination LC-IR techniques use an

interface that evaporates the LC eluent and deposits the separated compounds onto a moving IR-transparent substrate, where IR spectra are measured from the solid spots, allowing for the acquisition of interference-free and highly informative IR spectra independently of the chromatographic conditions. One option is that the deposited traces are moved offline through the IR beam after the LC separation is complete, and the reconstructed LC-IR chromatogram is assembled by the software after the scanning is complete; alternatively, collection of the IR spectra may take place in real time during the deposition process (Kok et al., 2003). Apart from the gain in sensitivity (down to nanograms) and resolution (typically, 4 cm^{-1}), a further advantage of LC-FTIR techniques based on trapping of analytes is the possibility for post-run signal averaging to improve detectability. Nonetheless, the LC-FTIR technique in the solid state is technical demanding and dictates a number of requirements for the coupling to be successful in terms of interface efficiency, LC flow rate, and composition of the eluent. Different approaches have been proposed over time based on various LC-IR interfaces, including thermospray, particle beam, electrospray, and pneumatic and ultrasonic nebulizer techniques (Somsen et al., 1998). Although capable of generating aerosols from the liquid stream and partial desolvation of the stream, none of those systems is able to effectively separate the solvent vapor and non-condensable carrier gas from the particulate stream in a reliable and robust manner. Likewise, the LC-IR sample delivery system developed by (Carson WW & Bourne S, 2014) relied on a small-scale self-regulating spray dryer, allowing for desolvation of the LC eluent stream while retaining temporal resolution of the dissolved substrates. Briefly, the system's operational steps include (i) the creation of a high-speed jet of micrometer-sized liquid droplets in an automated nebulizer, (ii) solvent evaporation from the droplets in a cyclone cavity, (iii) solvent vapor elimination onto cooled condenser walls, and (iv) focused deposition of the dried analytes onto a ZnSe disc for continuous transmission IR analysis. During operation, the temperature of the disc surface is controlled to trap the sample particles, and the vacuum provides thermal insulation and facilitates rapid removal of any residual solvent captured on the disc. Notably, this interface allows for operation with all common chromatography solvents (from 100% water through low- and high boiling point organic and halogenated solvents), with mobile-phase flows compatible with conventional LC columns (typically between 0.5

and 2 mL/min). This analytical tool has been demonstrated for the analysis of copolymer excipients, aimed at measuring lot-to-lot variations, and identification and characterization of melt processing degradation and compositional stability (Carson et al., 2011).

The present study aimed to investigate the potential of pneumatically assisted LC-FTIR in terms of the limit of identification and limit of quantification, and the way that the different interface operational parameters may affect the detection of small polar molecules like coumarins. These compounds are used in the food and fragrance industries (Garrard, 2014), and also display a remarkable array of biochemical and pharmacological activity, as shown by studies of the structure– activity relationship (SAR) (Önder, 2020; Penta, 2016). Among the coumarin groups, furanocoumarins have unique phototoxicity, which occurs under UV radiation; harmful effects include photodermatitis and cytotoxic and mutagenic disorders. Furanocoumarins are subdivided into a linear type, generically known as psoralens, where a furan ring is attached at the 6,7 positions of the benzopyrane-2-one ring, and an angular type, generically known as angelicins, where the ring is attached at the 7,8 positions of the coumarin structure (Christensen, 2018). In this research, psoralen and angelicin were selected as the parent molecules of the two types to demonstrate the proof of concept of the potential of LC-FTIR to discriminate between structural isomers in a fast, accurate, and reliable way.

7.2 Materials and methods

7.2.1 Solvents and chemicals

LiChrosolv water (LC-MS grade) and methanol (hypergrade for LC-MS) used as LC eluents and ethanol used as diluent for preparing stock and diluted analyte solutions were obtained from Merck Life Science (Darmstadt, Germany). Analytical standard grade (>98%) psoralen (furo[3,2-g]chromen-7-one, $C_{11}H_6O_3$, MW186.16) and angelicin (furo[2,3-h]chromen-2-one, $C_{11}H_6O_3$, MW 186.16) were obtained from Labochem Science (Catania, Italy).

7.2.2 Sample preparation

Standard solutions Stock solutions of the standard psoralen and angelicin (1000 μg/mL each) were prepared in ethanol, filtered through a 0.22 μm nylon membrane (Merck Life Science, Darmstadt, Germany), and stored at −6 °C until use. Working solutions of the standard material for linearity and repeatability studies and for determining the limit of detection (LOD) and the limit of quantification (LOQ) were prepared in a concentration range of 50–1000 μg/mL at five concentration levels, i.e., 50, 100, 250, 500, and 1000 μg/mL, in ethanol. The precision was estimated from three consecutive 5 μL injections performed on an intraday basis. The intermediate precision was estimated from 15 injections (5 μL) performed over three consecutive days.

7.3 Instrumentation and analytical conditions

7.3.1 LC analyses

A Nexera XR high-performance liquid chromatography (HPLC)-photodiode array detector (PDA) system (Shimadzu Europa, Duisburg, Germany) was used for the LC analyses. The instrument consisted of a CBM-20A controller, two LC 20AD parallel-flow pumps, a DGU-20A5R degassing unit, a CTO-20AC column oven, a SIL-20AC autosampler, and an SPD-M20A PDA detector. The separations were carried out on an Ascentis Express C18, 150 mm L × 4.6 mm i.d., 2.7 μm d.p. from Merck Life Science (Darmstadt, Germany). The mobile phase consisted of water (solvent A) and methanol (solvent B), and the elution gradient was as follows: 0 min, 15% B; 4.5 min, 28% B; 7 min, 60% B; 11 min, 85%B; 14min, 85%B. The flow rate was 1mL/min, and the injection volume was 5 μL. UV-Vis spectra were acquired at a sampling frequency of 4.1667 Hz (time constant 0.480 s) in a wavelength range of 190–370 nm, and a wavelength of 315 nm was selected for extracting the chromatograms.

7.3.2 LC-FTIR interface and FTIR analyses

The capillary exiting the HPLC-PDA system was connected to a hyphenated solvent removal interface (Spectra Analysis Instruments, Inc., Marlborough, MA, USA). After the majority of the solvent vapor had been removed by the interface, the sample aerosol was drawn to the DiscovIR-LC system (Spectra Analysis Instrument Inc., Marlborough, MA, USA). The aerosol was directed through a nozzle that focused the

particles onto the surface of an IR-transparent ZnSe disc, which was maintained at a controlled temperature (20 °C) by means of liquid nitrogen and cleaned daily with acetone. The DiscovIR-LC system was equipped with a mercury cadmium telluride (MCT) cryogenically cooled detector. Solid phase IR spectra of the LC-eluted compounds were recorded in real time from 10 μm × 10 μm spots in a range of 4000–650 cm^{-1} at a resolution of 4 cm^{-1}. Interface parameters were set as follows: nebulizer voltage, 16 W; cyclone temperature, 180 °C; condenser temperature, 4 °C. Disc rotation speed was varied from 1 mm/min to 10 mm/min. To synchronize data acquisition from the PDA and IR detectors, the optimum optic lag setting was found as equal to 512.

7.3.3 LC and LC-FTIR data acquisition and processing

The LC instrument was controlled by LabSolution software (Shimazdu Europa, Duisburg, Germany). LC-FTIR data acquisition and processing were performed using the Thermo Galactic GRAMS/AI spectroscopy and chromatography software version 9.3 (Thermo Fisher Scientific, Waltham, MA, USA). A full spectrum was collected every 0.4 s. The spectra and updated chromatogram were displayed less than a minute after elution from the chromatograph and visualized and elaborated by DiscovIR 10 software (Spectra Analysis Instruments, Inc.). Compounds were identified through a library search program using a first derivative correlation algorithm by comparison with a solid-phase IR spectral library made in-house. The results expressed by the software in 0–1 units (where 0 represents the maximum value for similarity or quality score) were converted into 1–100% units (where 100 represents the maximum value for similarity or quality score), using the formula: Quality score = (1 − GRAMS value) × 100.

7.4 Results and discussion

In this research, instrumentation and a method are presented based on a pneumatically assisted LC-FTIR interface, and the feasibility of the hyphenated technique is demonstrated for reliable analysis of structural isomers in a fast and accurate manner. The chemical structures of furo[3,2-g]chromen-7-one and furo[2,3-h]chromen-2-one (commonly known as psoralen and angelicin, or isopsoralen) selected as the case study

are depicted in figure 7.1. A variety of approaches have been presented for the analysis of coumarins, including furanocoumarins, aiming to fulfill the requirements of the current regulations. The most commonly used method for the separation of these compounds has been reversed-phase (RP) and, to a lesser extent, normal-phase (NP) LC, used in conjunction with UV and MS detection (Boysen & Hearn, 2010; Dugo et al., 2012).

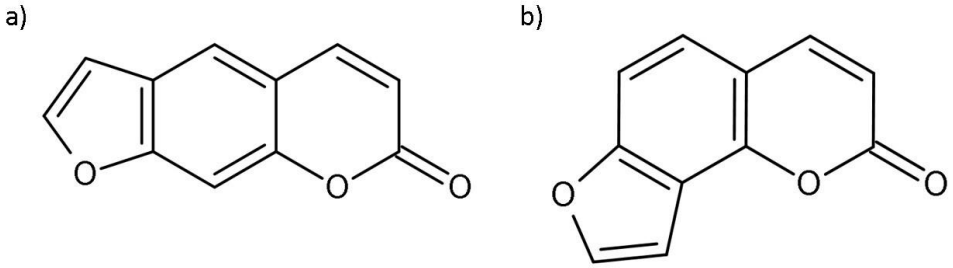

Figure 7.1 The chemical structures of a) psoralen (furo[3,2-g]chromen-7-one) and b) angelicin (furo[2,3-h]chromen-2-one).

These compounds exhibit strong absorbing chromophores, and these data, combined with tandem MS spectra recorded at different voltages, often provide the specificity of information needed for identification of the individual components in the samples. However, this is not the case for pairs of structural isomers such as bergapten/isobergapten or psoralen/angelicin (or isopsoralen) since these molecules undergo the same fragmentation pattern. The *m/z* transitions usually monitored for identification and quantification purposes (the so-called qualifier and quantifier ions) are identical, and moreover, their intensity ratios do not differ enough to allow for unambiguous discrimination. In such cases, the use of an additional parameter consisting of linear retention indices (LRI) to the spectral data is necessary, as well as consideration of the intrinsic limit of the MS/MS spectral library, which is based on only two fragment ions (Arigò et al., 2021). Unlike the retention time, which can change significantly with the instrument or laboratory used, the LRI depicts the retention behaviour of an analyte in a normalized manner, as independently as possible from the operating conditions.

7.4.1 Optimization of the LC-FTIR interface

The solvent-elimination approach is, by any evidence, more technically demanding than online LC-FTIR coupling. The first step of this research consisted in the optimization of the operational parameters of the interface to achieve effective evaporation of the eluent while at the same time preserving the chromatographic resolution during the deposition process. In this respect, the type of substrate material, the nature of the analytes, the LC flow rate, and the LC eluent composition are key factors. The substrate material used for deposition of the analytes must satisfy two key requirements, i.e., full compatibility with the chosen IR mode, and the absence of additional interference. As for the analytes, the general requisite of lower volatility with respect to the eluent is easily accomplished in LC. In our study, separation of the target compounds psoralen and angelicin was achieved under RP-LC conditions on a 15 cm octadecyl functionalized silica column of conventional diameter, operated at an optimum mobile-phase flow of 1.0 mL/min. The use of non-volatile additives was obviously precluded, and the rapid evaporation of such a volumetric flow of aqueous eluents (namely, a methanol gradient into water) required careful adjustment of the pneumatically assisted LC-FTIR interface parameters, and specifically the nebulizer voltage, cyclone temperature, and condenser temperature. Within the spray drier system of this interface, the LC eluent was pumped through a heated nebulizer which converted the liquid stream into a high-speed aerosol jet of micrometer-sized liquid droplets. The nebulizer was electrically heated by passing a current from end to end; the thin-wall metal capillary tube nebulizer must be regulated to evaporate approximately half the solvent. Mobile phases composed of solvents like chloroform and pure acetonitrile can be effectively nebulized without requiring any electrical power; likewise, under the LC gradients used in our study, in terms of composition, the nebulizer power was set using the highest power requirement. Specifically, for the water-to-methanol gradient employed, the nebulizer was set at 16 watts, while flowing at initial conditions of 1 mL/min of 85% water. The small offset from the theoretical 50% evaporation requirement (22 watts) took into account the initial percentage of eluent B (15%), as well as the amount of heat transferred to the nebulizer by thermal conduction from the cyclone body. A single setting of the control circuit automatically adjusts the nebulizer power (from 0 to 15 volts and up to 40 watts) to accommodate

wide changes in solvent composition (from pure water to pure organic solvent) and flow rate (from 0.2 to 2 mL/min). Solvent expansion upon conversion to vapor increases the nebulizer back pressure, which increases the solvent boiling point and the nebulizer operating temperature. The nebulizer wall temperature was monitored by changes in the tube's electrical resistance, and the nebulizer power was adjusted continuously using the capillary electrical resistance for feedback control (Carson WW & Bourne S, 2014).

The next operational step comprised solvent evaporation, i.e., centrifugal forces caused the liquid droplets to travel along the diameter of a hot cylindrical cavity, the so-called cyclone. The cavity surface was heated at 180 °C, which is far above the boiling point of the water component of the fluid stream, to cause the droplets to undergo film boiling. In film boiling, the evaporated solvent vapor blankets the heater surface, preventing droplet contact with the cavity wall, thereby retaining the solute in the droplets. A short residence time within the cavity and retention within the droplets is crucial to protecting the solute from thermal degradation. Afterwards, solvent vapor was eliminated by condensation onto a cooled unit, which was operated at 4 °C, i.e., above the freezing point of the solvent, to produce a liquid condensate that was continuously drained. The final critical step was to achieve focused deposition of the dried analytes, which were impacted through an orifice onto the optical surface, for continuous transmission IR analysis. The deposition interface, consisting of a rotating ZnSe disc, was located in an evacuated chamber and was temperature-controlled to freeze liquid solutes while allowing for sublimation of residual solvent. A low-level-vacuum (≈ 102 Pa) in the chamber was maintained by roughing pumps, preventing carbon dioxide and moisture in the environment from interfering with the measurements. The performance of the LC-FTIR technique ultimately relied on the proper setting of the parameters related to the disc operation, i.e., the disc temperature and the disc rotation speed. Both parameters require optimization to achieve the compound deposition into narrow spots in order to minimize band broadening and attain optimum IR sensitivity. A sufficient amount of chilling must be supplied to the disc to achieve trapping of the analytes, depending on their vapor pressures; a temperature of 20 °C was used for the compounds under study. Solid-phase IR spectra of the LC-eluted compounds were recorded in real time from 10 μm × 10 μm spots in

the range of 4000 650 cm^{-1} at a resolution of 4 cm^{-1}. A full spectrum was collected every 0.4 s; the spectra and updated chromatogram were displayed as they were collected, less than a minute after elution from the chromatograph. The calculation of IR response versus time was done with the use of a standard software package which utilizes a Gram-Schmidt reconstruction (GSR), resulting in the LC-FTIR chromatogram in figure 7.2.

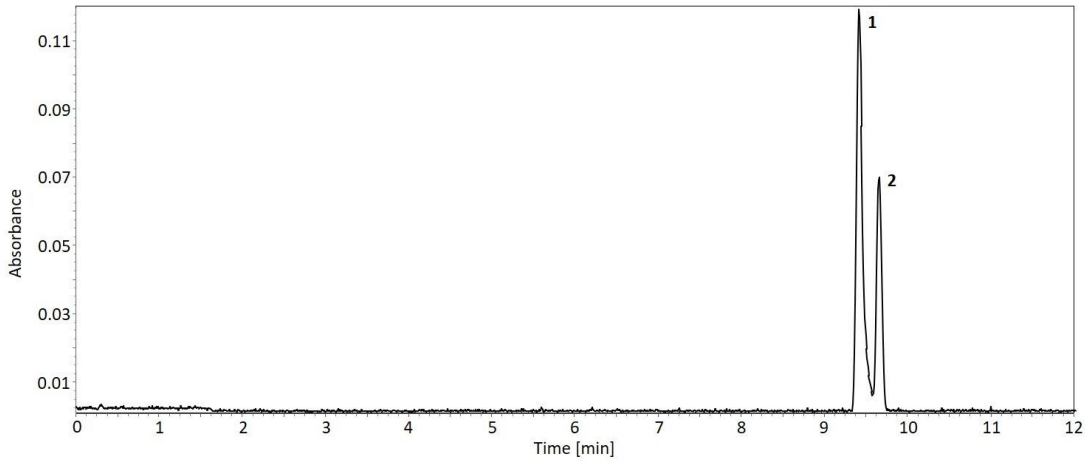

Figure 7.2 The Gram-Schmidt reconstructed LC-FTIR chromatogram of a standard psoralen (1) and angelicin (2) mixture in EtOH (max S/N chromatogram). Column: Ascentis Express C18, 150 mm L × 4.6 mm i.d., 2.7 μm d.p. (Merck Life Science, Darmstadt, Germany).

As the result of this reconstruction process, in a peak chromatogram the maximum absorbance detected anywhere in the mid-IR spectrum is plotted for every point in time. Under the selected experimental conditions, psoralen and angelicin were eluted within the first 10 min of the gradient; a 5 μL injection of the standard compound solution, corresponding to 1.25 μg of each analyte injected on the column, gave average chromatographic base peak widths of 15.8 s (peak 1, 39 data points) and 10.3 s (peak 2, 26 data points), at a disc rotation speed of 3 mm/min. Disc rotation continuously carried the deposit through the focal point of the internal IR microscope; thus careful control of the speed of the substrate should allow for concentrated deposits to be obtained, which will enhance analyte detectability. Matching the disc rotation speed to the amount of analyte being delivered by the deposition tip should afford a sufficient number of data points across the peak, depending on the detector acquisition

rate and the chromatographic peak width. However, in the case of closely eluting peaks, too slow a disc rotation rate would impair the chromatographic resolution. To address this concern, LC-FTIR analyses of the standard mixture were performed under the optimized conditions by increasing the disc speed from 1 to 10 mm/min in stepwise fashion to determine the best compromise between preserving the chromatographic resolution and maximizing the deposit thickness. The dependence of resolution (R_S) and signal intensity (maximum Y) as a function of the disc rotation rate is plotted in figure 7.3. In cases where incomplete peak separation occurred, by assuming the peak width at half the height for a Gaussian peak equal to 2.354σ, R_S was determined by the formula:

$$R_S = 1.18 \frac{t_{R2} - t_{R1}}{w_{h1} + w_{h2}} \qquad 7.1$$

where w_{h1} and w_{h2} are the peak widths measured at half the peak height. As expected, the two plots exhibited opposite trends, as the maximum signal intensity (0.177 AU) was obtained at the lowest disc speed (1 mm/min), albeit at the cost of (chromatographic) resolution, with R_S = 0.65. The latter gradually increased with increasing disc speed, and reached its maximum value (R_S = 2.15) at a disc speed of 10 mm/min. However, at such a high disc rotation speed, less time was allotted for the analyte deposition from the tip, and this inevitably led to a loss in sensitivity (0.062 AU). It can be appreciated from the plots in figure 7.3 that the two curves intersect at an x-axis value corresponding to a disc rotation speed of 3 mm/min, which thus represents the best compromise between peak resolution and sensitivity.

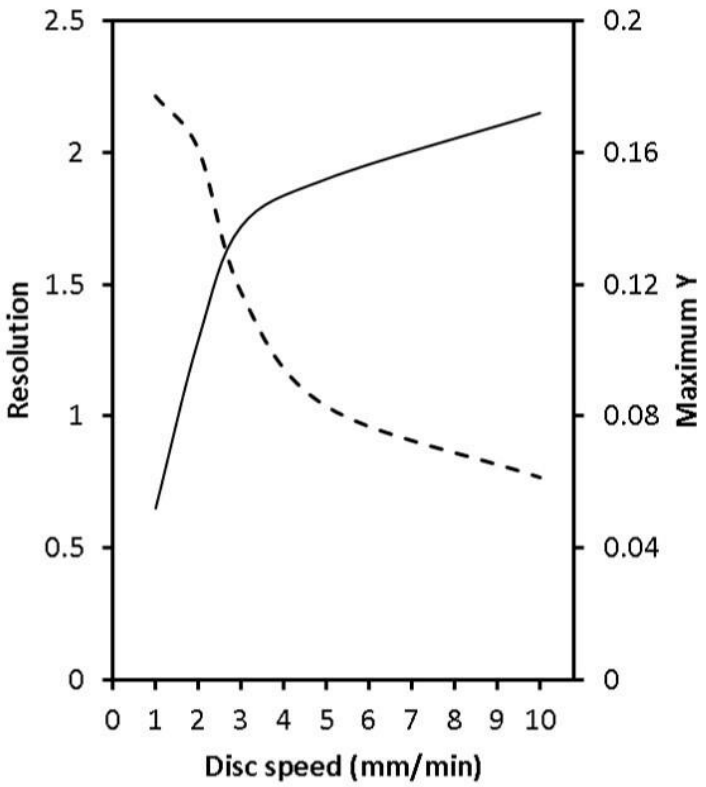

Figure 7.3 The dependence of peak resolution (RS, solid line) and FTIR signal intensity (maximum Y, dashed line) as a function of the ZnSe disc rotation rate. Data obtained for 5 μL injection of a standard psoralen and angelicin mixture (1.25 μg each on the column) under the same conditions as for figure 7.2.

7.4.2 Performance of the LC-FTIR technique for identification

The FTIR transmittance spectra of the LC-separated psoralen and angelicin (peak 1 and peak 2 in figure 7.2) recorded in the range of 650–4000 cm^{-1} at a resolution of 4 cm^{-1} is shown in Figure 7.4 while figure 7.5 shows an expansion of the relevant part of the FTIR spectrum, including the fingerprint region of the two molecules. It must be noted at this point that the FTIR spectra obtained from solid-deposited analytes after LC separation are characterized by much sharper absorption bands than those obtained by means of flow cell devices commonly employed in LC-FTIR techniques. With the molecules free to rotate, the FTIR spectra measured from flow cells in fact show significantly broadened bands, and centrifugal distortion has a further detrimental effect on the spectral specificity (and the technique sensitivity as well) (Salerno et al., 2020; Smith et al., 2018). Conversely, the sharp absorption bands obtained by LC-FTIR from solid-deposited analytes are very informative and allow us to easily

differentiate between very similar compounds (Frison et al., 2021), as may be appreciated from a visual inspection of the spectra in figure 7.5.

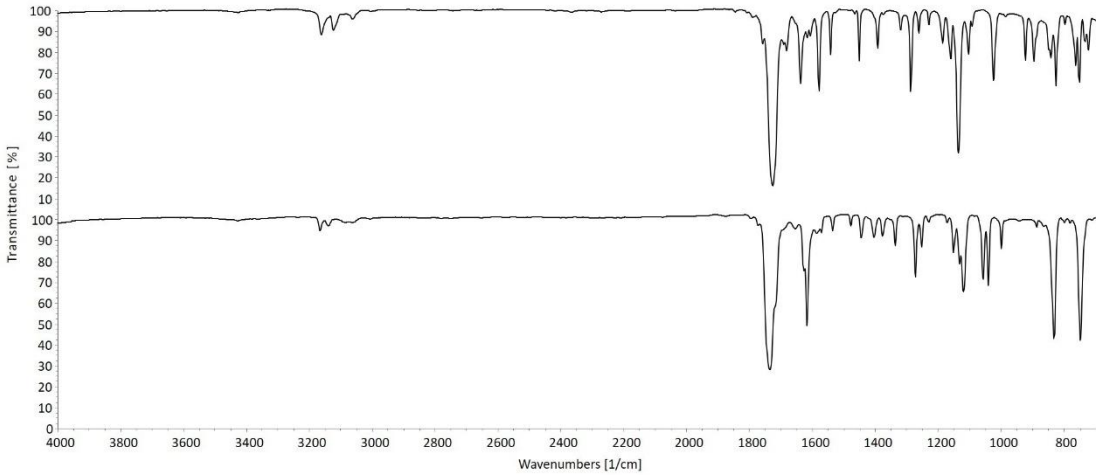

Figure 7.4 The FTIR transmittance spectra of the LC separated standard psoralen (top) and angelicin (bottom), recorded in the 650-4000 cm^{-1}, at a resolution of 4 cm^{-1} (as in figure 7.2).

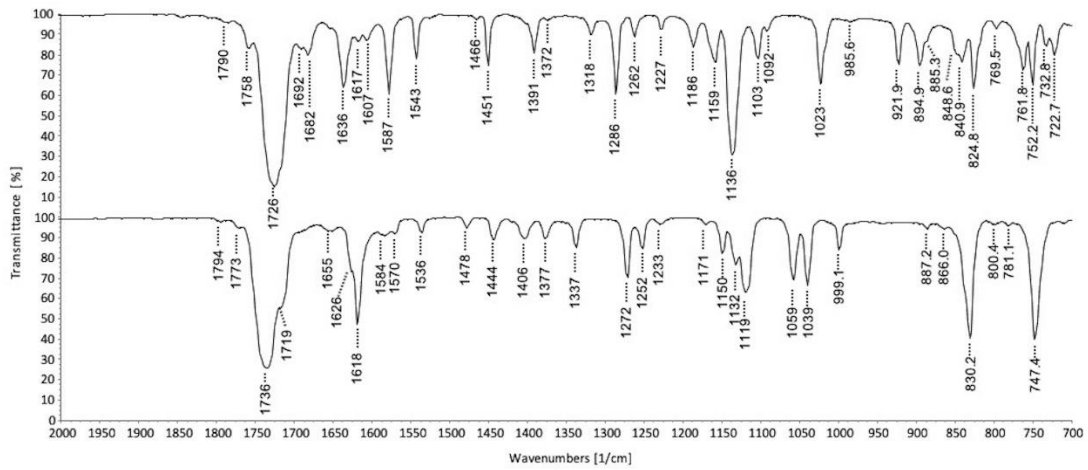

Figure 7.5 Part of the mid-IR spectra obtained for psoralen (top) and angelicin (bottom) by solid-deposition LC-FTIR analysis (as in figure 7.2).

Remarkable differences between the two spectra can be observed in the carbonyl stretching frequency region, where strong bands are centred at 1730 cm^{-1}, as well as in the frequency region of the C=C stretching modes, where two bands of medium intensity can be observed. The latter were assigned to the ν(C=C) mode of the furan ring (around 1630 cm^{-1}) and to the ν(C=C) mode of the pyrone ring (around 1580

cm^{-1}) (Laczkó et al., 1985). At the lower wavenumbers, considerable changes appeared in the spectral range characteristic of the C–O–C stretching modes (1250–1050 cm^{-1}) and in the frequency region of the C–H out-of-plane vibrational modes (900–700 cm^{-1}). Even though the discriminative power of the technique is not discussed, manual interpretation of IR spectral data is often a time-consuming process, requiring subjective interpretation by skilled analysts, whereas algorithm-based criteria rely on quantitative data evaluation by matching the experimental spectra into libraries, and afford a more trustworthy (and user-friendly) approach to unbiased results. As already demonstrated in previous studies, the high specificity afforded by IR spectral data allowed for the setting of a very strict tolerance for compound identification by library search (Frison et al., 2021; Salerno et al., 2020). A minimum hit quality or quality match factor (QMF) equal to or greater than 90% was assumed for a correct identification to reduce the likelihood of false positives and increase confidence in the results. However, the success of such an identification approach is also a matter of quantity, in that the amount of LC-separated analyte deposited on the ZnSe disc must be sufficient to provide a fully informative FTIR spectrum. In this respect, the LOD estimation would not represent a suitable parameter for assessing the performance of the technique investigated, in that a detectable signal is to be obtained, but the information gathered must also allow for a correct identification to be made, by searching a commercial or inhouse database. The limit of identification (LOI) was investigated in this study as the key parameter for the reliable identification of an unknown compound, contained at a certain amount in a given sample, and often in the presence of a noisy background (Lanzarotta et al., 2017). The spectra obtained after LC-FTIR analysis of the standard mixture of psoralen and angelicin, at concentration levels investigated for a linear dynamic range (0.25–5 μg and 0.5–5 μg for psoralen and angelicin, respectively), were searched in a solid-phase FTIR library made in-house (Oxygenated_Heterocyclic_Compounds), containing the spectra of standard coumarins, furanocoumarins, and polymethoxyflavones. As expected, the quality of the IR spectra increased with an increasing amount of analyte as a result of an increased signal-to-noise ratio (S/N, data shown in Figure 7.6), and a logarithmic dependence of the QMF values was found for both compounds from the amount measured. Specifically, the S/N of the spectrum increased from 12.28 (yielding a QMF of 35.83)

for the 0.25 μg injection of the standard psoralen, to S/N of 696.21 for the 5 μg injection (QMF of 99.89). For the standard angelicin, the corresponding values were S/N of 12.54 and QMF of 39.67 for the 0.25 μg injection, and S/N of 537.42 and QMF of 99.15 for the 5 μg injection.

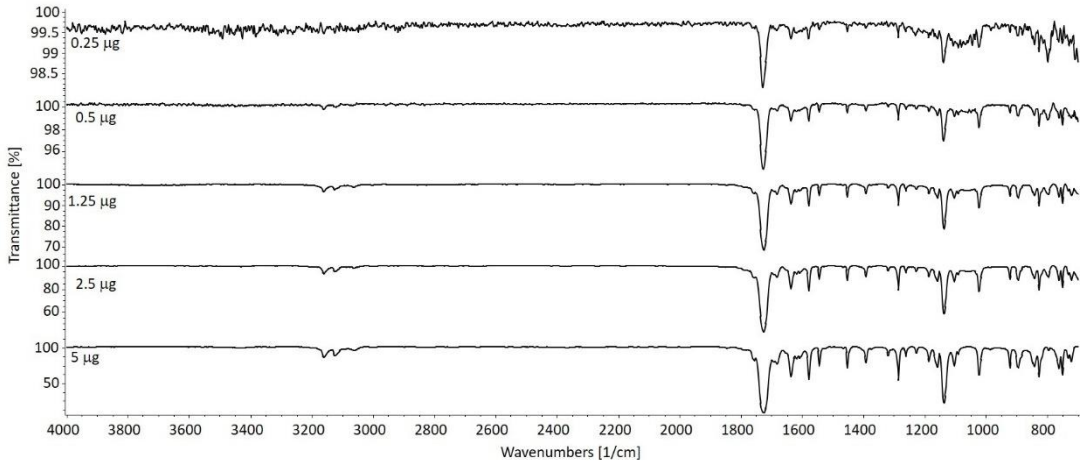

Figure 7.6 Solid-phase LC-FTIR spectra recorded for psoralen in the 650-4000 cm-1 at a resolution of 4 cm^{-1}. Top to bottom: increase in the signal-to-noise ratio resulting from increasing amounts of analyte deposited.

Based on the previously established criterion, the LOI value, as the minimum amount of substance yielding a library-searchable IR spectrum (QMF ≥ 90%), was determined to be equal to 0.6 μg (120 ppm) and 1.25 μg (250 ppm) for psoralen and angelicin, respectively. It is worth noting that both values correspond to analyte amounts which are far above the LOD (discussed later). The results obtained by searching the IR spectral data for both molecules in the custom FTIR spectral library are illustrated in tables 7.1 and 7.2 and demonstrated that both compounds could be differentiated and dentified, with no ambiguity. It can be appreciated from the results in table 7.1 that psoralen could be identified unambiguously, ranking as hit 1 in the list of candidates, with a QMF value which approximated 100% (i.e., 99.9%). It is also noteworthy that the QMF values obtained for the incorrect matches were dramatically lower, decreasing to 8.7% for hit 2 (bergapten), while the angular isomer angelicin showed up as hit 6, with a QMF of only 0.5%. Similarly, the high specificity of molecular/bond related information contained in the LC-FTIR spectrum allowed for highly confident identification of the angelicin molecule (hit 1, QMF 99.8%) to the exclusion of closely

related compounds, particularly the isomeric psoralen (hit 5, QMF 0.6%), on the basis of the QMF differential.

Table 7.1 The quality match factors obtained for Psoralen spectrum against the correct and incorrect matches by searching into a LC-FTIR spectral library made in-house.

Hit	Hit quality	Hit name	Library name
1	99.9	Psoralen	Oxygenated_Heterocyclic_Compounds
2	8.7	Bergapten	Oxygenated_Heterocyclic_Compounds
3	3.4	Bergamottin	Oxygenated_Heterocyclic_Compounds
4	2.3	Isobergapten	Oxygenated_Heterocyclic_Compounds
5	2.2	8-methoxypsoralen	Oxygenated_Heterocyclic_Compounds
6	0.5	Angelicin	Oxygenated_Heterocyclic_Compounds

Table 7.2 The quality match factors obtained for Angelicin spectrum against the correct and incorrect matches by searching into a LC-FTIR spectral library made in-house.

Hit	Hit quality	Hit name	Library name
1	99.8	Angelicin	Oxygenated_Heterocyclic_Compounds
2	11.2	Bergamottin	Oxygenated_Heterocyclic_Compounds
3	9.6	Bergapten	Oxygenated_Heterocyclic_Compounds
4	5.6	Citropten	Oxygenated_Heterocyclic_Compounds
5	0.6	Psoralen	Oxygenated_Heterocyclic_Compounds

7.4.3 Other performance parameters of the LC-FTIR technique

Hyphenated chromatographic-spectroscopic techniques often rely on absorbance measurement of the most intense IR peak as a function of time to enhance the selectivity and sensitivity in targeted approaches to analyte determination (Laczkó et al., 1985). Herein, by mimicking an untargeted approach to unknown compound identification/quantification in samples, the LOD and LOQ parameters of the solid-phase LC-FTIR technique were estimated by plotting the chromatographic peak area as a function of the amount of analyte measured. To construct the calibration curve

and determine the experimental LOD and LOQ, the IR response versus the amount injected was found to be linear over a range of 50–1000 μg/mL (0.25–5 μg injected) for psoralen and 100–1000μg/mL (0.5–5 μg injected) for angelicin. The linear regression equation obtained for psoralen was y = 0.0829x − 5.0989, with a correlation coefficient of 0.9927; for angelicin it was y = 0.0564x − 7.0409, with a correlation coefficient of 0.9918. The precision was estimated from three consecutive intraday 5 μL injections, while the intermediate precision was estimated from 15 injections of 5 μL performed over three consecutive days. The experimental data obtained from replicate analyses at each concentration level and the %RSD calculated are reported in the (table 7.3). LOD values of 12 ppm (0.06 μg injected) and 26 ppm (0.13 μg injected) were estimated for psoralen and angelicin, respectively, as the sample amount yielding a peak equal to three times the peak-to-peak noise level without any post-run treatment. The low end of the linear detection range (LDR) was calculated as an LOQ value of 40 ppm (0.2 μg injected) for psoralen and 80 ppm (0.4 μg injected) for angelicin. It is worth mentioning that because the LC-FTIR technique is free from time constraints, analyte deposits can be scanned repeatedly to obtain spectra at an increased signal-to-noise ratio over the entire chromatogram, or only for a portion of interest. Multiple analyte deposition can be performed to increase the sensitivity, and analyte spots can be analyzed repeatedly without any time constraints for signal averaging.

Table 7.3 Intra and inter-day variabilities for solid-deposition LC-FTIR analysis of two standard furanocoumarins (5 μL injections).

	Psoralen				Angelicin			
	Intra-day (n=3)		Inter-day (n=15)		Intra-day (n=3)		Inter-day (n=15)	
ppm	Area RSD%	t_R RSD%	Area RSD%	t_R RSD%	Area RSD%	t_R RSD%	Area RSD%	t_R RSD%
1000	7.34	0.15	8.24	0.20	10.64	0.05	13.57	0.15
500	9.39	0.09	17.50	0.16	12.53	0.11	10.06	0.06
250	9.90	0.07	20.50	0.13	18.69	0.05	10.71	0.05
100	7.40	0.10	18.17	0.04	12.24	0.09	17.68	0.08
50	11.70	0.03	21.74	0.07	nd	nd	nd	nd

7.5 Conclusions

Apart from the advantages of shorter analysis time and a higher degree of automation, additional arguments in favour of the pneumatically assisted LC-FTIR interface include the possibility for careful control of the interface performance and the speed of the substrate. Thus, concentrated deposits may be obtained to enhance analyte detectability, along with the use of microscope optics for examination. Insight was provided on the capability of the technique in terms of analyte identification and differentiation between closely related molecules, in a highly accurate and highly selective way, to reduce false positives or false negatives. The coupling to a solid-deposition detector led to an increase in the resolution (8 to 4 cm^{-1}) as well as in the specificity, in terms of differentiation between closely related molecules (quality match factors >99%). Qualitatively, the technique may be a very useful approach for the determination of target and unknown chemicals, affording pure fractions of chemical components in a mixture, and selective information for their identification using standards or library spectra. The technique may effectively complement the commonly used LC-MS approaches, which sometimes do not afford the reliable identification of unknown compounds with the exclusion of other possible regioisomeric molecules. It is worth mentioning that, in contrast to MS detection, quick recording of compound IR fingerprints does not require ionization in a probe, and thus is less prone to failure. This also alleviates common matrix effects, such as ionization suppression encountered during the validation and implementation of MS- and tandem MS based analytical methods. From a quantitative standpoint, the higher quantification limit (at the level of parts per million) actually poses severe limitations for widespread use of the LC-FTIR technique, with respect to more sensitive techniques such as MS-based methods. The practicability of the technique for real samples will depend on the target application, as it is it suitable for the determination of major sample constituents and not for minor components and contaminants. There is still much room for improving the sensitivity of the technique to address the need for analyte detection in the sub-microgram/microliter concentration range. Further developments in this direction would provide a unique platform in areas such as the biomedical field, in light of the high sensitivity of vibrational spectroscopy to changes at the molecular level.

Part III

Development of high-resolution GC-FTIR/MS prototype

Chapter 8

Application of a new integrated GC-*sd*-FTIR/MS approach for the univocal *cis/trans* fatty acid isomer discrimination

8.1 Introduction

Mass spectrometer (GC-MS) equipped with an electron ionization (EI) source is considered as the gold standard detector for detection of gas chromatographic eluting compounds, because of its high sensitivity (Nolvachai et al., 2015), its simplicity and the large availability of spectral databases which allows a fast identification of the eluting compounds. However, it has limitations in differentiating isomers or compounds with a very similar fragmentation pattern (Zavahir et al., 2018). This is the case of cis/trans fatty acid isomers, which are of particular interest because of the cardiovascular disease risk factors of the trans-fat (Ganguly & Pierce, 2015). Due to the identical fragmentation pattern of these compounds, information provided by GC-MS may not be sufficient for a definitive identification. For this compound class, mass spectrometry is not able to provide alone a definitive identification, because it does not manage to discriminate either the double bond position or its configuration.

The former, because the unsaturation has the tendency of migrating along the carbon chain during the fragmentation (McCloskey, 1971), and can only be deduced after studying mass spectra of corresponding derivatives (Jensen & Gross, 1987), such as the ones obtained by the reaction with 2-alkenyl-4,4-dimethyloxazoline (DMOX) (Wahl et al., 1994). Regarding the configuration, cis and trans fatty acids show an identical fragmentation pattern, therefore mass spectrometry fails in the discrimination.

This emphasizes the need for other information, capable of completing the ones provided by the already mentioned technique. Infrared spectroscopy provides a wealth of molecular vibrational information, especially in the fingerprint region, related to molecular functionalities and structures.

Indeed, its use for structural identification of fatty acids methyl esters (FAMEs) geometrical isomers is reported (Doumenq et al., 1989; Mossoba et al., 1990, 1997; Sémon et al., 1998). The discrimination of the cis/trans isomers is possible due to the specific absorptions that they show. In particular, the spectral band at 969 cm^{-1} corresponds to the trans double bond CH out-of-plane the out of plane bending is a specific absorption, while the cis configuration shows two bands at 723 cm^{-1}. Moreover, cis configuration presents the characteristic sp^2 $C = C - H$ stretching at 3001 cm^{-1} which is not present in the trans isomer due to its higher symmetry (Sémon et al., 1998). The two characteristic absorptions are shown in figure 8.1 for oleic acid methyl ester (cis isomer) and elaidic acid methyl ester (trans isomer).

The easiest infrared spectroscopy determination of trans fat is by Attenuated Total Reflection infrared spectroscopy (ATR-FTIR). However, for a more detailed study of the content of fatty acid in a fat sample, it is necessary to perform a gas chromatographic analysis to separate and then identify each component after a transesterification reaction to obtain fatty acids methyl esters (FAMEs). The hyphenation between gas chromatography and infrared spectroscopy was widely used for identification of such isomers, either by using gas phase (Doumenq et al., 1989, 1990), or solid phase (Mossoba et al., 1990) interphases, matrix isolation (MI) or direct deposition (dd), also for conjugated linoleic acid geometrical isomers. The molecular specificity can complement MS which provides information about the molecular weight, which is necessary for the determination of the chain length. However, one practical problem is that IR spectral libraries are much smaller compared to the MS ones.

MS remains the first choice for gas chromatographic analyses because its ease and for the larger availability of spectral libraries. However, in some cases it is not capable to discriminate between molecules with similar molecular structure such as isomers.

Therefore, the hyphenation of gas chromatography with one or more detectors is mandatory when a highly reliable identification of compounds as in this case for FAMEs is needed. To combine the complementary information coming from mass spectrometry and infrared spectroscopy, in this study a GC-*sd*-FTIR/MS system was developed making possible the unambiguous identification of such compounds.

Many types of GC-FTIR/MS configurations are reported in literature, but the most used is the one in which the flow is split in parallel and in a tunable ratio to the two detectors (Visser, 2002). The first capillary GC-FTIR/MS configuration was reported in 1982, in which the previously mentioned parallel configuration was used with a vapor phase IR detection (Crawford et al., 1982). Otherwise, other configurations included the usage of two identical columns connected to a unique injector (Smyrl et al., 1992).

Being a non-destructive detector, infrared spectroscopy was also serially linked to a mass spectrometer, using a configuration in which the light pipe was serially connected to mass spectrometer so that the outlet flow from the column can be directed into the mass spectrometer after its passage from the light pipe. (Hedges & Wilkins, 1991). The parallel and serial connection of the two detectors were compared for the identification of fatty acids methyl esters, concluding that the serial coupling has the advantage of guaranteeing a better sensitivity (Wahl et al., 1994).

The integration of GC with MS and FTIR was also developed with the matrix interphase infrared spectrometer and with direct deposition. The latter was used for analysis of designer steroids in dietary supplement (Lorenz et al., 2019).

The development of a new GC-sd-FTIR-MS instrumentation is here reported and exploited for FAMEs isomers identification. Separation of these compounds was obtained on a highly polar ion liquid column which is the only one that allows the separation of such compounds due to their similar boiling point (Delmonte et al., 2011).

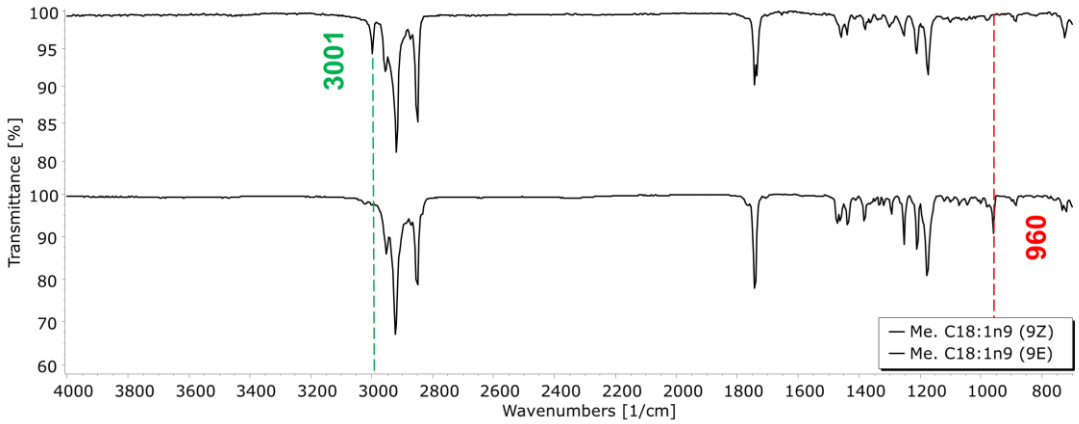

Figure 8.1 The infrared spectra of oleic acid methyl ester (9Z) above and (9E).

8.2 Material and methods

8.2.1 Chemicals

A standard mix containing 37 different fatty acids dissolved in dichloromethane at different concentration (Supelco 37 Component FAME Mix) and Linoleic Acid Methyl Ester Mix at the concentration of 10 mg/mL in dichloromethane were purchased from Merck Life Science (Darmstadt, Germany), GLC REFERENCE STANDARDS GLC-481-B was purchase from Nu-Chek.

8.2.2 Instrumentation and analytical conditions

To obtain a highly reliable identification of the chemical compounds the analyses were performed using two detection tools directly connected to the end of the column: mass spectrometry and Fourier transform infrared spectroscopy.

8.2.3 Analytical instrumentation

Gas chromatographic separation was performed on a Nexis GC-2030 gas chromatograph equipped with an AOC-20i auto sampler (Shimazdu, Kyoto, Japan) and a split-splitless injector. An ionic liquid stationary phase column was installed: SLB-IL 111 Capillary GC Column 200 m L × 0.25 mm i.d., 0.20 µm d_f (Supelco). This IL (ionic liquid) column is specifically designed for separation of geometric-positional (cis/trans) isomers of fatty acid methyl esters (FAMEs). Helium 99.9% was used as carrier gas and was flushed into the column using a constant linear velocity of 23

cm/sec and an initial column flow of 2.99 mL/min and an injector pressure of 627.7 KPa were used at the temperature of 50ºC.

The injections were performed in split 20 mode using an injector temperature of 270ºC and an injection volume of 1 µL. The analyses were performed starting from the temperature of 50 ºC to 260 ºC with an increase of 3 ºC/min.

After separation onto the column, the flow was split to the two detectors using a Siltek MXT low dead volume Y connector for 0.25 mm i.d. column (Restek). Two non-polar fused silica capillaries were used: the first (1.80 m L × 0.20 mm I.D.) was connected to the FTIR detector, the second (1.2 m L × 0.10 mm I.D.) to the mass spectrometer, in order to deliver 1:10 of the flow to the MS and the mayor part to the FTIR because of its lower sensitivity.

The mass spectrometer used was a QP2020 NX (Shimazdu, Kyoto, Japan) equipped with an electron impact source and a single quadrupole analyzer. The transfer line was set at the temperature of 250°C and the ion source at 200 °C. The MS analyses were performed in scan mode using the mass range of 40-360 *m/z*.

The FTIR capillary was connected to the DiscovIR solid phase FTIR detector (Spectra-Analysis Instrument Inc., Marlborough, MA, USA) by means of a heated external transfer line (1.30 m of length) made in laboratory whose temperature was set to 300°C. The extremity of the restrictor was positioned directly above a ZnSe disc, which was placed into an evacuated chamber ($4x10^{-4}$ torr) which was also chilled down to −50°C by means of liquid nitrogen to allow the entrapment of the analytes. The DiscovIR FTIR instrument was equipped with a Mercury-Cadmium-Telluride (MCT) cryogenically cooled detector. Solid phase IR spectra of the GC eluted compounds were recorded in real time from 10 µm × 10 µm spots in the 700–4,000 cm^{-1} range, with a resolution of 4 cm^{-1} and a scan rate of 2Hz, at a disc rotation speed of 3 mm/min.

8.2.3 Margarine derivatization

To 10 mg of margarine 100 µL of internal standard Glyceryl triundecanoate ($C_{11}C_{11}C_{11}$) 5000 ppm in heptane was added. Then 500 µL of MeONa 0,5 M in MeOH wad added and the solution was vortexed for 2 min at 3000 rpm. Then the reaction was performed at the temperature of 100 °C for 15 min. Then, 500 µL of BF_3 (14% in

MeOH) was added to the solution and it was vortexed for 2 min at 3000 rpm. Afterwards, it was let react at 100 °C for 15 min, and after cooling, extraction was performed by adding 350 µL of heptane and 200 µL of saturated saline water (NaCl). It was vortexed for 5 min at 3000 rpm. In the end, organic phase was taken, and injected into the system (0.5 µL split 10).

8.3 Results and discussion

The scheme of the analytical instrumentation is reported in figure 8.2. It allowed the parallel detection of fatty acid methyl esters.

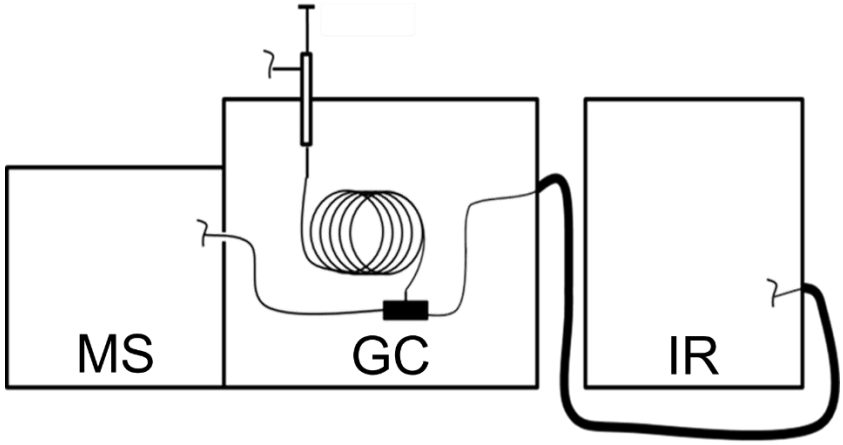

Figure 8.2 Scheme of the GC-FTIR/MS system.

Since the two detectors had the interphase entrance on their left the construction of an external transfer line was necessary to allow the connection of the column with the infrared detector. This must be flexible and heated in all parts to avoid the condensation of the separated analytes.

The developed instrumentation was tested for the correct identification of fatty acid methyl esters (FAMEs). Firstly, the mix of the cis/trans isomers of the linoleic acid methyl ester was injected into the system to assess it efficacy in delivering the separated analytes to both detectors while keeping the chromatographic separation.

Chromatographic separation was performed on a ion liquid based stationary phase column, which is the most suitable for the separation of such isomers.

Figure 8.3 shows the two chromatograms obtained, above GC-MS and below GC-FTIR. By a visually inspection, it is possible to notice that the separated analytes are efficiently delivered to the FTIR detector through the developed external transfer line because they maintain the same chromatographic profile.

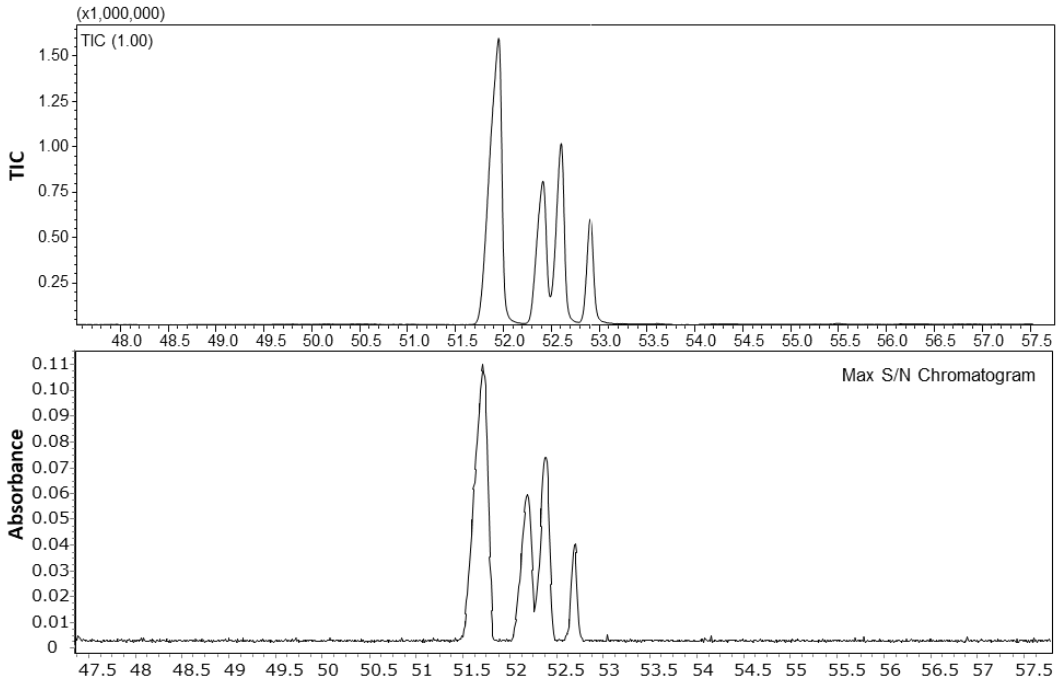

Figure 8.3 The GC-MS (above) and GC-FTIR (below) chromatograms of the Linoleic Acid Methyl Ester Mix.

As figure 8.4 shows, the mass spectra of these four isomers are almost identical, and it is demonstrated by performing the library search of the firs peak, reported in table 8.1. Due to the same fragmentation pattern, the first three results are Me. C18:2n6 (9Z,12E), Me. C18:2n6 (9E,12E) and Me. C18:2n6 (9E,12E) with a similarity of 97%, 97% and 96% respectively. Therefore, the identification is not definitive.

On the other hand, infrared spectroscopy provides a wealth of information (figure 8.5) related to the different vibration of these double bonds which allow the unbiased discrimination.

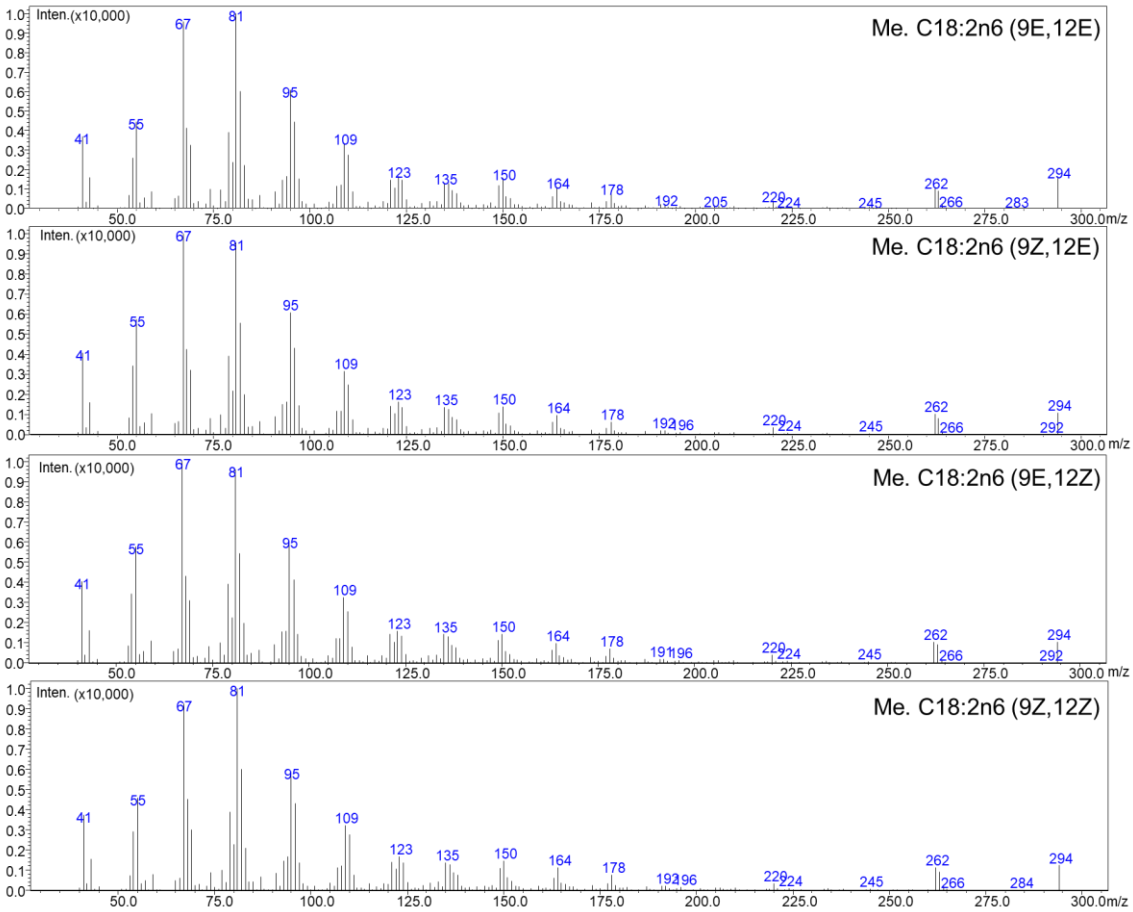

Figure 8.4 The EI mass spectra of the four cis/trans isomers of linoleic acid methyl ester.

Table 8.1 The infrared spectra of the Linoleic Acid Methyl Ester cis trans isomers.

HIT	Similarity	Compound name	Mol. Wt.	Formula
1	97	Me. C18:2n6 (9Z,12E)	294	$C_{19}H_{34}O_2$
2	97	Me. C18:2n6 (9E,12E)	294	$C_{19}H_{34}O_2$
3	96	Me. C18:2n6 (9E,12E)	294	$C_{19}H_{34}O_2$
4	93	Et. C18:2n6 (9E, 12E)	309	$C_{20}H_{36}O_2$

To this regard, figure 8.5 shows the infrared spectra of the four isomers. There are many differences in these spectra and the specific absorption of the two double bond configurations are evident.

Indeed, the 9E,12E isomer does not show any absorption above 3000 cm^{-1}. On the other hand, the 9Z,12Z isomer does not absorb at the specific wavelength of trans double bond (960 cm^{-1}). The two 9E,12Z and 9Z,12E isomers show both absorptions at 960 and 3000 cm^{-1}.

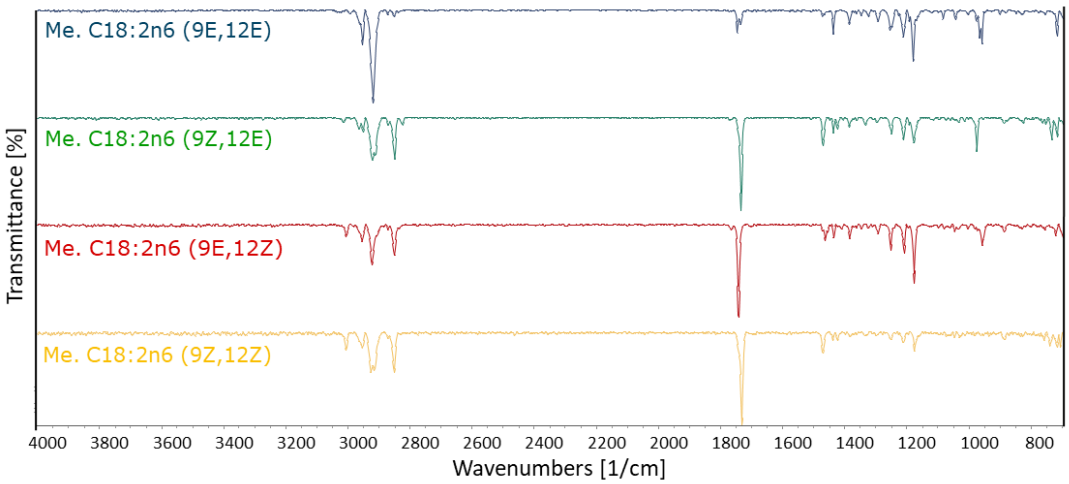

Figure 8.5 The infrared spectra of the four cis/trans isomers of linoleic acid methyl ester.

The confirmation of the structure is achieved by the library search which is reported in table 8.2 for the first peak of figure 8.3. The first result was Me. C18:2n6 (9E,12E) with a similarity of 94%, while the second was Me. C15:1n5 (10E) with a similarity of 54%. The huge difference in term of similarity between the first two results of the library search means that a much greater selectivity was achieved. This because the IR

spectrum provides a huge number of information which are specific of a single molecule, especially in the fingerprint region.

Looking for the other isomers, they resulted at the positions 16 (9Z,12E), 27 (9Z,12Z) and 57 (9E,12Z) with similarities of 25, 22 and 11%. This allows the definitive identification of the first peak as Me. C18:2n6 (9E,12E).

Table 8.2 The FTIR library search results for the first peak of figure 8.3.

HIT	Similarity	Compound name	Mol. Wt.	Formula
1	94	Me. C18:2n6 (9E,12E)	294	$C_{19}H_{34}O_2$
2	54	Me. C15:1n5 (10E)	254	$C_{16}H_{30}O_2$
3	49	Me. C17:1n7 (10E)	282	$C_{18}H_{34}O_2$
4	45	Me. C18:1n12 (6E)	296	$C_{19}H_{36}O_2$
5	38	Me. C18:1n9 (9E)	296	$C_{19}H_{36}O_2$
…	…	…		
16	25	Me. C18:2n6 (9Z,12E)	294	$C_{19}H_{34}O_2$
…	…	…		
27	22	Me. C18:2n6 (9Z,12Z)	294	$C_{19}H_{34}O_2$
…	…	…		
57	11	Me. C18:2n6 (9E,12Z)	294	$C_{19}H_{34}O_2$

The usefulness of tis prototype system was also demonstrated performing the analysis of the standard mix of 37 FAMEs. Figure 8.6 shows the GC-MS Total Ion Current (TIC) from 42.5 to 54.5 min. In this case the effectiveness of the use of this two complementary information was used for the identification of a peak resulted from a coelution. To do so the peak at t_R 49.1 min was taken into consideration.

The first part of the peak, at t_R 49.064 min was identified as Me. C18:0 by mass spectrometry. The results of MS library search for the shoulder of this peak at t_R 49.128 min are displayed in table 8.3. The first result was Me.C17:1n7 *cis* with 97% of similarity score and the second was Me.C17:1n7 *trans* with a similarity of 96%. On

these bases, it was not possible to elucidate the double bond configuration only by using mass spectrometry data.

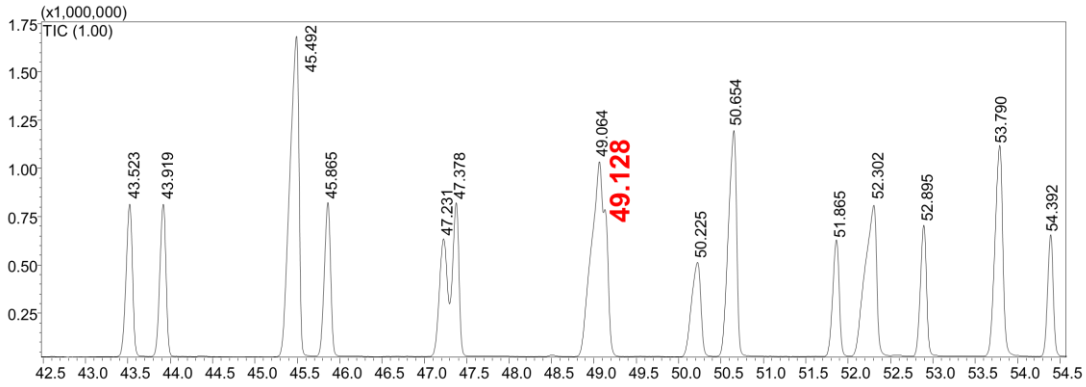

Figure 8.6 Total ion current chromatogram of Supelco 37 standard mix chromatogram from 42.5 to 54.5 min.

Table 8.3 GC-MS library search for the peak at t_R 49.128 min.

HIT	Similarity	Compound name	Mol. Wt.	Formula
1	97	Me. C17:1n7 (10Z)	282	$C_{18}H_{34}O_2$
2	96	Me. C17:1n7 (10E)	282	$C_{18}H_{34}O_2$
3	91	Me. 9,10-methylene C16:0	282	$C_{18}H_{34}O_2$
4	84	Et. C17:1n7 (10E)	296	$C_{19}H_{36}O_2$

In case of coelutions FTIR library search is not effective in the identification, because the IR peak spectrum is the result of the combination of two or more spectra, depending on how many compounds are present. In this case, from the IR search Me. C17:1n7 (10Z) resulted first with a similarity of 81%, while the trans isomer resulted 9 with a similarity of 60%. These results are informative, but in this case, since the uncertainty was between Me. C17:1n7 (10Z) and Me. C17:1n7 (10E), the two characteristic infrared bands made the discrimination between *cis* and *trans* possible. Therefore, the GC-FTIR chromatograms at the characteristic wavelengths of the *cis*- (@3001 cm^{-1} in figure 8.7) and *trans*- (@960 cm^{-1} in figure 8.8) isomers were displayed. Whereas in the @3001 cm^{-1} chromatogram it can be noticed a little peak under the last part of the Max S/N chromatogram peak, in the @960 cm^{-1} no peaks are present. It means that

there is an absorption at 3001 cm^{-1} and while no absorptions are present at 3001 cm^{-1}. These considerations allowed to demonstrate that the peak was Me. C17:1n7 (10Z).

The selection of the characteristic wavelength chromatogram is also effective when the compound is not present into the IR spectral library. This can frequently happen due to the fact that IR libraries are less complete and diffuse than GC-MS ones.

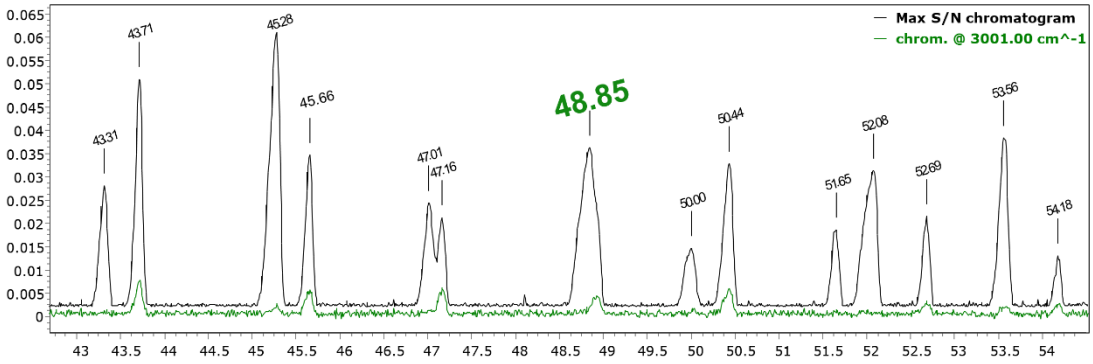

Figure 8.7 FTIR chromatogram of Supelco 37 standard mix chromatogram (42.5-54.5 min). In green the band chromatogram at the specific wavelength of cis fatty acids: 3001 cm^{-1}.

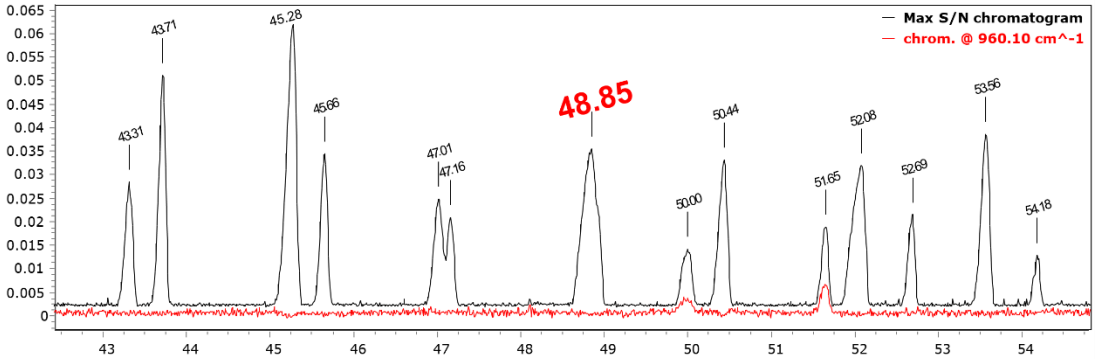

Figure 8.8 FTIR chromatogram of Supelco 37 standard mix chromatogram (42.5-54.5 min). In red the band chromatogram at the specific wavelength of the trans fatty acids at 960 cm^{-1}.

Afterwards, for the analysis a real sample containing fatty acid isomers, a commercial margarine was selected and first subjected to transesterification to obtain the corresponding fatty acid methyl esters (FAMEs). Figure 8.9 shows the chromatograms

of the margarine sample and the comparison with reference standard mixtures containing fatty acids methyl esters (GLC-481 or Supelco 37).

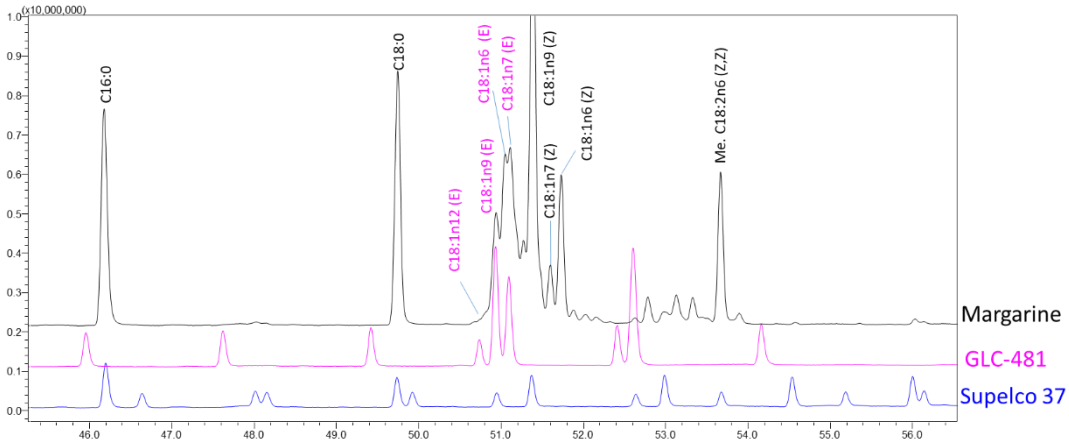

Figure 8.9 GC-MS chromatograms of trans esterified margarine (black), GLC-481 (pink), Supelco 37 (blue).

In the first region, there are only the saturated FAMEs, Me.C16:0 and Me.C18:0, which can be easily identified based on the retention index and mass spectra or IR spectra. In the region around 50.5 and 52.5 min the monounsaturated fatty acids elutes; this region is quite complex since several coelution occurs. Furthermore, the compound eluting, possess the same mass and very similar mass spectra. In this contest, the combined use of the information obtained from two different detector and the linear retention index filter was necessary. The trans monounsaturated fatty acids Me.C18:1n9 (E) and Me.C18:1n7 (E) were identified by comparison to the GLC-481 standard on the base of their retention time. The cis monounsaturated fatty acids Me.C18:1n9 (Z) and Me.C18:1n7 (Z) were confirmed by FTIR spectral library (95% and 91% of similarity obtained, respectively). For the same compound MS similarity were 97% and 98%, however in the mass search list other compound with similarity above 90% were present (opposite to the IR results where other compounds similarity was below 80%). Unfortunately, minor components were not detected using FTIR. In this case, signal averaging should be performed to enhance the S/N. The present work is still under development with application to other samples.

8.4 Conclusions

The use of the hyphenated instrumentation based on two types of detectors (FTIR and MS) resulted successful in achieving the confident identification of the cis/trans fatty acid isomers because of their distinct absorption in the mid-infrared, either with IR library search, or without in case of peaks are not completely separated. Remarkably, the complementary MS and FTIR information can be obtained with a single injection. The not perfect chromatographic separation negatively affects the results of the infrared spectroscopy library search, therefore especially in case of the margarine will be improves. Moreover, the not enough signal of some of the less abundant peaks will be improved by performing the redeposition and rescanning functions.

References

Andersen, A. J., Yamada, S., Pramodkumar, E. K., Andresen, T. L., Boisen, A., & Schmid, S. (2016). Nanomechanical IR spectroscopy for fast analysis of liquid-dispersed engineered nanomaterials. *Sensors Actuators B Chem*, *233*, 667–673. https://doi.org/10.1016/j.snb.2016.04.002

Arigò, A., Dugo, P., Rigano, F., & Mondello, L. (2021). Linear retention index approach applied to liquid chromatography coupled to triple quadrupole mass spectrometry to determine oxygen heterocyclic compounds at trace level in finished cosmetics. *J Chromatogr A*, *1649*, 462183. https://doi.org/10.1016/j.chroma.2021.462183

Arihara, K., & Ohata, M. (2010). Functional meat products. *Handbook of Meat Processing*, *24*, 423–439. https://doi.org/10.1002/9780813820897.ch24

Association of Official Agricultural Chemists (AOAC). (1996). Crude protein in meat and meat products including pet foods. Combustion method. *AOAC 992.15-1992*.

Bahar, A. A., & Ren, D. (2013). Antimicrobial peptides. *Pharmaceuticals*, *6*(12), 1543–1575. https://doi.org/10.3390/ph6121543

Balan, V., Mihai, C. T., Cojocaru, F.-. D., Uritu, C.-. M., Dodi, G., Botezat, D., & Gardikiotis, I. (2019). Vibrational Spectroscopy Fingerprinting in Medicine: from Molecular to Clinical Practice. *Materials*, *12*(18), 2884. https://doi.org/10.3390/ma12182884

Barman, P., Joshi, S., Sharma, S., Preet, S., Sharma, S., & Saini, A. (2023). Strategic Approaches to Improvise Peptide Drugs as Next Generation Therapeutics. *Int J Pept Res Ther*, *29*, 61. https://doi.org/10.1007/s10989-023-10524-3

Bersuder, P., Hole, M., & Smith, G. (1998). Antioxidants from a heated histidine-glucose model system. I: Investigation of the antioxidant role of histidine and isolation of antioxidants by high-performance liquid chromatography. *J Am Oil Chem Soc*, *75*(2), 181–187. https://doi.org/10.1007/s11746-998-0030-y

Bianco, M., Calvano, C. D., Ventura, G., Bianco, G., Losito, I., & Cataldi, T. R. I. (2020). Regiochemical assignment of N-acylphosphatidylethanolamines(NAPE) by liquid chromatography/electrospray ionization with multistage mass spectrometry and its application to extracts of lupin seeds. *J Am Soc Mass Spectrom*, *31*(9), 1994–2005. https://doi.org/10.1021/jasms.0c00267

Bose, B., Downey, T., Ramasubramanian, A. K., & Anastasiu, D. C. (2022). Identification of Distinct Characteristics of Antibiofilm Peptides and Prospection of Diverse Sources for Efficacious Sequences. *Front Microbiol*, *12*, 783284. https://doi.org/10.3389/fmicb.2021.783284

Boysen, R. I., & Hearn, M. T. W. (2010). 9.02 - High Performance Liquid Chromatographic Separation Methods. *Comprehensive Natural Products II*, *9*, 5–49. https://doi.org/10.1016/B978-008045382-8.00183-0

Brodkorb, A., Egger, L., Alminger, M., Alvito, P., Assunção, R., Ballance, S., Bohn, T., Bourlieu-Lacanal, C., Boutrou, R., Carrière, F., Clemente, A., Corredig, M., Dupont, D., Dufour, C., Edwards, C., Golding, M., Karakaya, S., Kirkhus, B., Le Feunteun, S., Lesmes, U., Macierzanka, A., Mackie, A. R., Martins, C., Marze, S., McClements, D. J., Ménard, O., Minekus, M., Portmann, R., Santos, C. N., Souchon, I., Singh, R. P., Vegarud, G. E., Wickham, M. S. J., Weitschies, W., Recio, I. (2019). INFOGEST static in vitro simulation of gastrointestinal food digestion. *Nat Protoc*, *14*(4), 991–1014. https://doi.org/10.1038/s41596-018-0119-1

Buszewski, B., & Noga, S. (2012). Hydrophilic interaction liquid chromatography (HILIC)-a powerful separation technique. *Anal Bioanal Chem*, *402*(1), 231–247. https://doi.org/10.1007/s00216-011-5308-5

Cai, B., Chen, H., Wan, P., Luo, L., Ye, Z., Huang, J., Chen, D., & Pan, J. (2022). Isolation and identification of immunomodulatory peptides from the protein hydrolysate of tuna trimmings (*Thunnas albacares*). *LWT*, *164*, 113614. https://doi.org/10.1016/j.lwt.2022.113614

Capriotti, A. L., Caruso, G., Cavaliere, C., Samperi, R., Ventura, S., Zenezini Chiozzi, R., & Laganà, A. (2015). Identification of potential bioactive peptides generated by simulated gastrointestinal digestion of soybean seeds and soy milk proteins. *J Food Compost Anal*, *44*, 205–213. https://doi.org/10.1016/j.jfca.2015.08.007

Capriotti, A. L., Cavaliere, C., Foglia, P., Piovesana, S., Samperi, R., Zenezini Chiozzi, R., & Laganà, A. (2015). Development of an analytical strategy for the identification of potential bioactive peptides generated by in vitro tryptic digestion of fish muscle proteins. *Anal Bioanal Chem*, *407*, 845–854. https://doi.org/10.1007/s00216-014-8094-z

Carson, W. W., Kearney, T., & Zhou, M. (2011). An LC–IR Hyphenated Approach to Characterize Polymeric Excipients in Pharmaceutical Formulations. *LCGC N Am*, *29*(4).

Carson WW, & Bourne S. (2014). Method and apparatus for desolvating flowing liquid (Patent 8920658.2014.). United States. https://www.freepatentsonline.com/8920658.html

Cerrato, A., Aita, S. E., Capriotti, A. L., Cavaliere, C., Montone, C. M., Laganà, A., & Piovesana, S. (2020). A new opening for the tricky untargeted investigation of natural and modified short peptides. *Talanta*, *219*, 121262. https://doi.org/10.1016/j.talanta.2020.121262

Cerrato, A., Aita, S. E., Cavaliere, C., Laganà, A., Montone, C. M., Piovesana, S., Zenezini Chiozzi, R., & Capriotti, A. L. (2021). Comprehensive identification of

native medium-sized and short bioactive peptides in sea bass muscle. *Food Chem*, 343, 128443. https://doi.org/10.1016/j.foodchem.2020.128443

Cerrato, A., Aita, S. E., Montone, C. M., Capriotti, A. L., Piovesana, S., & Laganà, A. (2021). Chapter 4 - Methodologies for extraction and separation of short-chain bioactive peptides. *Biologically Active Peptides*, *4*, 75–86. https://doi.org/https://doi.org/10.1016/B978-0-12-821389-6.00002-9

Cerrato, A., Capriotti, A. L., Capuano, F., Cavaliere, C., Montone, A. M. I., Montone, C. M., Piovesana, S., Chiozzi, R. Z., & Laganà, A. (2020). Identification and antimicrobial activity of medium-sized and short peptides from yellowfin tuna (*Thunnus albacares*) simulated gastrointestinal digestion. *Foods*, *9*(9), 1185. https://doi.org/10.3390/foods9091185

Cerrato, A., Lammi, C., Capriotti, A. L., Bollati, C., Cavaliere, C., Montone, C. M., Bartolomei, M., Boschin, G., Li, J., Piovesana, S., Arnoldi, A., & Laganà, A. (2023). Isolation and functional characterization of hemp seed protein-derived short- and medium-chain peptide mixtures with multifunctional properties for metabolic syndrome prevention. *Food Res Int*, *163*, 112219. https://doi.org/10.1016/j.foodres.2022.112219

Christensen, L. P. (2018). Chapter 29 - Polyphenols and Polyphenol-Derived Compounds From Plants and Contact Dermatitis. *Polyphenols: Prevention and Treatment of Human Disease*, 29, 349-384. https://doi.org/10.1016/B978-0-12-813008-7.00029-1

chromatography. (2006). *IUPAC Compendium of Chemical Terminology, 3rd ed. International Union of Pure and Applied Chemistry* (3.0.1). https://doi.org/doi:10.1351/goldbook.C01075

Cooks, R. G. (1995). Collision-induced Dissociation : Readings and Commentary. *J Mass Spectrom*, *30*(9), 1215–1221. https://doi.org/10.1002/jms.1190300902

Coppola, D., Lauritano, C., Esposito, F. P., Riccio, G., Rizzo, C., & de Pascale, D. (2021). Fish Waste: From Problem to Valuable Resource. *Mar Drugs*, *19*(2), 116. https://doi.org/10.3390/MD19020116

Corrêa, A. P. F., Daroit, D. J., Fontoura, R., Meira, S. M. M., Segalin, J., & Brandelli, A. (2014). Hydrolysates of sheep cheese whey as a source of bioactive peptides with antioxidant and angiotensin-converting enzyme inhibitory activities. *Peptides*, *61*, 48–55. https://doi.org/10.1016/j.peptides.2014.09.001

Cotter, R. J. (1999). The New Time-of-flight Mass Spectrometry. *Anal Chem*, *71*(13), 445A-451A. https://doi.org/10.1021/ac9904617

Cox, J., & Mann, M. (2008). MaxQuant enables high peptide identification rates, individualized p.p.b.-range mass accuracies and proteome-wide protein quantification. *Nat Biotechnol*, *26*(12), 1367–1372. https://doi.org/10.1038/nbt.1511

Cox, J., Neuhauser, N., Michalski, A., Scheltema, R. A., Olsen, J. V., & Mann, M. (2011). Andromeda: A peptide search engine integrated into the MaxQuant environment. *J Proteome Res*, *10*(4), 1794–1805. https://doi.org/10.1021/pr101065j

Crawford, R. W., Hirschfeld, Tomas., Sanborn, R. H., & Wong, C. M. (1982). Organic analysis with a combined capillary gas chromatograph mass spectrometer Fourier transform infrared spectrometer. *Anal Chem*, *54*(4), 817–820. https://doi.org/10.1021/ac00241a051

Cutajar, N., Lia, F., Deidun, A., Galdies, J., Arizza, V., & Zammit Mangion, M. (2022). Turning Waste into A Resource: Isolation and Characterization of High-Quality Collagen and Oils from Atlantic Bluefin Tuna Discards. *Appl Sci*, *12*(3), 1542. https://doi.org/10.3390/app12031542

Dass, C. (2006). Chapter 3 - Mass Analysis and Ion Detection. *Fundamentals of Contemporary Mass Spectrometry*, *3*, 67–117. https://doi.org/10.1002/0470118490

Dávalos, A., Gómez-Cordovés, C., & Bartolomé, B. (2004). Extending Applicability of the Oxygen Radical Absorbance Capacity (ORAC-Fluorescein) Assay. *J Agric Food Chem*, *52*(1), 48–54. https://doi.org/10.1021/jf0305231

Delmonte, P., Fardin Kia, A. R., Kramer, J. K. G., Mossoba, M. M., Sidisky, L., & Rader, J. I. (2011). Separation characteristics of fatty acid methyl esters using SLB-IL111, a new ionic liquid coated capillary gas chromatographic column. *J Chromatogr A*, *1218*(3), 545–554. https://doi.org/10.1016/j.chroma.2010.11.072

Di Vaio, A., Hasan, S., Palladino, R., & Hassan, R. (2023). The transition towards circular economy and waste within accounting and accountability models: a systematic literature review and conceptual framework. *Environ Dev Sustain*, *25*(1), 734–810. https://doi.org/10.1007/s10668-021-02078-5

Donato, P., Cacciola, F., Mondello, L., & Dugo, P. (2011). Comprehensive chromatographic separations in proteomics. In *J Chromatogr A*, *1218*(49), 8777–8790. https://doi.org/10.1016/j.chroma.2011.05.070

Donato, P., Cacciola, F., Sommella, E., Fanali, C., Dugo, L., Dachà, M., Campiglia, P., Novellino, E., Dugo, P., & Mondello, L. (2011). Online comprehensive RPLC × RPLC with mass spectrometry detection for the analysis of proteome samples. *Anal Chem*, *83*(7), 2485–2491. https://doi.org/10.1021/ac102656b

Donato, P., Dugo, P., Cacciola, F., Dugo, G., & Mondello, L. (2009). High peak capacity separation of peptides through the serial connection of LC shell-packed columns. *J Sep Sci*, *32*(8), 1129–1136. https://doi.org/10.1002/jssc.200800639

Donnarumma, D., La Tella, R., Vento, F., Salerno, T. M. G., Micalizzi, G., Rigano, F., & Mondello, L. (2021). Evaluation of the Level of Toxic Contaminants and Essential Molecules in the Context of the Re-Use of Tuna Fishery Industry by-

Products. *Food Anal Methods*, *14*(10), 2161–2174. https://doi.org/10.1007/s12161-021-02045-w

Dos Santos Aguilar, J. G., & Sato, H. H. (2018). Microbial proteases: Production and application in obtaining protein hydrolysates. In *Food Res Int*, 103, pp. 253–262). Elsevier Ltd. https://doi.org/10.1016/j.foodres.2017.10.044

Doumenq, P., Guiliano, M., Bertrand, J. C., & Mille, G. (1990). GC/FT-IR Analysis of Fatty Acid Methyl Esters. *Appl Spectrosc*, *44*(8), 1355–1359. https://doi.org/10.1366/0003702907896196 76

Doumenq, P., Guiliano, M., & Mille, G. (1989). GC/FTIR potential for structural analysis of marine origin complex mixtures. *Int J Environ Anal Chem*, *37*(4), 235–244. https://doi.org/10.1080/03067318908026900

Dugo, P., Russo, M., Sarò, M., Carnovale, C., Bonaccorsi, I., & Mondello, L. (2012). Multidimensional liquid chromatography for the determination of chiral coumarins and furocoumarins in Citrus essential oils. *J Sep Sci*, *35*(14), 1828-1836. https://doi.org/10.1002/jssc.201200078

Dupree, E. J., Jayathirtha, M., Yorkey, H., Mihasan, M., Petre, B. A., & Darie, C. C. (2020). A critical review of bottom-up proteomics: The good, the bad, and the future of this field. *Proteomes*, *8*(3), 1–26. https://doi.org/10.3390/proteomes8030014

Eng, J. K., Mccormack, A. L., & Yates, J. R. (1994). An approach to correlate tandem mass spectral data of peptides with amino acid sequences in a protein database. *J Am Soc Mass Spectrom*, *5*(11), 976–989. https://doi.org/10.1016/1044-0305(94)80016-2

Eng, J. K., Searle, B. C., Clauser, K. R., & Tabb, D. L. (2011). A face in the crowd: recognizing peptides through database search. *Mol Cell Proteomics*, *10*(11), R111.009522. https://doi.org/10.1074/mcp.R111.009522

Erdem Büyükkiraz, M., & Kesmen, Z. (2022). Antimicrobial peptides (AMPs): promising class of antimicrobial compounds. *J Appl Microbiol*, *132*(3), 1573–1596. https://doi.org/10.1111/jam.15314

Escudero, E., Toldrá, F., Sentandreu, M. A., Nishimura, H., & Arihara, K. (2012). Antihypertensive activity of peptides identified in the in vitro gastrointestinal digest of pork meat. *Meat Sci*, *91*(3), 382–384. https://doi.org/10.1016/j.meatsci.2012.02.007

Esposito, M., Tse, T., & Soufani, K. (2018). Introducing a circular economy: new thinking with new managerial and policy implications. *Calif Manage Rev*, *60*(3), 5–19. https://doi.org/10.1177/0008125618764691

European Commission, & Directorate-General for Environment. (2020). *Investing in the circular economy – A blueprint for a green recovery*. Publications Office. https://data.europa.eu/doi/10.2779/48431

Exarchou, V., Godejohann, M., van Beek, T. A., Gerothanassis, I. P., & Vervoort, J. (2003). LC-UV-Solid-Phase Extraction-NMR-MS Combined with a Cryogenic Flow Probe and Its Application to the Identification of Compounds Present in Greek Oregano. *Anal Chem*, *75*(22), 6288–6294. https://doi.org/10.1021/ac0347819

Fadeeva, Z., & Van Berkel, R. (2023). Towards circular economy of food systems: an explorative appraisal of opportunities in fish, seafood value chains. *Sustainable Food Value Chain Development: Perspectives from Developing and Emerging Economies*, 61–86. Springer Nature Singapore. https://doi.org/10.1007/978-981-19-6454-1_4

Famiglini, G., Palma, P., Termopoli, V., & Cappiello, A. (2021). The history of electron ionization in LC-MS, from the early days to modern technologies: A review. *Anal Chim Acta*, 1167, 338350. https://doi.org/10.1016/j.aca.2021.338350

FAO. (2022). The State of World Fisheries and Aquaculture 2022. Towards Blue Transformation. *The State of World Fisheries and Aquaculture 2022*. FAO. https://doi.org/10.4060/cc0461en

Fenn, J. B. (2003). Electrospray wings for molecular elephants (Nobel lecture). *Angew Chem Int Ed*, *42*(33), 3871–3894. https://doi.org/10.1002/anie.200300605

Fenn, J. B., Mann, M., Meng, C. K., Wong, S. F., & Whitehouse, C. M. (1989). Electrospray ionization for mass spectrometry of large biomolecules, *Science*, *246*(4926), 64-71. https://doi.org/10.1126/science.2675315

Fenn, J. B., Mann, M., Meng, C. K., Wong, S. F., & Whitehouse, C. M. (1990). Electrospray ionization-principles and practice, *Mass Spectrom Rev*, *9*(1) 37–70.

Fernández-Costa, C., Martínez-Bartolomé, S., McClatchy, D. B., Saviola, A. J., Yu, N. K., & Yates, J. R. (2020). Impact of the identification strategy on the reproducibility of the DDA and DIA results. *J Proteome Res*, *19*(8), 3153–3161. https://doi.org/10.1021/acs.jproteome.0c00153

Ferraro, V., Carvalho, A. P., Piccirillo, C., Santos, M. M., Paula, P. M., & E. Pintado, M. (2013). Extraction of high added value biological compounds from sardine, sardine-type fish and mackerel canning residues - A review. *Mater Sci Eng C*, *33*(6), 3111–3120. https://doi.org/10.1016/j.msec.2013.04.003

Frison, G., Zancanaro, F., Frasson, S., Quadretti, L., Agnati, M., Vlassich, F., Gagliardi, G., Salerno, T. M. G., Donato, P., & Mondello, L. (2021). Analytical Characterization of 3-MeO-PCP and 3-MMC in Seized Products and Biosamples: The Role of LC-HRAM-Orbitrap-MS and Solid Deposition GC-FTIR. *Front Chem*, *8*, 618339. https://doi.org/10.3389/fchem.2020.618339

Fuoco, Roger., Shafer, K. H., & Griffiths, P. R. (1986). Capillary gas chromatography/Fourier transform infrared microspectrometry at subambient

temperature. *Anal Chem*, *58*(14), 3249–3254. https://doi.org/10.1021/ac00127a073

Gallego, M., Grootaert, C., Mora, L., Aristoy, M. C., Van Camp, J., & Toldrá, F. (2016). Transepithelial transport of dry-cured ham peptides with ACE inhibitory activity through a Caco-cell monolayer. *Journal of Functional Foods*, *21*, 388–395. https://doi.org/10.1016/j.jff.2015.11.046

Gallego, M., Mauri, L., Aristoy, M. C., Toldrá, F., & Mora, L. (2020). Antioxidant peptides profile in dry-cured ham as affected by gastrointestinal digestion. *J Funct Foods*, *69*, 103956. https://doi.org/10.1016/j.jff.2020.103956

Gallego, M., Mora, L., Escudero, E., & Toldrá, F. (2018). Bioactive peptides and free amino acids profiles in different types of European dry-fermented sausages. *Int J Food Microbiol*, *276*, 71–78. https://doi.org/10.1016/j.ijfoodmicro.2018.04.009

Gallego, M., Mora, L., & Toldrá, F. (2018). Characterisation of the antioxidant peptide AEEEYPDL and its quantification in Spanish dry-cured ham. *Food Chem*, *258*, 8–15. https://doi.org/10.1016/j.foodchem.2018.03.035

Ganguly, R., & Pierce, G. N. (2015). The toxicity of dietary trans fats. *Food Chem Toxicol*, *78*, 170–176. https://doi.org/https://doi.org/10.1016/j.fct.2015.02.004

Garrard, A. (2014). Coumarins. *Encyclopedia of Toxicology (Third Edition)*, 1052–1054. https://doi.org/10.1016/B978-0-12-386454-3.00798-3

Gathungu, R. M., Kautz, R., Kristal, B. S., Bird, S. S., & Vouros, P. (2020). The integration of LC-MS and NMR for the analysis of low molecular weight trace analytes in complex matrices. *Mass Spectrom Rev*, *39*(1-2), 35–54. https://doi.org/10.1002/mas.21575

Giromini, C., Cheli, F., Rebucci, R., & Baldi, A. (2019). Invited review: Dairy proteins and bioactive peptides: Modeling digestion and the intestinal barrier. *J Dairy Sci*, *102*(2), 929–942. https://doi.org/10.3168/jds.2018-15163

Guo, J., & Huan, T. (2020). Comparison of full-scan, data-dependent, and data-independent acquisition modes in liquid chromatography-mass spectrometry based untargeted metabolomics. *Anal Chem*, *92*(12), 8072–8080. https://doi.org/10.1021/acs.analchem.9b05135

Haag, A. M. (2016). Mass analyzers and mass spectrometers. Modern Proteomics – Sample Preparation, Analysis and Practical Applications. Advances in Experimental Medicine and Biology, vol 919, 157–169. https://doi.org/10.1007/978-3-319-41448-5_7

Hackshaw, K. V, Miller, J. S., Aykas, D. P., & Rodriguez-Saona, L. (2020). Vibrational spectroscopy for identification of metabolites in biologic samples. *Molecules*, *25*(20), 4725. https://doi.org/10.3390/molecules25204725

Halim, N. R. A., Yusof, H. M., & Sarbon, N. M. (2016). Functional and bioactive properties of fish protein hydrolysates and peptides: s comprehensive review. *Trends Food Sci Technol*, *51*, 24–33. https://doi.org/10.1016/j.tifs.2016.02.007

Hashimoto, K., & Badarla, V. R. (2019). Kawai1 A, Ideguchi T. Complementary vibrational spectroscopy. *Nat Commun*, *10*, 4411. https://doi.org/10.1038/s41467-019-12442-9

Hayes R N, & Gross M L. (1990). Collision-induced dissociation. *Meth Enzymol*, *193*, 237–263. https://doi.org/https://doi.org/10.1016/0076-6879(90)93418-K

Hedges, L. M., & Wilkins, C. L. (1991). Component Analysis of Eucalyptus Oil by Gas Chromatography-Fourier Transform-Infrared Spectrometry-Mass Spectrometry. *J Chromatogr Sci*, *29*(8), 345–350. https://doi.org/10.1093/chromsci/29.8.345

Hellinger, R., Sigurdsson, A., Wu, W., Romanova, E. V., Li, L., Sweedler, J. V., Süssmuth, R. D., & Gruber, C. W. (2023). Peptidomics. *Nature Rev Methods Primers*, *3*, 25. https://doi.org/10.1038/s43586-023-00205-2

Henzel, W. J., Billeci, T. M., Stults, J. T., Wong, S. C., Grimley, C., & Watanabe, C. (1993). Identifying proteins from two-dimensional gels by molecular mass searching of peptide fragments in protein sequence databases. *Proc Natl Acad Sci*, *90*(11), 5011–5015. https://doi.org/10.1073/pnas.90.11.5011

Huan, Y., Kong, Q., Mou, H., & Yi, H. (2020). Antimicrobial Peptides: Classification, Design, Application and Research Progress in Multiple Fields. In *Front Microbiol*, 11, 582779. https://doi.org/10.3389/fmicb.2020.582779

Huang, S.-J., Tsai, S.-Y., & Mau, J.-L. (2006). Antioxidant properties of methanolic extracts from Agrocybe cylindracea. *LWT*, *39*(4), 379–387. https://doi.org/10.1016/j.lwt.2005.02.012

James, P., Quadroni, M., Carafoli, E., & Gonnet, G. (1993). Protein Identification by Mass Profile Fingerprinting. *Biochem Biophys Res Commun*, *195*(1), 58–64. https://doi.org/10.1006/bbrc.1993.2009

Jensen, N. J., & Gross, M. L. (1987). Mass spectrometry methods for structural determination and analysis of fatty acids. *Mass Spectrom Rev*, *6*(4), 497–536. https://doi.org/10.1002/mas.1280060403

Johnson, R. S., Martin, S. A., Biemann, K., Stults, J. T., & Throck Watson, J. (1987). Novel fragmentation process of peptides by collision-induced decomposition in a tandem mass spectrometer: differentiation of leucine and isoleucine. *Anal Chem*, *59*(21), 2621–2625. https://doi.org/10.1021/ac00148a019

Juhasz, P., Vestal, M. L., & Martin, S. A. (1997). On the initial velocity of ions generated by matrix-assisted laser desorption ionization and its effect on the calibration of delayed extraction time-of-flight mass spectra. *J Am Soc Mass Spectrom*, *8*, 209–217. https://doi.org/10.1016/S1044-0305(96)00256-5

Karas, M., & Bahr, U. (1990). Laser desorption ionization mass spectrometry of large biomolecules. *TrAC, Trends Anal Chem*, *9*(10), 321–325. https://doi.org/https://doi.org/10.1016/0165-9936(90)85065-F

Kebukawa, Y., Kobayashi, H., Urayama, N., Baden, N., Kondo, M., Zolensky, M. E., & Kobayashi, K. (2019). Nanoscale infrared imaging analysis of carbonaceous chondrites to understand organic-mineral interactions during aqueous alteration. *PNAS*, *116*(3), 753–758. https://doi.org/10.1073/pnas.1816265116

Kok, S. J., Wold, C. A., Hankemeier, T., & Schoenmakers, P. J. (2003). Comparison of on-line flow-cell and off-line solvent-elimination interfaces for size-exclusion chromatography and Fourier-transform infrared spectroscopy in polymer analysis. *J Chromatogr A*, *1017*(1-2), *83*–96. https://doi.org/10.1016/j.chroma.2003.08.026

Kuehl, D., & Griffiths, P. R. (1979). Novel approaches to interfacing a high performance liquid chromatograph with a fourier transform infrared spectrometer. *J Chromatogr Sci*, *17*(8), 471–476. https://doi.org/10.1093/chromsci/17.8.471

Kyte, J., & Doolittle, R. F. (1982). A simple method for displaying the hydropathic character of a protein. *J Mol Biol*, *157*(1), 105–132. https://doi.org/10.1016/0022-2836(82)90515-0

Laczkó, Z., Harsányi, L., & Dobos, S. (1985). Studies of UV photochemistry of psoralen and angelicin by infrared spectroscopy. *J Mol Struct*, *130*(3–4), 227–234. https://doi.org/10.1016/0022-2860(85)87004-6

Lanzarotta, A., Lorenz, L., Voelker, S., Falconer, T. M., & Batson, J. S. (2017). Forensic drug identification, confirmation, and quantification using a fully integrated gas chromatography-Fourier transform infrared-mass spectrometer (GC-FT-IR-MS). *Appl Spectrosc*, *72*(5), 750–756. https://doi.org/10.1177/0003702817746964

Lassoued, I., Mora, L., Nasri, R., Jridi, M., Toldrá, F., Aristoy, M. C., Barkia, A., & Nasri, M. (2015). Characterization and comparative assessment of antioxidant and ACE inhibitory activities of thornback ray gelatin hydrolysates. *J Funct Foods*, *13*, 225–238. https://doi.org/10.1016/j.jff.2014.12.042

Lee, A. C. L., Harris, J. L., Khanna, K. K., & Hong, J. H. (2019). A comprehensive review on current advances in peptide drug development and design. *Int J Mol Sci*, *20*(10), 2383. https://doi.org/10.3390/ijms20102383

Lorenz, L. M., Toomey, V. M., Lanzarotta, A. C., Flurer, R. A., & Falconer, T. M. (2019). Identification of the designer steroid Androsta-3,5-diene-7,17-dione in a dietary supplement. *Drug Test Anal*, *11*(7), 1109–1115. https://doi.org/10.1002/dta.2589

Ma, B., & Johnson, R. (2012). De novo sequencing and homology searching. *Mol Cell Proteomics*, *11*(2), O111.014902. https://doi.org/10.1074/mcp.O111.014902

Mahlapuu, M., Björn, C., & Ekblom, J. (2020). Antimicrobial peptides as therapeutic agents: opportunities and challenges. *Crit Rev Biotechnol*, *40*(7), 978–992. https://doi.org/10.1080/07388551.2020.1796576

Mamyrin, B. A., Karataev, V. I., Shmikk, D. V, & Zagulin, V. A. (1973). The mass-reflectron, a new nonmagnetic time-of-flight mass spectrometer with high resolution. *J Exp Theor Phys*, *37*, 45. https://api.semanticscholar.org/CorpusID:106399404

Mann, M., Højrup, P., & Roepstorfis, P. (1993). Use of mass spectrometric molecular weight information to identify proteins in sequence databases. *Biol Mass Spectrom*, *22*(6), 338–345. https://doi.org/10.1002/bms.1200220605

Mann, M., Hendrickson, R. C., & Pandey, A. (2001). Analysis of proteins and proteomes by mass spectrometry. *Annu Rev Biochem*, 70, 437–473. https://doi.org/10.1146/annurev.biochem.70.1.437

Martínez-Vázquez, R. M., Milán-García, J., & de Pablo Valenciano, J. (2021). Challenges of the blue economy: evidence and research trends. *Environ Sci Eur*, *33*, 61. https://doi.org/10.1186/s12302-021-00502-1

McCloskey, J. A. (1971). *Topics in Lipid Chemistry*, vol 1, 369–440.

Meher, P. K., Sahu, T. K., Saini, V., & Rao, A. R. (2017). Predicting antimicrobial peptides with improved accuracy by incorporating the compositional, physico-chemical and structural features into Chou's general PseAAC. *Sci Rep*, *7*, 42362. https://doi.org/10.1038/srep42362

Miller, P. E., & Denton, M. B. (1986). The Quadrupole Mass Filter: Basic Operating Concepts. *J Chem Educ*, *63*, 617–622. https://doi.org/10.1021/ed063p617

Minekus, M., Alminger, M., Alvito, P., Ballance, S., Bohn, T., Bourlieu, C., Carrière, F., Boutrou, R., Corredig, M., Dupont, D., Dufour, C., Egger, L., Golding, M., Karakaya, S., Kirkhus, B., Le Feunteun, S., Lesmes, U., Macierzanka, A., Mackie, A., Marze, S., McClements, D. J., Ménard, O., Recio, I., Santos, C. N., Singh, R. P., Vegarud, G. E., Wickham, M. S. J., Weitschies W., Brodkorb, A. (2014). A standardised static *in vitro* digestion method suitable for food-an international consensus. *Food Funct*, *5*(6), 1113–1124. https://doi.org/10.1039/c3fo60702j

Minkiewicz, P., Iwaniak, A., & Darewicz, M. (2019). BIOPEP-UWM database of bioactive peptides: Current opportunities. *Int J Mol Sci*, *20*(23), 5978. https://doi.org/10.3390/ijms20235978

Mohamed, M. A., Jaafar, J., Ismail, A. F., Othman, M. H. D., & Rahman, M. A. (2017). Chapter 1 - Fourier Transform Infrared (FTIR) Spectroscopy. *Membrane Characterization*, *1*, 3–29. https://doi.org/https://doi.org/10.1016/B978-0-444-63776-5.00001-2

Mondello, L., Donato, P., Cacciola, F., Fanali, C., & Dugo, P. (2010). RP-LC x RP-LC analysis of a tryptic digest using a combination of totally porous and partially

porous stationary phases. *J Sep Sci*, *33*(10), 1454–1461. https://doi.org/10.1002/jssc.200900816

Mora, L., Escudero, E., Arihara, K., & Toldrá, F. (2015). Antihypertensive effect of peptides naturally generated during Iberian dry-cured ham processing. *Food Res Int*, *78*, 71–78. https://doi.org/10.1016/j.foodres.2015.11.005

Mora, L., Escudero, E., & Toldrá, F. (2016). Characterization of the peptide profile in Spanish Teruel, Italian Parma and Belgian dry-cured hams and its potential bioactivity. *Food Res Int*, *89*, 638–646. https://doi.org/10.1016/j.foodres.2016.09.016

Mora, L., González-Rogel, D., Heres, A., & Toldrá, F. (2020). Iberian dry-cured ham as a potential source of α-glucosidase-inhibitory peptides. *J Funct Foods*, *67*, 103840. https://doi.org/10.1016/j.jff.2020.103840

Mora, L., Reig, M., & Toldrá, F. (2014). Bioactive peptides generated from meat industry by-products. *Food Res Int*, *65*(PC), 344–349. https://doi.org/10.1016/j.foodres.2014.09.014

Mora, L., Sentandreu, M. A., & Toldrá, F. (2007). Hydrophilic chromatographic determination of carnosine, anserine, balenine, creatine, and creatinine. *J Agric Food Chem*, *55*(12), 4664–4669. https://doi.org/10.1021/jf0703809

Morseletto, P. (2020). Targets for a circular economy. *Resour Conserv Recycl*, *153*, 104553. https://doi.org/10.1016/j.resconrec.2019.104553

Mossoba, M. M., Mcdonald, R. E., Chen, J.-Y. T., Armstrong, D. J., & Page, S. W. (1990). Identification and quantitation of trans-9, trans-12-octadecadienoic acid methyl ester and related compounds in hydrogenated soybean oil and margarines by capillary gas chromatography/matrix isolation/Fourier transform infrared spectroscopy. *J Agric Food Chem*, *38*(1), 86–92. https://doi.org/10.1021/jf00091a016

Mossoba, M. M., McDonald, R. E., Roach, J. A. G., Fingerhut, D. D., Yurawecz, M. P., & Sehat, N. (1997). Spectral confirmation of trans monounsaturated C_{18} fatty acid positional isomers. *J Am Oil Chem Soc*, *74*(2), 125–130. https://doi.org/10.1007/s11746-997-0156-3

Mune Mune, M. A. (2015). Influence of Degree of Hydrolysis on the Functional Properties of Cowpea Protein Hydrolysates. *J Food Process Preserv*, *39*(6), 2386–2392. https://doi.org/10.1111/jfpp.12488

Neubauer, D., Jaśkiewicz, M., Migoń, D., Bauer, M., Sikora, K., Sikorska, E., Kamysz, E., & Kamysz, W. (2017). Retro analog concept: comparative study on physico-chemical and biological properties of selected antimicrobial peptides. *Amino Acids*, *49*(10), 1755–1771. https://doi.org/10.1007/s00726-017-2473-7

Nielsen, P. M., Petersen, D., & Dambmann, C. (2001). Improved method for determining food protein degree of hydrolysis. *J Food Sci*, *66*(5), 642–646. https://doi.org/10.1111/j.1365-2621.2001.tb04614.x

Nolvachai, Y., Kulsing, C., & Marriott, P. J. (2015). Pesticides Analysis: Advantages of Increased Dimensionality in Gas Chromatography and Mass Spectrometry. *Crit Rev Env Sci Tec*, *45*(19), 2135–2173. https://doi.org/10.1080/10643389.2015.1010431

Önder, A. (2020). Chapter 3 - Anticancer activity of natural coumarins for biological targets. *Studies in Natural Products Chemistry*, *64*, 85–109. https://doi.org/10.1016/B978-0-12-817903-1.00003-6

Pachetti, M., Zupin, L., Venturin, I., Mitri, E., Boscolo, R., D'Amico, F., Vaccari, L., Crovella, S., Ricci, G., & Pascolo, L. (2020). FTIR Spectroscopy to Reveal Lipid and Protein Changes Induced on Sperm by Capacitation: Bases for an Improvement of Sample Selection in ART. *Int J Mol Sci*, *21*. https://doi.org/10.3390/ijms21228659

Pappin, D. J. C., Hojrupt, P., & Bleasby, A. J. (1993). Rapid identification of proteins by peptide-mass fingerprinting. *Curr Biol*, *3*(6), 327–332. https://doi.org/10.1016/0960-9822(93)90195-t

Penta, S. (2016). Introduction to Coumarin and SAR. Chapter 1 - Introduction to Coumarin and SAR. *Advances in Structure and Activity Relationship of Coumarin Derivatives*, 1–16. https://doi.org/10.1016/B978-0-12-803797-3.00001-1

Pepe, G., Sommella, E., Ventre, G., Scala, M. C., Adesso, S., Ostacolo, C., Marzocco, S., Novellino, E., & Campiglia, P. (2016). Antioxidant peptides released from gastrointestinal digestion of "Stracchino" soft cheese: Characterization, in vitro intestinal protection and bioavailability. *J Funct Foods*, *26*, 494–505. https://doi.org/10.1016/j.jff.2016.08.021

Perkins, D. N., Pappin, D. J. C., Creasy, D. M., & Cottrell, J. S. (1999). Probability-based protein identification by searching sequence databases using mass spectrometry data. *Electrophoresis*, *20*(18), 3551–3567. https://doi.org/10.1002/(SICI)1522-2683(19991201)20:18<3551::AID-ELPS3551>3.0.CO;2-2

Pihlanto-Leppälä, A. (2001). Bioactive peptides derived from bovine whey proteins: opioid and ace-inhibitory peptides. *Trends Food Sci Technol*, *11*, 347–356.

Piovesana, S., Capriotti, A. L., Caruso, G., Cavaliere, C., La Barbera, G., Zenezini Chiozzi, R., & Laganà, A. (2016). Labeling and label free shotgun proteomics approaches to characterize muscle tissue from farmed and wild gilthead sea bream (*Sparus aurata*). *J Chromatogr A*, *1428*, 193–201. https://doi.org/10.1016/j.chroma.2015.07.049

Pirtskhalava, M., Vishnepolsky, B., Grigolava, M., & Managadze, G. (2021). Physicochemical features and peculiarities of interaction of amp with the membrane. *Pharmaceuticals*, *14*(5), 471. https://doi.org/10.3390/ph14050471

Pizzano, R., Nicolai, M. A., & Addeo, F. (1998). Antipeptide Antibodies as Analytical Tools to discriminate among bovine αs1-Casein components. *J Agric Food Chem*, *46*(2), 766–771. https://doi.org/10.1021/jf9706336

Prior, R. L., Wu, X., & Schaich, K. (2005). Standardized methods for the determination of antioxidant capacity and phenolics in foods and dietary supplements. In *J Agric Food Chem*, *53*(10), 4290–4302. https://doi.org/10.1021/jf0502698

Ragunathan, N., Krock, K. A., Klawun, C., Sasaki, T. A., & Wilkins, C. L. (1999). Gas chromatography with spectroscopic detectors. *J Chromatogr A*, *856*(1), 349–397. https://doi.org/https://doi.org/10.1016/S0021-9673(99)00819-5

Re, R., Pellegrini, N., Proteggente, A., Pannala, A., Yang, M., & Rice-Evans, C. (1999). Antioxidant activity applying an improved ABTS radical cation decolorization assay, *Free Radic Biol Med*, *26*(9-10), 1231–1237. https://doi.org/10.1016/S0891-5849(98)00315-3

Reedy, G. T., Ettinger, D. G., Schneider, J. F., & Bourne, Sidney. (1985). High-resolution gas chromatography/matrix isolation infrared spectrometry. *Anal Chem*, *57*(8), 1602–1609. https://doi.org/10.1021/ac00285a024

Rigano, F., Arena, P., Mangraviti, D., Donnarumma, D., Dugo, P., Donato, P., Mondello, L., & Micalizzi, G. (2021). Identification of high-value generating molecules from the wastes of tuna fishery industry by liquid chromatography and gas chromatography hyphenated techniques with automated sample preparation. *J Sep Sci*, *44*(8), 1571–1580. https://doi.org/10.1002/jssc.202100108

Roepstorff, P., & Fohlman, J. (1984). Proposal for a Common Nomenclature for Sequence Ions in Mass Spectra of Peptides. *Biomed Mass Spectrom*, *11*(11), 601. https://doi.org/https://doi.org/10.1002/bms.1200111109

Ryder, K., Bekhit, A. E. D., McConnell, M., & Carne, A. (2016). Towards generation of bioactive peptides from meat industry waste proteins: Generation of peptides using commercial microbial proteases. *Food Chem*, *208*, 42–50. https://doi.org/10.1016/j.foodchem.2016.03.121

Salerno, T. M. G., Donato, P., Frison, G., Zamengo, L., & Mondello, L. (2020). Gas Chromatography-Fourier Transform Infrared Spectroscopy for Unambiguous Determination of Illicit Drugs: A Proof of Concept. *Front Chem*, *8*, 624. https://doi.org/10.3389/fchem.2020.00624

Samaei, S. P., Ghorbani, M., Tagliazucchi, D., Martini, S., Gotti, R., Themelis, T., Tesini, F., Gianotti, A., Gallina Toschi, T., & Babini, E. (2020). Functional, nutritional, antioxidant, sensory properties and comparative peptidomic profile of faba bean (*Vicia faba*, L.) seed protein hydrolysates and fortified apple juice. *Food Chem*, *330*, 127120. https://doi.org/10.1016/j.foodchem.2020.127120

Santiago-López, L., Aguilar-Toalá, J. E., Hernández-Mendoza, A., Vallejo-Cordoba, B., Liceaga, A. M., & González-Córdova, A. F. (2018). Invited review: Bioactive

compounds produced during cheese ripening and health effects associated with aged cheese consumption. *J Dairy Sci*, *101*(5), 3742–3757. https://doi.org/10.3168/jds.2017-13465

Schwarzenberg, A., Dossmann, H., Cole, R. B., Machuron-Mandard, X., & Tabet, J.-. C. (2014). Differentiation of isomeric dinitrotoluenes and aminodinitrotoluenes using electrospray high resolution mass spectrometry. *J Mass Spectrom*, *49*(12), 1330–1337. https://doi.org/10.1002/jms.3471

Sémon, E., Ferary, S., Auger, J., & Le Quéré, J. L. (1998). Gas chromatography-fourier transform infrared spectrometry of fatty acids: New Applications with a direct deposition interface. *J Am Oil Chem Soc*, *75*(2), 101–105. https://doi.org/10.1007/s11746-998-0018-7

Sentandreu, M. A., Stoeva, S., Aristoy, M. C., Laib, K., Voelter, W., & Toldrá, F. (2003). Identification of small peptides generated in Spanish dry-cured ham. *J Food Sci*, *68*(1), 64–69. https://doi.org/10.1111/j.1365-2621.2003.tb14115.x

Smith, L. W., Thaxton-Weissenfluh, A., Abiedalla, Y., DeRuiter, J., Smith, F., & Clark, C. R. (2018). Correlation of vapor phase infrared spectra and regioisomeric structure in synthetic cannabinoids. *Spectrochim Acta A Mol Biomol Spectrosc*, *196*, 375–384. https://doi.org/10.1016/j.saa.2018.02.052

Smyrl, N. R., Hembree, D. M., Davis, W. E., Williams, D. M., & Vance, J. C. (1992). Simultaneous GC-FT-IR/GC-MS analysis for isomer-specific identification and quantitation of complex mixture components. *Appl Spectrosc*, *46*(2), 277–282. https://doi.org/10.1366/0003702924125636

Sobott, F., Watt, S. J., Smith, J., Edelmann, M. J., Kramer, H. B., & Kessler, B. M. (2009). Comparison of CID Versus ETD based MS/MS fragmentation for the analysis of protein ubiquitination. *J Am Soc Mass Spectrom. 20*(9), 1652–1659. https://doi.org/10.1016/j.jasms.2009.04.023

Somsen, G. W., Gooijer, C., & Brinkman, U. A. (1999). Liquid chromatography-Fourier-transform infrared spectrometry. *J Chromatogr A*, *856*(1-2), 213–242. https://doi.org/10.1016/s0021-9673(99)00280-0

Somsen, G. W., Gooijer, C., & Brinkman, U. A. T. (1998). Analyte-deposition-based Detection in Column Liquid Chromatography: Concept and Examples. *TrAC Trends Anal Chem*, *17*(3), 129–140. https://doi.org/10.1016/s0165-9936(98)00005-3

Somsen, G. W., & Visser, T. (2000). Liquid Chromatography/Infrared Spectroscopy. *Encyclopedia of Analytical Chemistry: Applications, Theory, and Instrumentation*. https://doi.org/10.1002/9780470027318.a5608

Strohalm, M., Kavan, D., Novák, P., Volný, M., & Havlíček, V. (2010). mMass 3: A cross-platform software environment for precise analysis of mass spectrometric data. *Anal Chem*, *82*(11), 4648–4651. https://doi.org/10.1021/ac100818g

Talapko, J., Meštrović, T., Juzbašić, M., Tomas, M., Erić, S., Horvat Aleksijević, L., Bekić, S., Schwarz, D., Matić, S., Neuberg, M., & Škrlec, I. (2022). Antimicrobial Peptides—Mechanisms of Action, Antimicrobial Effects and Clinical Applications. *Antibiotics*, *11*(10), 1417. https://doi.org/10.3390/antibiotics11101417

Thakur, A., Sharma, A., Alajangi, H. K., Jaiswal, P. K., Lim, Y. beom, Singh, G., & Barnwal, R. P. (2022). In pursuit of next-generation therapeutics: antimicrobial peptides against superbugs, their sources, mechanism of action, nanotechnology-based delivery, and clinical applications. *Int J Biol Macromol*, *218*, 135–156. https://doi.org/10.1016/j.ijbiomac.2022.07.103

Thiede, B., Höhenwarter, W., Krah, A., Mattow, J., Schmid, M., Schmidt, F., & Jungblut, P. R. (2005). Peptide mass fingerprinting. *Methods*, *35*(3), 237–247. https://doi.org/10.1016/j.ymeth.2004.08.015

Toldrá, F., Gallego, M., Reig, M., Aristoy, M. C., & Mora, L. (2020). Bioactive peptides generated in the processing of dry-cured ham. *Food Chem*, *321*, 126689. https://doi.org/10.1016/j.foodchem.2020.126689

Toldrá, F., & Mora, L. (2021). Chapter 2 - Enzymatic mechanisms for the generation of bioactive peptides. *Biologically Active Peptides: From Basic Science to Applications for Human Health*, *2*, 27–46. https://doi.org/10.1016/B978-0-12-821389-6.00031-5

Toldrá, F., Mora, L., & Reig, M. (2016). New insights into meat by-product utilization. *Meat Sci*, *120*, 54–59. https://doi.org/10.1016/j.meatsci.2016.04.021

Toldrá, F., Reig, M., Aristoy, M. C., & Mora, L. (2018). Generation of bioactive peptides during food processing. *Food Chem*, *267*, 395–404. https://doi.org/10.1016/j.foodchem.2017.06.119

Tranchida, P. Q., Aloisi, I., Giocastro, B., Zoccali, M., & Mondello, L. (2019). Comprehensive two-dimensional gas chromatography-mass spectrometry using milder electron ionization conditions: A preliminary evaluation. *J Chromatogr A*, *1589*, 134–140. https://doi.org/10.1016/j.chroma.2019.01.006

Valero, Y., Saraiva-Fraga, M., Costas, B., & Guardiola, F. A. (2020). Antimicrobial peptides from fish: beyond the fight against pathogens. *Rev Aquac*, *12*(1), 224–253. https://doi.org/10.1111/raq.12314

Van Deemter, J. J., Zuiderweg, F. J., & Klinkenberg, A. (1956). Longitudinal diffusion and resistance to mass transfer as causes of nonideality in chromatography, Chem Eng Sci, *50*(24), 3867. https://doi.org/10.1016/0009-2509(96)81812-4

Vestal, M. L., Juhasz, P., & Martin, S. A. (1995). Delayed extraction matrix-assisted laser desorption time-of-flight mass spectrometry. *Rapid Commun Mass Spectrom*, *9*(11), 1044–1050. https://doi.org/10.1002/rcm.1290091115

Vierros, M., & De Fontaubert, C. (2017). The potential of the blue economy: increasing long-term benefits of the sustainable use of marine resources for small

island developing states and coastal least developed countries. *Washington, D.C. : World Bank Group.*, *1*. http://documents.worldbank.org/curated/en/523151496389684076/The-potential-of-the-blue-economy-increasing-long-term-benefits-of-the-sustainable-use-of-marine-resources-for-small-island-developing-states-and-coastal-least-developed-countries

Visser, T. (2002). FT-IR detection in gas chromatography. *TrAC Trends Anal Chem*, *21*(9), 627–636. https://doi.org/https://doi.org/10.1016/S0165-9936(02)00812-9

Wahl, H. G., Habel, S.-Y., Schmieder, N., & Liebich, H. M. (1994). Identification of cis/trans isomers of methyl ester and oxazoline derivatives of unsaturated fatty acids using GC–FTIR–MS. *J High Resol Chromatogr*, *17*(7), 543–548. https://doi.org/https://doi.org/10.1002/jhrc.1240170707

Wan, P., Cai, B., Chen, H., Chen, D., Zhao, X., Yuan, H., Huang, J., Chen, X., Luo, L., & Pan, J. (2023). Antidiabetic effects of protein hydrolysates from *Trachinotus ovatus* and identification and screening of peptides with α-amylase and DPP-IV inhibitory activities. *Curr Res Food Sci*, *6*, 100446. https://doi.org/10.1016/j.crfs.2023.100446

Wang, G. D. (2015). LC-MS in plant metabolomics. *Plant Metabolomics: Methods and Applications*, 45–61. https://doi.org/10.1007/978-94-017-9291-2_3

Want, E. J. (2018). LC-MS untargeted analysis. *Metabolic Profiling. Methods Mol Biol*, *1738*, 99–116 https://doi.org/10.1007/978-1-4939-7643-0_7

Wood, T. D., Moy, M. A., Dolan, A. R., Bigwarfe, P. M., White, T. P., Smith, D. R., & Higbee, D. J. (2003). Miniaturization of electrospray ionization mass spectrometry. *Appl Spectrosc Rev*, *38*(2), 187–244. https://doi.org/10.1081/ASR-120021167

Xiao, Y., Vecchi, M. M., & Wen, D. (2016). Distinguishing between Leucine and Isoleucine by Integrated LC-MS Analysis Using an Orbitrap Fusion Mass Spectrometer. *Anal Chem*, *88*(21), 10757–10766. https://doi.org/10.1021/acs.analchem.6b03409

Xie, J., Zhao, Q., Li, S., Yan, Z., Li, J., Li, Y., Mou, L., Zhang, B., Yang, W., Miao, X., Jiang, X., & Wang, R. (2017). Novel antimicrobial peptide CPF-C1 analogs with superior stabilities and activities against multidrug-resistant bacteria. *Chem Biol Drug Des*, *90*(5), 690–702. https://doi.org/10.1111/cbdd.12988

Yaghoubzadeh, Z., Peyravii Ghadikolaii, F., Kaboosi, H., Safari, R., & Fattahi, E. (2020). Antioxidant activity and anticancer effect of bioactive peptides from rainbow trout (*Oncorhynchus mykiss*) skin hydrolysate. *Int J Pept Res Ther*, *26*(1), 625–632. https://doi.org/10.1007/s10989-019-09869-5

Yates, J. R., Speicher, S., Griffin, P. R., & Hunkapiller, T. (1993). Peptide mass maps: a highly informative approach to protein identification. *Anal Biochem*, *214*(2), 397–408. https://doi.org/https://doi.org/10.1006/abio.1993.1514

Yathisha, U. G., Bhat, I., Karunasagar, I., & Mamatha, B. S. (2019). Antihypertensive activity of fish protein hydrolysates and its peptides. *Crit Rev Food Sci Nutr*, *59*(15), 2363–2374. https://doi.org/10.1080/10408398.2018.1452182

Yu, X.-Y. (2016). *Advances in Microfluidics*. https://doi.org/10.5772/60788

Zavahir, J. S., Nolvachai, Y., & Marriott, P. J. (2018). Molecular spectroscopy – Information rich detection for gas chromatography. In *TrAC - Trends Anal Chem*, *99*, 47–65. https://doi.org/10.1016/j.trac.2017.11.014

Zhang, Y., Fonslow, B. R., Shan, B., Baek, M. C., & Yates, J. R. (2013). Protein analysis by shotgun/bottom-up proteomics. *Chem Rev* 113, Issue 4, pp. 2343–2394). https://doi.org/10.1021/cr3003533

Zhu, Y., Lao, F., Pan, X., & Wu, J. (2022). Food Protein-Derived Antioxidant Peptides: Molecular Mechanism, Stability and Bioavailability. *Biomolecules*, *12*(11), 1622. https://doi.org/10.3390/biom12111622

Zou, T. Bin, He, T. P., Li, H. Bin, Tang, H. W., & Xia, E. Q. (2016). The structure-activity relationship of the antioxidant peptides from natural proteins. *Molecules*, *21*(1). https://doi.org/10.3390/molecules21010072

Zubarev, R. A., & Makarov, A. (2013). Orbitrap mass spectrometry. *Anal Chem*, *85*(11), 5288–5296. https://doi.org/10.1021/ac4001223

Publications

1 The online coupling of liquid chromatography to Fourier transform infrared spectroscopy using a solute deposition interface: A proof of concept

Tania Maria Grazia Salerno, **Carmelo Coppolino**, Paola Donato, Luigi Mondello

Anal. Bioanal. Chem. 414, 703–712 (2022)

https://doi.org/10.1007/s00216-021-03693-x

2 Circular Economy in the food chain: retrieval and characterization of antimicrobial peptides from fish waste Hydrolysates

Tania Maria Grazia Salerno, **Carmelo Coppolino**, Paola Arena, Ahmed Aichouni, Andrea Cerrato, Anna Laura Capriotti, Francesca Rigano, Danilo Donnarumma, Paola Donato, Alice Mondello, Luigi Mondello

Food and analytical methods

https://doi.org/10.1007/s12161-023-02543-z

3 Determination of methorphan enantiomers and other illicit drugs in seized drugs and biological specimens by means of HPLC-MS/MS and GC-MS

Article submitted (Analytical and Bioanalytical Chemistry)

4 Development of a novel integrated GC-*sd*-FTIR/MS approach and its application for the univocal cis/trans fatty acid isomer discrimination

Article submitted (Analytical and Bioanalytical Chemistry)

5 Characterization of short- and medium-chain antioxidant peptides from fish protein hydrolysate and evaluation of gastrointestinal effect

Article submitted (Food Research International)

Contributes at conferences

1 2021 On-line Forensic Symposium - Current Trends in Seized Drug Analysis, January 18-22, 2021

Paola Donato, Tania Maria Grazia Salerno, **Carmelo Coppolino**, Giampietro Frison, Luigi Mondello

Solid-Phase GC-FTIR for the Analysis of Illicit Drug Isomers

Invited Oral Communication

2 2021 On-line Forensic Symposium- Current Trends in Seized Drug Analysis, January 18-22, 2021

Paola Donato, Tania Maria Grazia Salerno, **Carmelo Coppolino**, Giampietro Frison, Luigi Mondello

Analysis of Synthetic Cannabinoids and Cathinones by Solid-Phase Deposition GC-FTIR

Poster Communication

3 18th GC×GC International Symposium, June 7-11, 2021

Tania Maria Grazia Salerno, **Carmelo Coppolino**, Mariosimone Zoccali, Luigi Mondello

GC×GC-*sd*-FTIR/MS for Reliable Identification in the Foodomics Field

Invited Oral Communication

4 XXVII Congresso Nazionale della Società Chimica Italiana - SCI 2021, on-line, September 14-23, 2021

Tania Maria Grazia Salerno, **Carmelo Coppolino**, Mariosimone Zoccali, Paola Donato, Luigi Mondello

The Coupling of Gas Chromatography - Mass Spectrometry with Infrared Spectroscopy for Reliable Identification of Unknowns in Complex Samples

Oral Communication

5 XXVII Congresso Nazionale della Società Chimica Italiana - SCI 2021, on-line, September 14-23, 2021

Carmelo Coppolino, Tania Maria Grazia Salerno, Paola Donato, Luigi Mondello

HPLC-FTIR: a proof of concept

Poster Communication

6 XXVII Congresso Nazionale della Società Chimica Italiana - SCI 2021, on-line, September 14-23, 2021

Carmelo Coppolino, Tania Maria Grazia Salerno, Paola Donato, Giampietro Frison, Luca Zamengo, Luigi Mondello

Chiral analysis of Methorphan's enantiomers by HPLC coupled with FTIR

Poster Communication

7 Doctochem 4th EDITION, Messina, 25-26 Novembre 2021

Carmelo Coppolino, Tania Maria Grazia Salerno, Paola Donato, Luigi Mondello

Confident discrimination of regioisomeric furanocoumarins by means of HPLC-FTIR

Oral Communication

8 Le indagini forensi e il contributo della spettrometria di massa, Rome, March 25, 2022

Tania Maria Grazia Salerno, **Carmelo Coppolino**, Paola Donato, Flavio Zancanaro, Samuela Frasson, Giampietro Frison, Luigi Mondello

The combined use of Solid Deposition GC-FTIR and LC-HRAM-Orbitrap-MS in forensic casework identification routine

Oral Communication

9 XXIX Congresso della Divisione di Chimica Analitica della Società Chimica Italiana, Milazzo (ME), September 11-15, 2022

Paola Donato, Tania Maria Grazia Salerno, **Carmelo Coppolino**, Luigi Mondello

GC-FTIR affords reliable forensic evidence for drugs of abuse

Oral Communication

10 XXIX Congresso della Divisione di Chimica Analitica della Società Chimica Italiana, Milazzo, Italy, September 11-15, 2022

Carmelo Coppolino, Tania Maria Grazia Salerno, Paola Donato, Luigi Mondello

Application of a new integrated GC-FTIR/MS approach for the univocal discrimination of regioisomers

Poster Communication

11 Incontri di Scienza delle Separazioni 2022, Firenze, November 17-18, 2022

Carmelo Coppolino, Andrea Cerrato, Anna Laura Capriotti, Paola Donato, Luigi Mondello

Recovery and valorisation of protein hydrolysate from tuna fishery industry waste

Oral communication

12 Doctochem 5th EDITION, Messina, 29-30 Novembre 2022

Carmelo Coppolino, Andrea Cerrato, Anna Laura Capriotti, Paola Donato, Luigi Mondello

HPLC-MS/MS characterization of tuna waste protein hydrolysate for reuse in novel formulations

Oral communication

13 HPLC 2023, 51st International Symposium on High Performance Liquid Phase Separations and Related Techniques, Duesseldorf, June 18-22, 2023

Carmelo Coppolino, Tania Maria Grazia Salerno, Giampiero Frison, Luca Zamengo, Paola Donato, Luigi Mondello

Determination of methorphan enantiomers in seizure drugs and biological specimens by means of chiral HPLC-MS/MS

Oral Communication

14 HPLC 2023, 51st International Symposium on High Performance Liquid Phase Separations and Related Techniques, Duesseldorf, June 18-22, 2023

Paola Donato, Francesca Rigano, Roberta La Tella, **Carmelo Coppolino**, Paola Dugo, Luigi Mondello

Investigation of a Novel Porous Graphitic Carbon Column as Stationary

Phase in Supercritical Fluid Chromatography

Oral Communication

15 HPLC 2023, 51st International Symposium on High Performance Liquid Phase Separations and Related Techniques, Duesseldorf, June 18-22, 2023

Mats Josefson, Gustaf Hulthe, Hasanain Al-Abas, Marta Luciani, Tania Maria Grazia Salerno, **Carmelo Coppolino**, Paola Donato, Luigi Mondello, Dario Ferracane, William W. Carson, P-O Quist

Characterization of modified celluloses for pharmaceutical formulation by Size Exclusion Chromatography/InfraRed detection and Machine Learning

Poster Communication

16 53rd International Symposium on Essential Oils (ISEO 2023), Milazzo (ME) September 13-16, 2023

Tania Maria Grazia Salerno, **Carmelo Coppolino**, Lorenzo Cucinotta, Paola Donato, Luigi Mondello

Boosting the confidence in identification in the Flavour and Fragrance field via a Gas Chromatography – Mass Spectrometry – Fourier Transform Infrared Spectroscopy instrument

Oral Communication

17 XXX Congresso della Divisione di Chimica Analitica della Società Chimica Italiana, Vasto (CH) September 17-21, 2023

Carmelo Coppolino, Tania Maria Grazia Salerno, Giampiero Frison, Luca Zamengo, Paola Donato, Luigi Mondello

Method for direct enantiomer determination of methorphan in seized drugs and biological specimens by means of chiral HPLC-MS/MS

Oral Communication

18 XXX Congresso della Divisione di Chimica Analitica della Società Chimica Italiana, Vasto (CH), September 17-21, 2023

Carmelo Coppolino, Tania Maria Grazia Salerno, Antonio Ferracane, Mariosimone Zoccali, Peter Quinto Tranchida, Paola Donato, Luigi Mondello

Fourier transform infrared spectroscopy (FTIR) coupled to comprehensive two-dimensional gas chromatography (GC×GC-*sd*-FTIR): a powerful tool for lipidomic studies

Poster Communication

19 Incontri di Scienza delle Separazioni, Termoli (CB), October 12-13, 2023

Carmelo Coppolino, Lorenzo Cucinotta, Tania Maria Grazia Salerno, Danilo Sciarrone, Paola Donato, Luigi Mondello

Application of a new integrated GC-FTIR/MS approach for the univocal cis/trans fatty acid isomer discrimination

Oral Communication

20 Doctochem 6th EDITION, Messina, November 29-30, 2023

Carmelo Coppolino, Lorenzo Cucinotta, Tania Maria Grazia Salerno, Danilo Sciarrone, Paola Donato, Luigi Mondello

Univocal differentiation of *cis/trans* fatty acid isomers by means of a novel integrated GC-FTIR/MS approach

Oral communication